Master Thesis in Geosciences

Deep basin and crustal configuration of the transition between the Møre and Vøring margins off mid-Norway

Barbara E. Klein

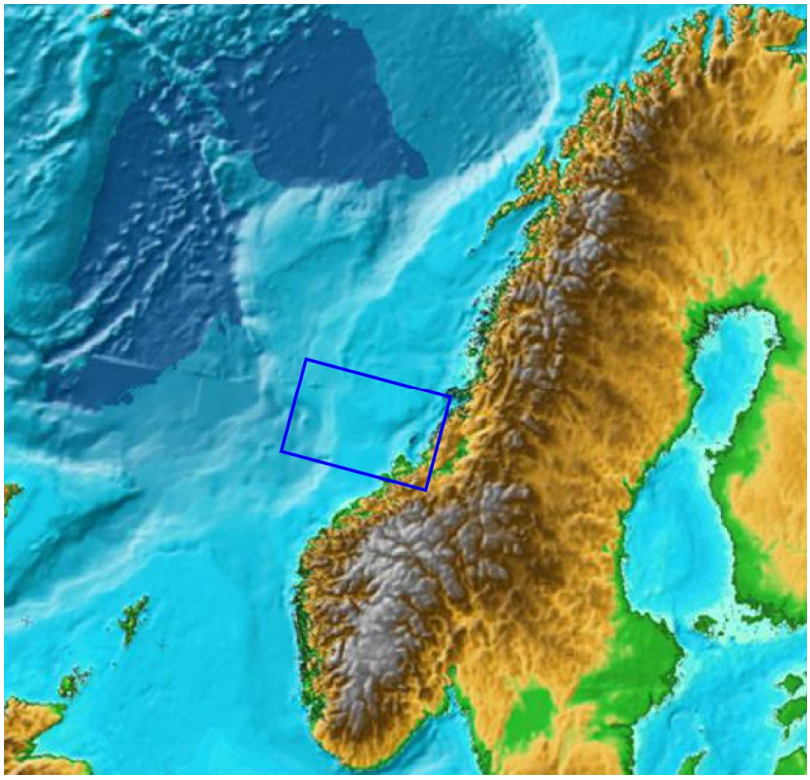

UNIVERSITY OF OSLO

FACULTY OF MATHEMATICS AND NATURAL SCIENCES

Deep basin and crustal configuration of the transition between the Møre and Vøring margins off mid-Norway

Barbara E. Klein

Master Thesis in Geosciences

Discipline: Petroleum Geology and Geophysics

Department of Geosciences

Faculty of Mathematics and Natural Sciences

UNIVERSITY OF OSLO

June 2006

PREFACE

This thesis was carried out at the Department of Geosciences, University of Oslo with Professor Jan Inge Faleide as supervisor.

I would like to address my very special thanks to Professor Jan Inge Faleide for his valuable guidance, constant support and encouragements during the data analysis work and writing process of the thesis. I am grateful for the boost he gave me during the difficult moments making me believe and carry on with the good work.

I am also very thankful to Jonas Wilson for helping me and advising me during the long days spent at the computer lab. I wouldn't have been able to achieve so much without his constructive comments and technical support, as I always seemed to have the computers against me.

I thank all my fellow students at the department for their nice company and cheerfulness at all the stages of this work. I would also like to express my gratitude to Professor Valerie Maupin who has made possible for me to come to Norway as an exchange student. This experience and first contact with the Norwegian life made me want to continue my studies in Oslo.

TGS-Nopec and WesternGeco are acknowledged for access to the regional MCS profiles.

Last but not least, thank you to my family and friends for their love and support. I wouldn't be where I am today without them.

Oslo, June 2006

Barbara E. Klein.

CONTENTS

1. Introduction

The present study focuses on the transition zone between the Møre and Vøring margins (Fig. 1.1) which are parts of a broader geological province defined as the continental margin off mid-Norway located between 62°N and 69°N. This province is described as a passive rifted margin (Blystad et al. 1995) corresponding to a seismically inactive continental transition to the deep ocean that has undergone a long period of extension and rifting. Our study area is defined as a wide NW-SE corridor extending from the southern part of the Trøndelag Platform close to mainland to the Møre Marginal High at the outer margin. The selection of this area is based on the distribution of our primary data, a set of two-ship wide-angle seismic profiles, analysed for the first time in this study. The results of this analysis are integrated with multichannel seismic and gravity data to construct geological models along five deep crustal transects across our study area on the continental margin.

The geological evolution of the continental margin off mid-Norway is linked to the tectono-magmatic history of the NE Atlantic margin. The passive rifted margin experienced a c. 350 m.y. history of intermittent extensional deformation and sediment basin formation from the the collapse of the Caledonian orogeny in Devonian time to the earliest Eocene continental break-up and opening of the Norwegian-Greenland Sea. The extensional history has been punctuated by three main rifting episodes in Late Palaeozoic-Early Mesozoic, Late Jurassic-Early Cretaceous, and Late Cretaceous to Early Eocene times; the latter leading to continental break-up. Such a long lasting tectonic activity resulted in the formation of massive Cretaceous sedimentary basins; the Møre and theVøring basins.

The analysis of the wide-angle seismic data, a set of Expanding Spread Profiles (ESP), provides us velocity-depth information through the crust at their geographical location in our study area. The selection of the key multichannel seismic (MCS) lines was guided by the location of these ESP's and the fact that they extend over the main part of the continental margin at this transition zone between the Møre and Vøring margins. The obtained velocity information from our ESP's, supplemented by Ocean Bottom Seismometer (OBS) and sonobuoys data are used in the interpretation and depth conversion of the selected MCS lines. The final depth-converted seismic sections form the basis for gravity modelling. The

integration of all results will allow us to construct deep crustal transects along the key seismic profiles. The upper crustal part of these geological models is well constrained by MCS data, whereas the geometry of deeper structures such as top basement and Moho discontinuity are determined based on ESP, OBS, and gravity data.

The main objectives of this work are to study of the deep basin configuration and crustal structures along main crustal transects in a NW-SE corridor crossing the southern and northern part of respectively the Møre and Vøring margins; to image the geology below inner flows and sills intrusions and study the geometry of the crustal thinning to discuss the modes of extension that accompanied the rifting history of the continental margin from the late Palaeozoic to early Tertiary times. We will also discuss the extent of the high velocity/density lower crustal body that is widespread and characteristic of the continent margin off mod-Norway.

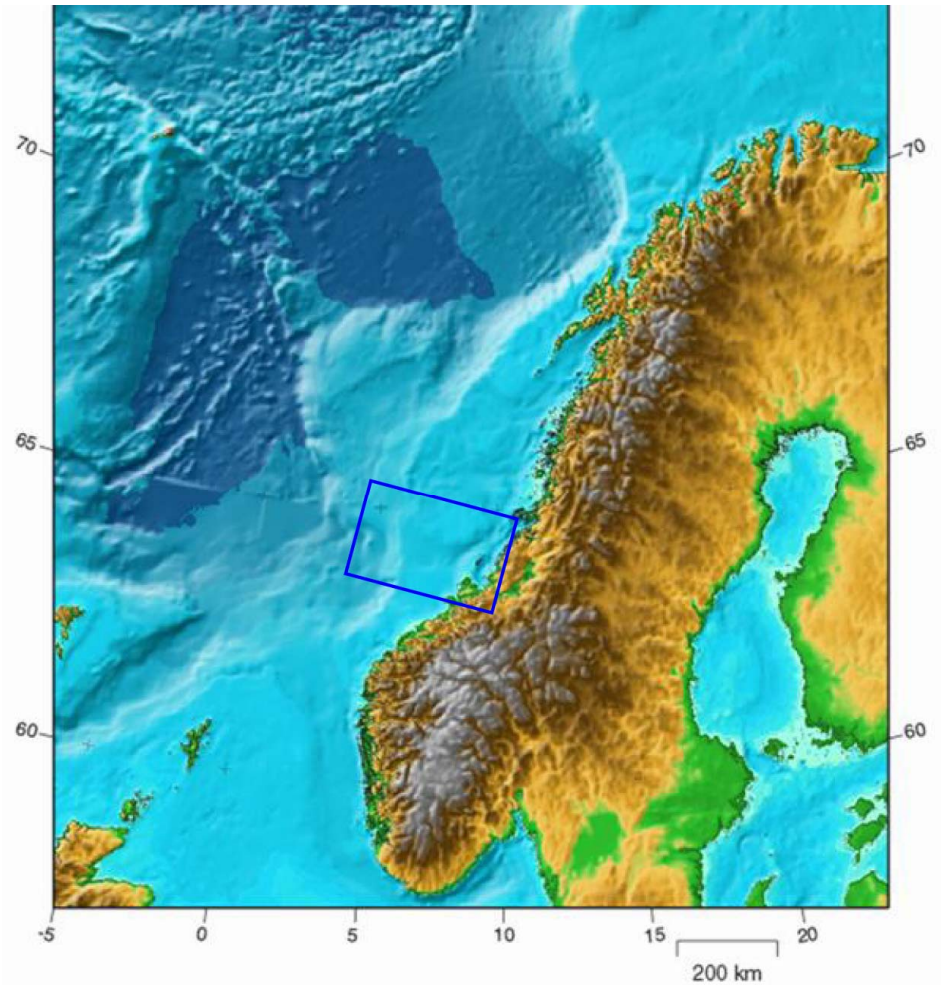

Figure 1.1. Map showing the location of the study area in relation to Norway. Bathymetry is also shown in this figure.

2. Geological framework

2.1. The continental margin off mid-Norway

The continental margin off mid-Norway is an offshore area extending from the coast of Norway westwards to oceanic crust of Cenozoic age (Fig. 2.1). The margin is located between latitude 62°N and 69°N and may be described as a rifted passive continental margin (Blystad et al., 1995). This type of geological province is by definition seismically inactive. It corresponds to the welding of adjoining oceanic and continental lithosphere as part of the same plate and finds its origins in a continental break-up process.

The continental margin is subdivided by two NW-SE lineaments into three structural provinces and has gone through a complex tectono-magmatic history of extension and rifting leading to a final continental rupture and the opening of the Norwegian-Greenland Sea. The development of this margin has also been marked by major subsidence with formation of thick sedimentary successions.

In this chapter we will first consider the regional setting of the NE Atlantic, followed by a description of the main structural elements of the continental margin off mid-Norway completed by a presentation of the stratigraphy. Finally, the geological evolution of the margin from the Late Palaeozoic to present will be summarized.

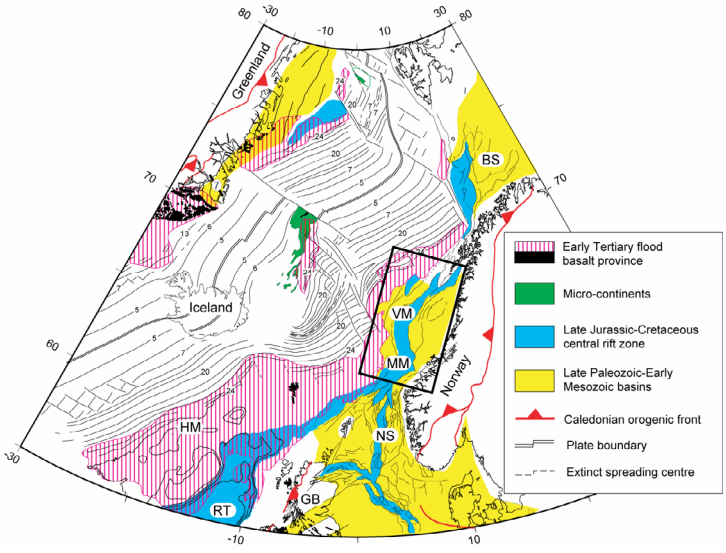

Figure 2.1. Location of the continental margin off mid-Norway in the NE Atlantic geological configuration (Skogseid et al., 2000). The area is located inside the blue rectangle. BS, SW Barents Sea; GB, Great Britain; MM, Møre margin; NS, North Sea; RT, Rockall Trough; VM, Vøring Margin; HM, Hatton-Rockall margin.

2.2. Regional NE Atlantic setting

2.2.1. Geological configuration

The continental margin off mid-Norway is part of a broader geological province defined as the NE Atlantic margin. This broader province (Fig. 2.2) is bounded to the west and the northwest by oceanic crust of Cenozoic age and extends for 3000 km from the western part of the Barents Sea to the termination of the Rockall Trough and Porcupine basin against the oceanic crust of Cretaceous age (Doré et al., 1999).

The NE Atlantic margin is defined by repeated structural patterns such as series of linked NE-SW trending Cretaceous-Cenozoic depocenters or NW-SE transfer lineaments. Because of the similarities in structures and timing of the different tectonic events over the whole or large parts of the margin, we see it as a benefit to focus first on the regional setting of the NE Atlantic margin and transfer this overall view to the study of the structure and evolution of the mid-Norwegian margin.

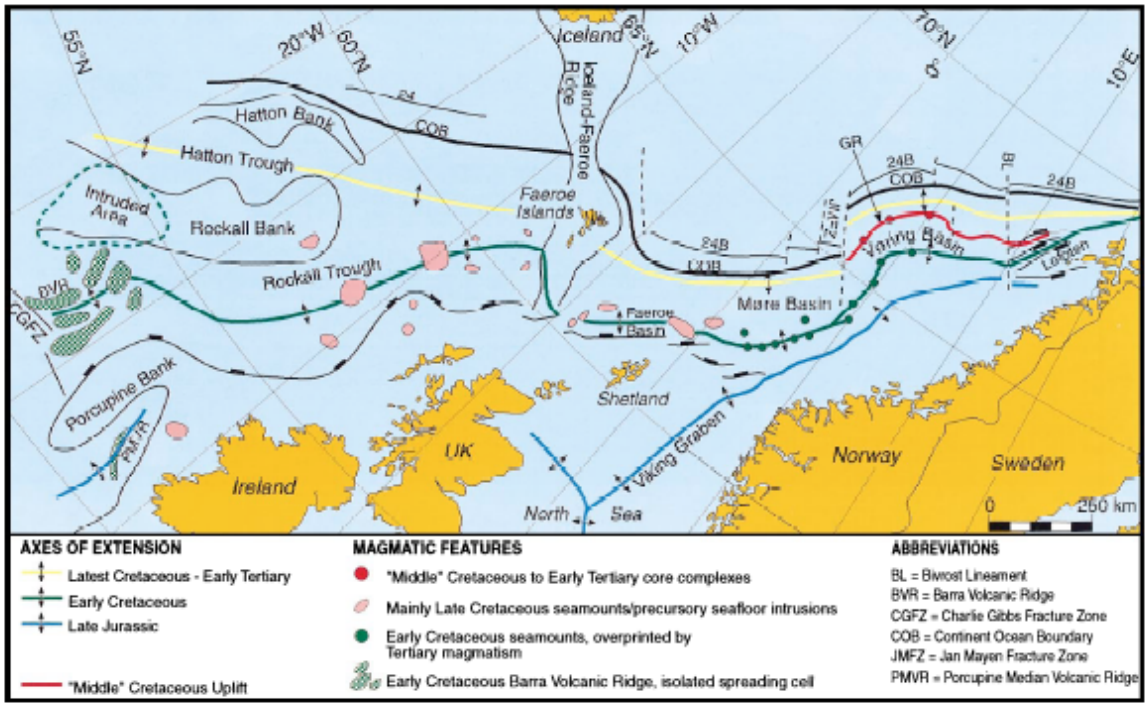

Figure 2.2. Simplified map of the NE Atlantic margin which gives also the interpreted location of rift axes between Jurassic and Early Tertiary (Lundin & Doré, 1997).

2.2.2. Extensional history

The NE Atlantic margin has gone through a c. 350 m.y. history of intermittent extensional deformation and sediment basin formation between the collapse of the Caledonian orogeny in Devonian time and the Early Eocene continental break-up. The development of the area has been punctuated by three main rifting episodes.

1) A Late Palaeozoic-Early Mesozoic phase initiated the formation of a series of large half-graben basins. Between Norway and Greenland, the NE Atlantic rift system is considered to have originated from the reactivation of the Caledonian fold belt (Doré et al., 1999). It followed the NE-oriented Caledonides into the SW Barents Sea. As to the part of the rift system located between Britain and Greenland, basin trends may indicate a reactivation of the Appalachian deformation system (Skogseid et al., 2000).

2) The second main rifting episode is the Late Jurassic-Early Cretaceous phase which is characterized by major crustal extension and subsequent thermal subsidence. This rifting phase is considered to be a precursor to the progressive continental separation in the southern part of the North Atlantic.

3) The final Maastrichtian-Paleocene rift episode, that lasted c. 20 m.y., led to continental separation and the onset of sea-floor spreading at the Paleocene-Eocene transition. The end of this extensional phase was associated with widespread igneous activity across a c. 300 km wide zone along the outer margin as evident by the presence of sill intrusions, flood basalts and magmatic underplating (Skogseid et al., 2000).

2.2.3. Lineament pattern

With the compilation of structural, stratigraphic and potential field data over the NE Atlantic margin Doré et al. (1997) discussed the lineament pattern of the area. The predominance of three major sets has been observed (Fig. 2.3).

1) The NE Atlantic margin is characterized by a dominant NE-SW left-stepping lineament set. The Møre-Trøndelag Fault Zone on the Mid-Norwegian Shelf and the Great Glen Fault, located southwards, can be used to illustrate NE-SW fault trends (Fig 2.3). It is possible to assign to this lineament set a basement origin as the NE Atlantic margin can be associated to a somewhat oblique re-opening along the Caledonian suture system and fold belt.

2) A second lineament set with a N-S trend interacts with the dominant NE-SW trends forming a repeated rhomboidal geometry along the margin (Fig. 2.3). The fact that these two lineament sets are linked suggests that they have a common origin. The E-W extension during Jurassic times may have reactivated some N-S faults inherited from basement structural grain.

3) The other major set corresponds to NW-SE transfer zones which strongly segment the Mesozoic-Cenozoic basin chain along most of the NE Atlantic margin. The Senja Fracture Zone (SFZ) on the Barents Sea margin, the Jan Mayen Lineament (JML) between the Vøring and the Møre Basins and the Anton Dohrn Transfer (ADT) in the Rockall Trough (Fig. 2.3) are the most prominent transfers and are linked to significant left-stepping basin offsets.

Doré et al. (1997) argued that the reason of the current dominance and visibility of these lineament sets is their convenient orientations that accommodated the extensional forces leading to the NE Atlantic break-up.

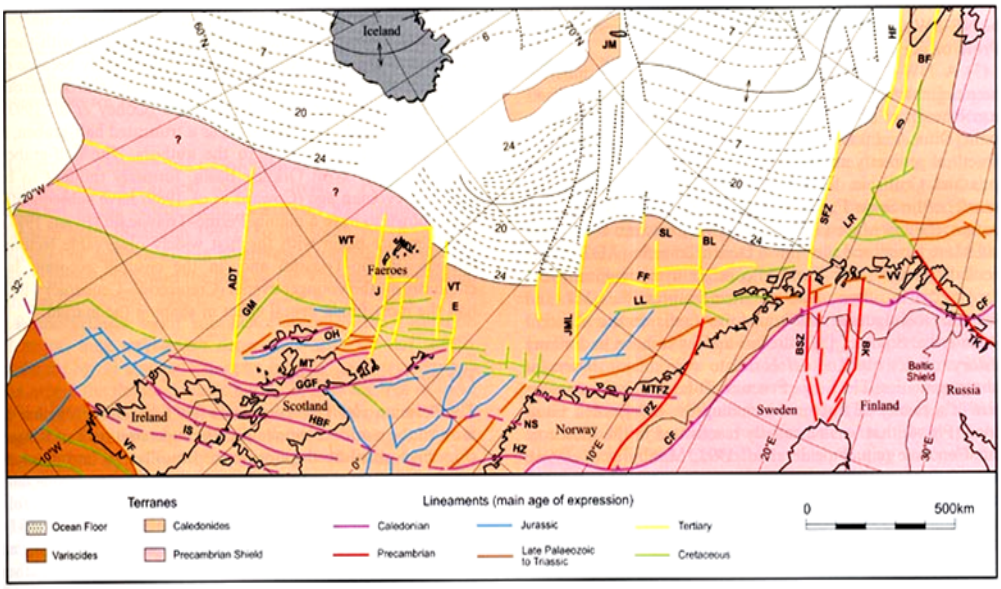

Figure 2.3. Map showing the major lineament sets. ADT, Anton Dohrn Transfer; BL, Bivrost Lineament; GGF, Great Glen Fault; JML, Jan Mayen Lineament; FF, Fles Fault Complex; MTFZ, Møre-Trøndelag Fault Zone; SFZ, Senja Fracture Zone; SL, Surt Lineament (Doré et al., 1999).

2.2.4. Rotation of the extensional vector

A fundamental event in the evolution of the NE Atlantic occurred during the Late Jurassic-Cretaceous rift episode. The Late Jurassic rift system was characterized by an E-W extension contrasting with the NW-NE extension direction that was established in Early Cretaceous times. This significant rotation of the extensional vector reflects changing stress directions through time. In plate tectonic terms, this rotation reflects the cessation of the Tethyan seafloor spreading in Early Cretaceous and north-eastwards propagation of Atlantic margin. This NW-SE extensional direction was maintained intermittently through to break-up.

2.3. Structure of the continental margin off mid-Norway

We will now focus on a part of the NE Atlantic margin located between 62°N and 69°N: the continental margin off mid-Norway. Our aim is to give a description of the main structural elements and the margin segments that compose this geological province. We present a map of the area (Fig. 2.4) to locate geographically the different elements described in this part of the paper.

2.3.1. Tectonic setting

The continental margin off mid-Norway consists of two major NE-SW trending basins of with a very thick Cretaceous basin fill: the Vøring and the Møre basins. These basins are flanked to the east by the uplifted mainland and the Trøndelag Platform and to the west by the Møre and Vøring Marginal Highs (Fig. 2.4). The highs are characterized by Eocene lavas overlying an unknown substrate. The basin area is separated from these marginal highs by the Faeroe-Shetland Escarpment to the south and the Vøring Escarpment to the north.

The continental margin is subdivided by two NW-SE trending lineaments into three structural provinces. The Bivrost Lineament, to the north, separates the wide and deep Vøring Basin from the narrow and tectonically uplifted continental margin around the Lofoten Ridge. The Jan Mayen Lineament separates the Møre Basin to the south from the Vøring Basin to the north. These two lineaments continue into the oceanic crust as respectively the Bivrost and Jan Mayen Fracture Zones.

As part of the NE Atlantic margin, the margin off mid-Norway has also gone through a long extensional history that began in Permo-Carboniferous times and experienced the three major rifting episodes indicated previously. In Carboniferous to Early Cretaceous time the extensional tectonics were related to intra-plate continental rifting. In Late Cretaceous-Tertiary times, the tectonic regime became controlled by the relative movements along plate boundaries prior and during continental break-up and the onset of seafloor spreading in the North Atlantic.

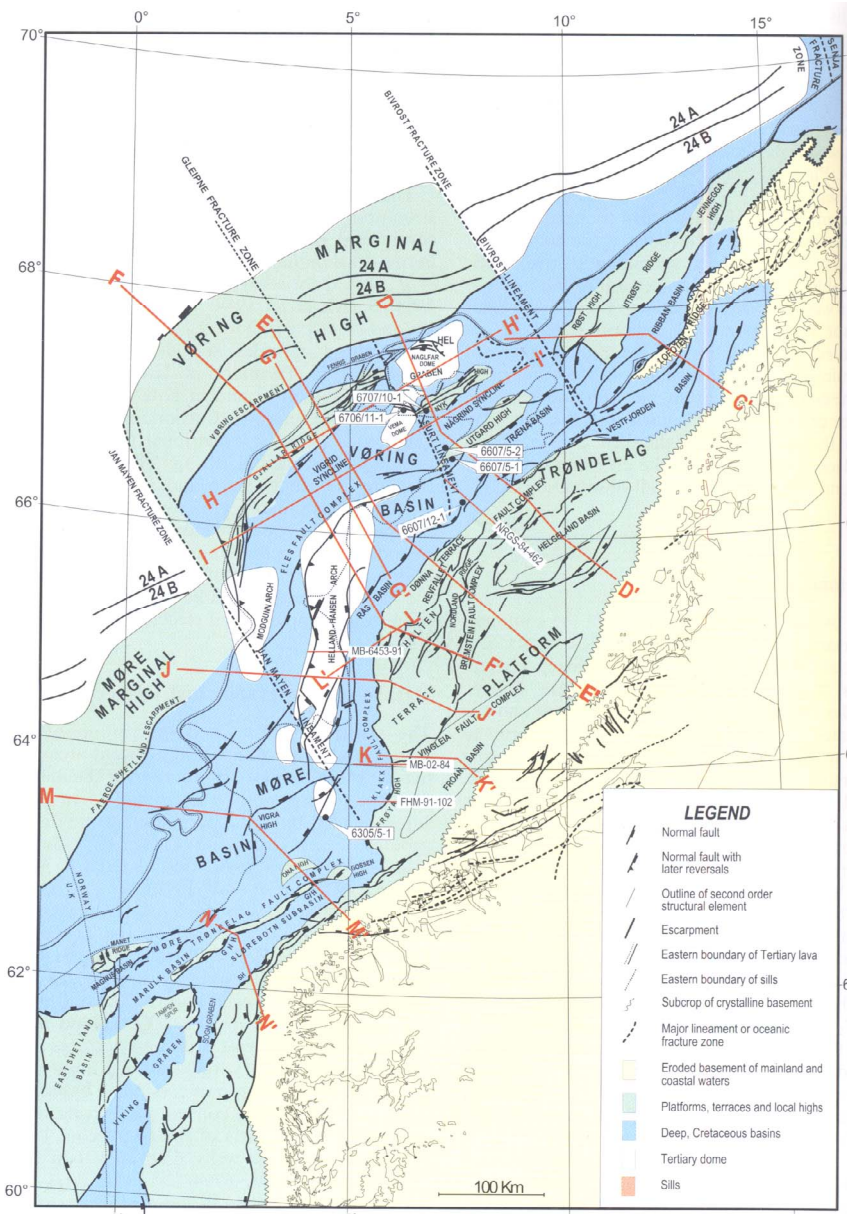

Figure 2.4. Simplified structural map presenting the main tectonic elements of the Norwegian Sea (Brekke, 2000). The AA', DD', FF', MM' and CC' regional profiles are shown in Fig. 2.5, 2.6 and 2.8.

2.3.2. Main structural elements

Before beginning the presentation of the different structural elements of the mid Norwegian Sea continental margin, we note that the nomenclature and definitions of these elements, and the regional profiles presented in Figure 2.6 and 2.8 are taken from the NPD-Bulletin No 8 by Blystad et al. (1995). We first present the Vøring and Møre basins as they are two major elements of the margin. These basins were formed as a result of the Late Jurassic-Early Cretaceous rifting episode and they both have a very thick Cretaceous sedimentary infill. On seismic sections, the axial part of the basins is generally deeper than 7 s two way travel time (Brekke, 2000). Figure 2.5 is one example of a regional profile across the Vøring basin showing the enormous Cretaceous thickness. In addition, we also show two regional profiles (Fig. 2.6) crossing the Vøring Marginal High, the Vøring Basin and the Trøndelag Platform. The location of these three profiles is indicated on Figure 2.4 by the red coloured AA', DD' and FF' segments.

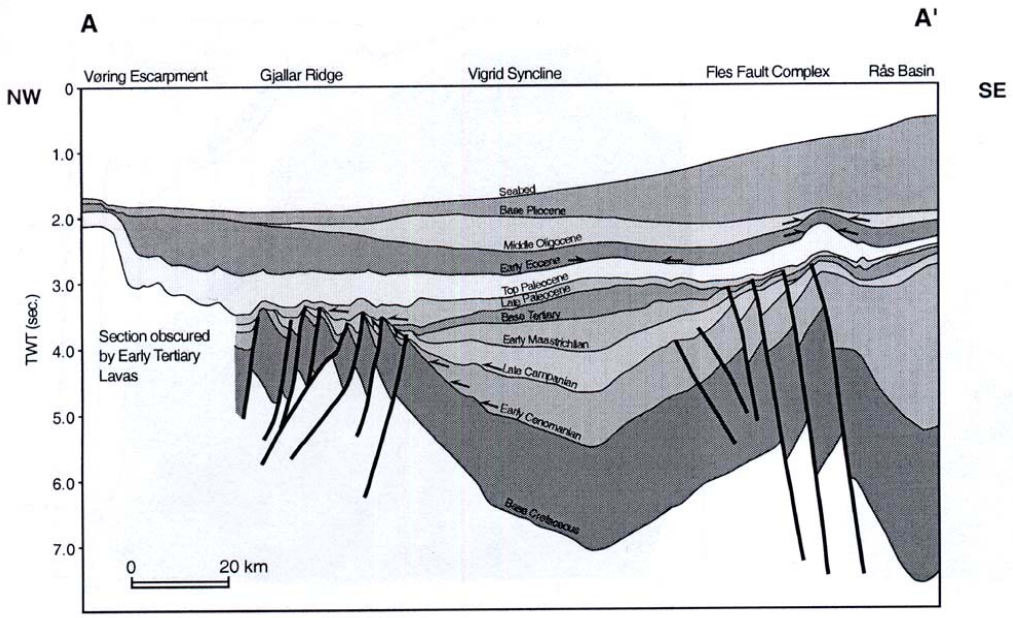

Figure 2.5. Regional profile across the Vøring Basin showing large Cretaceous thickness in two of its sub-basins (Bjørnseth et al., 1997). Location of the profile in Figure 2.4.

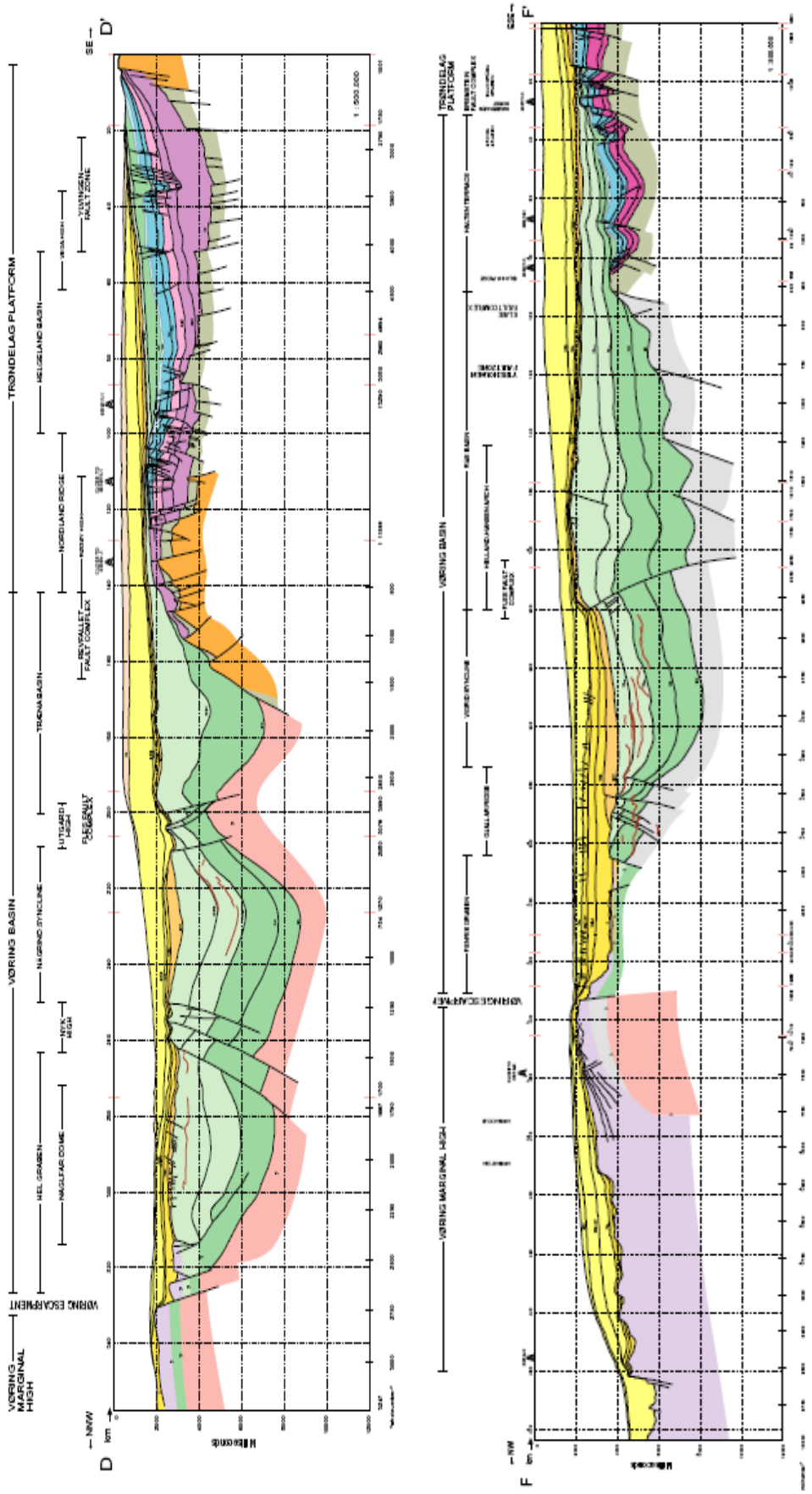

Figure 2.6. Regional profiles across the Vøring Marginal High, the Vøring Basin and the Trøndelag Platform. Color code: yellow and light orange, Tertiary sediments; light and dark green, Cretaceous; blue, Jurassic; pink and violet, Triassic and Late Permian; light violet, Eocene lavas (Blystad et al. 1995). The two profiles are located on Figure 2.4 by the red colored DD' and FF' segments

The **Vøring Basin** has experienced several extensional and compressional episodes that led to the formation of a diversity of structures and sedimentary distributions. It is composed by grabens, sub basins and structural highs and is bounded to the north and to the south by, respectively, the Bivrost and the Jan Mayen Lineaments. Parallel to these bounding NW-SE trending features, the Surt Lineament is an important tectonic divide within the basin. South of this divide, the Vøring basin is regionally folded into a central anticline, the Helland Hansen Arch, flanked by two synclines: the Vigrind Syncline to the west and the Rås Basin to the east. This anticline is located along the Fles Fault Complex of Late Jurassic-Early Cretaceous age. The fault complex bisects the basin and extends from the Bivrost to the Jan Mayen Lineaments. North of the Surt Lineament, the Vøring Basin reveals another configuration: three synclines (the Hel Graben to the west, the Någrind Syncline and the Træna Basin to the east) separated by Nyk and Utgard structural highs.

A tectonic phase in late Middle Jurassic to Late Cenomanian times is the first phase describing the development of the Vøring Basin. During this phase, major crustal extension created the basin area constituted of deep depocenters. Subsequent thermal subsidence in Cenomanian time led these depocenters to merge into a large one defined as the Vøring basin *sensu stricto*. The final Maastrichtian-Paleocene rifting phase, which was also associated with compressional tectonics, ended the development of the basin after uplift of the area and erosion. This phase was followed by Paleocene-Eocene igneous activity.

The Vøring Basin is bounded to the west by the Vøring Escarpment which separates it from the Vøring Marginal High (Fig. 2.6). This high developed during Maastrichtian-Paleocene times in response to continental extension leading to Eocene break-up and was later on further separated from the basin area by differential subsidence along the Vøring Escarpment. The marginal high and the outer part of the Vøring Basin experienced uplift and erosion during latest Paleocene and were covered by Upper Paleocene-Eocene flood basalts.

East of the Vøring Basin, we find the Trøndelag Platform which covers an area of more than 50 000 km². This structural element was initiated during the late Middle Jurassic-Early Cretaceous rifting episode but the area was also tectonically active during earlier episodes in Late Palaeozoic to Early Mesozoic times. The Trøndelag Platform has been a large stable area since the Jurassic and is covered by rather flat-lying and parallel bedded strata. The thickness

of the Cretaceous sediments of the platform is very different from the Vøring Basin: the Cretaceous strata are thin and partly absent in some parts of the platform (Fig. 2.6) which can be explained by uplift and erosion episodes in Late Cretaceous.

Considering now the structural province south of the Jan Mayen Lineament, there are three main elements to describe: the Møre Basin, the Møre Marginal High and the Møre-Trøndelag Fault Complex (Fig. 2.4). The Møre Basin, which was initiated during the late Middle Jurassic-Early Cretaceous rifting phase, has the NE-SW trend and a deep Cretaceous sedimentary infill in common with the Vøring Basin. Since this first rifting episode, the basin has been tectonically rather quiet by undergoing passive subsidence. The area did not experience observable Cretaceous and Tertiary reactivations except for minor movements along the Faeroe-Shetland Escarpment in the west and the Jan Mayen Lineament. This contrasts with the active tectonic history of the Vøring Basin (Fig. 2.7).

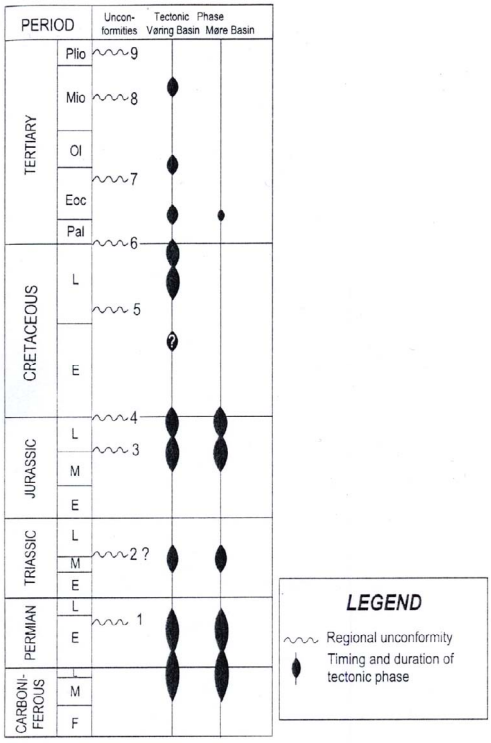

Figure 2.7. Tectonic history of the Norwegian Sea Continental Margin showing the difference in activity between the Vøring and Møre Basins and also the regional unconformities found in the stratigraphy of the area (Brekke et al., 1999).

To the west, the Møre Marginal High is separated from the Møre Basin by the Faeroe-Shetland Escarpment, which mainly developed as a volcanic escarpment associated with the continental break-up and formation of the Norwegian Sea. The marginal high, bounded to the

west by the transition to “normal” oceanic crust, developed as part of the volcanic passive margin during early Tertiary rifting, break-up and initial seafloor spreading. As for the Vøring Basin, the outer parts of the Møre Basin and the marginal high experienced uplift and magmatic activity.

The third main element of the southern province is the Møre-Trøndelag Fault Complex (Fig. 2.4) which represents a fundamental zone of basement weakness as it was initiated in Precambrian times and experienced multiple reactivations during the following tectonic history. The most important tectonic activity along the complex took place in Permo-Triassic and Late Jurassic-Cretaceous times.

North to the Bivrost Lineament, the continental margin is narrow and has a horst and graben geometry formed during the late Middle Jurassic-Early Cretaceous rifting phase. One of the main elements of this northern province is the 350 km long NE-SW trending Lofoten Ridge. This ridge is a basement horst symmetrically separating two Cretaceous half-grabens: the Vestfjorden Basin in the east and Ribban Basin in the west. These two basins were initiated in response to the crustal stretching and subsidence that took place during the rifting phase named above. Another elevated area of the province is the Utrøst Ridge located westwards from the Ribban Basin. This element is mainly related to Late Cretaceous and Tertiary plate tectonism linked to the opening of the Norwegian Sea. The whole northern province has been uplifted and experienced deep erosion in latest Cretaceous to Early Tertiary times. This is the reason why it is, for example, difficult to give details about the Tertiary history of the Lofoten Ridge or why the Ribban Basin is mainly filled with Early Cretaceous sediments. The development of the main structural elements of this area is closely related.

Two regional profiles, crossing the main structural elements in the southern part of the continental margin and north to the Bivrost Lineament respectively, are shown in Figure 2.8. Profile MM’ illustrates the structure of the Møre Marginal High, the Møre Basin and the Møre-Trøndelag Fault Complex. Profile CC’ illustrates the horst and graben geometry of the narrow northern structural province.

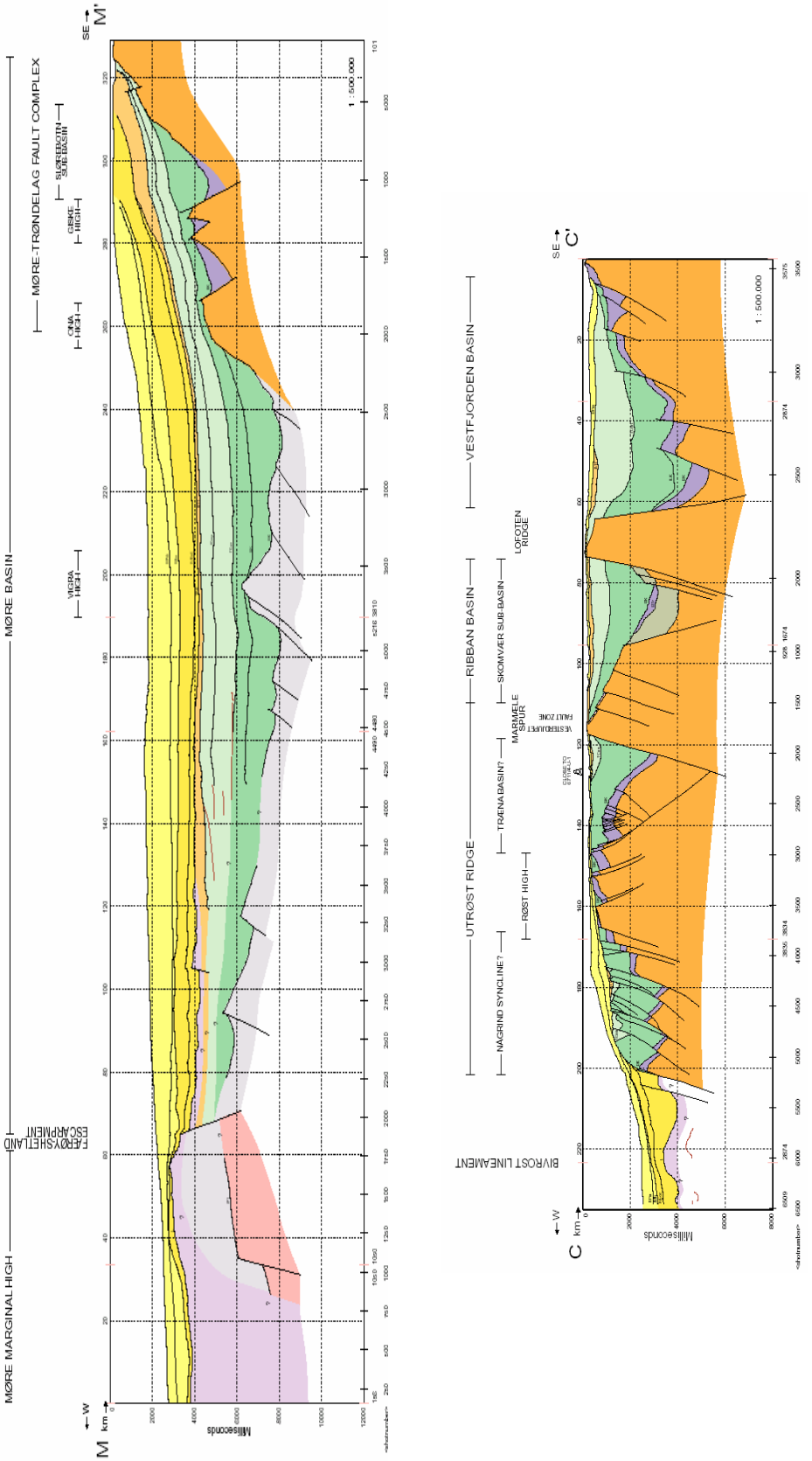

Figure 2.8. Regional profiles across the main structural elements of the southern part (profile MM') and the northern part (profile CC') of the continental margin off mid-Norway. **Color code**: yellow, Tertiary sediments; green, Cretaceous; light violet, Eocene lavas; violet, Triassic; dark orange, Permian and basement rocks (Blystad et al. 1995). The two profiles are located on **figure 2.4** by the red colored MM' and CC' segments.

2.3.3. Main lineaments

Two of the main lineaments crossing the continental margin are the Jan Mayen and the Bivrost lineaments bounding the Vøring Basin to the south and the north respectively. These NW-SE oriented bounding lineaments could possibly be linked to the oceanic Jan Mayen and Bivrost Fracture Zones. They are deep and probably reflect an old structural grain in the crystalline basement. These lineaments had a major control on the post-Caledonian development of the continental margin as they divide the margin into three differentiated structural provinces.

The Jan Mayen lineament is defined by a sinistral shift of the basin axes and basin flanks in contrast with the Bivrost Lineament defined by a dextral shift. The Jan Mayen Lineament seems to have played an important role through Late Cretaceous and Tertiary times as a tectonic barrier between the tectonically active Vøring Basin and the quiet Møre Basin (Brekke, 2000). A third important lineament defined as the Surt Lineament crosses the Vøring Basin and is parallel to the others.

2.4. Stratigraphy

The stratigraphy of the sediments building the continental margin off mid-Norway is linked to the tectonic evolution of a broader area : the northern North Atlantic. From Carboniferous to Jurassic times, the area between Norway and Greenland was a central zone of continental rifting and intermittent shallow seaways separating a northern ocean (the Boreal Ocean) and a southern ocean (the Proto-Tethys and Tethys). Experiencing a long extensional history with various rifting episodes, the central zone became a permanent seaway between the two oceans (Brekke et al. 2001). From the Devonian to continental break-up in Eocene time, a progressive northward continental drift occurred leading to climate changes over the area: the initial equatorial climate evolved to successively temperate and arctic climates. These paleogeographic developments led to changes in the nature of the deposited sediments.

The sedimentary stratigraphy is known from exploration wells. As the margin is composed by very deep depocenters, it is difficult to have information about pre-Triassic rocks for these structural elements. Most of the wells on the continental margin have been drilled on the

Trøndelag Platform and the Halten Terrace to the east of the Vøring Basin leading to a good knowledge of the post-Lower Triassic stratigraphy of these structures. This knowledge has been used to make extrapolations about pre-Cenomanian sequences of the Vøring Basin that are located too deep to be reached by exploration wells.

From exploration wells and seismic surveys, nine regional unconformities have been identified in the stratigraphy of the area (Fig. 2.7; Brekke, 2000). Details on these unconformities will be given later in parallel with the presentation of the sedimentary environments of the continental margin using the publication of Brekke et al. (2001).

Continental alluvial, fluvial and lacustrine environments prevailed in the region during Carboniferous times. Red fluvial sandstones and siltstones, yellow fluvial sandstones, grey siltstones, thin coal seams and lacustrine black shales are typical Carboniferous sediments on the Norwegian shelf and in East Greenland. The Early Permian is characterized by the continuation of the alluvial and fluvial facies of the Carboniferous over the present Norwegian Shelf. In middle to Late Permian times, episodes of uplift and erosion caused an erosional hiatus representing the first unconformity in the stratigraphy. An important change in sedimentary environments occurred in Late Permian times: transgression in the Norwegian Sea region, accompanied by an arid to temperate climatic change, created open marine conditions favourable to the formation of shallow marine carbonate deposits. Deposits of continental clastics were also recorded in the area.

The Triassic period is defined as a period of thermal relaxation after the rifting episode of Late Permian-Early Triassic age. The Early Triassic corresponds to a period of marine deposits. The deposits of Middle to Late Triassic age comprise continental clastics, molasses and deltaic sands interbedded with marine deposits originating from marine incursions cycles. A second regional unconformity in the stratigraphy is placed at the base of the Upper Triassic but the existence of this unconformity is questioned. The stratigraphy shows a relative sea-level rise in Early to Middle Jurassic that caused the Norwegian Sea region to be dominated by shallow clastic shelf environments.

The dominant lithology of the Lower Jurassic is an alternation of sandstones and shale/siltstone units with sandstones. This lithology is characteristic of shallow marine to deltaic environments. The Middle Jurassic units are composed of three lithologies: a lower

sandstone with numerous shaly interbeds, a middle mudstone and an upper massive fine to coarse-grained sandstone. The depositional environments are similar to that of the Early Jurassic. An erosional hiatus is visible in Bathonian times and corresponds to the third regional unconformity of the studied region. This hiatus is explained by a phase of uplift and erosion during Middle Jurassic. A major rifting phase started at the end of Middle Jurassic times accompanied by a major sea-level rise, which finally drowned the area between East Greenland and Norway. This drowning created open marine conditions and the stratigraphy of Late Middle and Late Jurassic times consists of an accumulation of marine shales and of large volumes of black shales with scattered sandstone stringers.

The base of the Cretaceous sedimentary sequence is defined across the whole area by an erosional unconformity on top of marine shales. During Early Cretaceous, subsidence and renewed sea-level rise led to the deposition of open marine mudstones and shales in the deep basin areas. In platform areas and structural highs the sea-level rise led to widespread accumulation of shales and marls. The Late Cretaceous was a period of accelerated basin subsidence accompanied by the uplift of the basin flanks and by the emergence of basin-bounding platforms. The unconformity of Turonian-Coniacian age is linked to the deep erosion of the flank uplifts and the platform areas. In basin areas the marine sediments were overlain by coarse-grained turbidites, which originated from the erosion of the western and northern emergent platform areas.

The sedimentary environments of the Tertiary reflect the tectonic and climatic evolution of the region. The base of the Tertiary corresponds to an unconformity linked to latest Cretaceous uplift and later erosion. An important uplift of the axial part of the Norwegian-Greenland Sea area occurred before continental break-up in Eocene times. This phenomenon led the region to be dominated by marine clastic deposits evolving to marine claystones in Eocene and Oligocene times. Two phases of compression during Oligocene-Miocene times coincide with the regional hiati of Late Eocene-Early Oligocene and Middle Miocene age. These hiati correspond to two of Tertiary stratigraphic unconformities and are associated with submarine erosion. The Neogene is characterized by periods of glaciations due to the deterioration of the climate. These glaciations led to a deep erosion of the surrounding mainland areas and caused huge inputs of progading clastic sediments into the Norwegian-Greenland Sea. The youngest unconformity in the stratigraphy is dated from Pliocene times and is linked to glacial erosion.

2.5. Geological evolution from Late Palaeozoic to present

The continental margin off mid-Norway has been very active tectonically from the Late Silurian to Early Eocene time. The history of the margin, following the collapse of the Caledonian Orogeny in the Late Devonian, can be divided into two epochs. The first one corresponds to an exceptionally long period of extensional deformation and basin formation characterized by three main rifting episodes culminating with a break-up and continental separation at the Paleocene-Eocene transition. The second epoch corresponds to the phase of seafloor spreading between Eurasia and Greenland from Early Eocene to present (Blystad et al., 1995).

2.5.1. Late Palaeozoic to Early Eocene

Extensional movements began after the collapse of the Caledonian Orogeny and led to the development of molasse basins in Norway and East Greenland in Late Devonian and Carboniferous times. However the sediment packages associated with these movements are poorly resolved seismically. This is mainly due to the overprint of these Palaeozoic tectonic events by younger ones (Doré et al., 1999). A first main rifting event in Late Carboniferous-Early Permian time corresponds to an active tectonic period over large parts of the proto-North Atlantic area. Basement-involved normal block faulting of late Early Permian age may have created the horst and half-graben configuration mapped beneath the Trøndelag Platform and the Halten Terrace. The Permian-Triassic time is characterized by the formation of the Pangea supercontinent and the beginning of intra-plate continental rifting between Norway and Greenland. This period corresponds to a basin development phase: the Froan and Vestfjorden basins are structural elements of the Norwegian continental margin that were formed during Permian-Triassic time. Other basement-involved block faulting occurred in Middle to Late Triassic time leading to the further development of the basinal area east of the Nordland Ridge and the Frøya High. The Triassic also saw the formation of evaporite intervals, which acted as important detachment levels for the later rifting episodes and the Triassic-Early Jurassic episode of growth faulting. This faulting episode ceased in late Early Jurassic and was followed by a phase of quiescence that lasted until late Middle Jurassic time. The Bathonian time is defined as the transition between this quiet tectonic period and a strong

late Middle Jurassic-Early Cretaceous rifting episode that played a very important role in the formation of many structures composing the Norwegian continental margin. This rifting episode is characterized by a significant stretching and thinning of the crust beneath the continental margin. A subdivision, between deep basins to the west and the platform area to the east, was probably instituted in the early stage of this tectonic episode (Brekke, 2000).

The Halten and Dønna terraces, at the western flank of the Trøndelag Platform, were tectonically very active in Bathonian to Kimmeridgian time. This period is also characterized by the pronounced flexuring and faulting along the eastern flanks of the Møre and Traena Basins. The Late Jurassic time is defined as a period of uplift and deep erosion of the western edges of the Halten Terrace, the Frøya High and the Nordland Ridge. These eroded highs were parts of the Late Jurassic peneplain of the Trøndelag Platform. Large-scale faulting and flexuring in the platform area initiated the development of the terraces as individual structural elements.

The late Middle Jurassic-Late Cenomanian was also a very important period for the development of the Vøring Basin area. Major crustal stretching and thinning, faulting and subsequent thermal subsidence led to the creation of a deep basin area with depocenters such as the Rås and the Træna basins and a shallower broader basin including the present Vigrid and Någrind synclines, Hel Graben and Nyk High. These two areas were separated by the Fles Fault Complex defined as important normal faults that were initiated during the second main rifting episode. In the narrow Lofoten-Vestfjorden area, north of the Bivrost Lineament, the general horst and graben geometry was initiated by the late Middle Jurassic-Early Cretaceous rifting episode. In the province south of the Jan Mayen Lineament, the deepest parts of the Møre Basin were elevated and erosion took place during Mid-Jurassic time. The rifting episode represents the main tectonic event of the area. Following major crustal stretching and thinning, thermal subsidence in Early Cretaceous time transformed the Møre Basin into a deep basin area with an overall geometry of symmetrical down-flexed flanks.

Some renewed tectonic activity, which started at the transition between Cenomanian and Turonian times, initiated the relative uplift of the Gjallar Ridge forming the western flank of the Vøring Basin. This tectonic activity and the associated subsidence, which reached its maximum in Campanian time, also led to the merging of the Halten and Dønna Terraces and different depocenters of Early Cretaceous age composing the Vøring Basin area. The Vøring

Basin *sensu stricto* is defined at the post-Cenomanian Cretaceous levels. The Campanian time corresponds to a period of maximum subsidence rate in the Vøring Basin but also coincides with an important faulting activity on the Nyk High and possibly the Gjallar Ridge and also along the Nordland Ridge, the Halten Terrace and the Fles Fault Complex. In the Lofoten-Vestfjorden area, the Mid-Cretaceous time is defined as a period of graben rotation and subsidence followed in latest Cretaceous and Early Tertiary by the uplift and deep erosion of the whole province.

The Møre Basin, in contrast to the Vøring Basin, seems to have been tectonically quiet in the period following the late Mid-Jurassic-Early Cretaceous rifting episode. After passive subsidence in Cretaceous time, the basin did not experience observable tectonic activity in Late Cretaceous and seemed to have been affected by only minor activity in Tertiary time. This lack of activity implies that the Jan Mayen Lineament must have acted as a regional transfer zone during the Late Cretaceous (Brekke, 2000). The Tertiary activity was mainly related to reactivations of the Jan Mayen Lineament and minor faulting along the Færoe-Shetland Escarpment.

In the Vøring Basin, the faulting activity in Campanian time was followed by a compressional event which led to a regional folding. This folding is considered to be of latest Campanian-Maastrichtian age according to certain clues in the sedimentary sequences. This phase of compression and the resulting geometry of the Vøring Basin suggest a reactivation along the Fles Fault Complex (Brekke, 2000). The geometry of the basin also suggests the active role of the Surt Lineament as a tectonic hinge zone in Late Cretaceous time. This latest Cretaceous compressional event may have also led to a shift in basin configuration with the inversion of the Rås Basin and the tightening of the Vigrid and Någrind Synclines (Bjørnseth et al., 1997). The development of the Någrind Syncline, north of the Surt Lineament, was closely linked with the Hel Graben, Nyk High and Utgard High. The present configuration of the syncline was mainly acquired during Late Cretaceous to Early Tertiary times. During the same time, the Hel Graben, which developed as the northern part of the Vigrind Syncline in Early Cretaceous, became an individual graben structure. The main development phase of the two highs is also dated to that age. The tectonics of this period involved both normal and inverse reactivations along the flanking of the Fles Fault Complex (Blystad et al., 1995).

The final intra-continental rifting episode between Eurasia and Greenland probably lasted from Maastrichitian to the Paleocene-Eocene transition, which corresponds to the time of continental break-up (Blystad et al., 1995). The rifting phase, that involved central rift uplift due to increased heat flow, strongly affected the western parts of the margin and the areas north of the Jan Mayen Lineament. This caused the erosion of the Møre and Vøring Marginal Highs and other ridges in the Vøring Basin and Lofoten-Vestfjorden area. This extensional phase was also associated with widespread intrusive activity along the rifting axis and the western parts of the Vøring and Møre basins. The Maastrichtian-Paleocene rifting episode also initiated the formation of the Vøring Escarpment separating the Vøring Marginal High from the Vøring Basin and the formation of the Færoe-Shetland Escarpment separating the Møre Marginal High from the Møre Basin. The continental break-up between Eurasia and Greenland occurred at the Paleocene-Eocene transition and was associated with enormous volumes of tholeiitic flood basalts flowing across the western eroded platforms of the margin.

2.5.2. Early Eocene to present

Continental break-up and onset of sea floor spreading marked the beginning of the second epoch of the tectonic history of the continental margin off mid-Norway. This period, which extends from earliest Eocene to present, corresponds to a phase of seafloor spreading and of different tectonic events that led to the present structural configuration of the margin.

After continental break-up, the margin experienced two main phases of flexuring in Late Eocene-Early Oligocene and Late Miocene times. These phases correspond to the reactivations in a reverse sense of the major tectonic lineaments: the Jan Mayen, Bivrost and Surt Lineaments and the Fles Fault Complex. The compressional regime and the associated reactivations might be the origin of the creation of major anticlines and domes in the area such as the Helland-Hansen Arch, the Vema Dome located south of the Hel Graben or the Nagflar Dome which was formed by inversion of the Hel Graben. This tectonic activity also gave rise to further elevation of the Nordland Ridge and, the Nyk and Utgard highs. The Lofoten-Vestfjorden area probably also experienced phases of renewed uplift and erosion during Tertiary times with the inversion of the Ribban Basin and the uplift of the Utrøst Ridge, but details are not known because of the erosion of the sedimentary sequences of Tertiary age.

A Lower to Middle Miocene hiatus is recorded all over the continental margin implying a period of erosion or non-deposition before the major Late Miocene folding episode. This could be explained by the uplift of the whole margin during a period of 7 m.y. in Early to Mid-Miocene time.

The last important tectonic period that started in latest Miocene to Early Pliocene times is characterized by strong differential tilting and asymmetric uplift of mainland Norway (Blystad et al., 1995). The uplift initiated strong erosion which led to the deposition of large important sediment volumes on the adjacent shelf. These events created an up to 1500 m thick Pliocene-Pleistocene sedimentary cover. During the Pliocene-Pleistocene period, uplift and erosion phases occurred in the area. Rapid erosion took place as a result of multiple glaciations, while net uplift was linked to interglacial periods as a result of isostatic response to lithosphere unloading.

3. Data

In this chapter, we present the geological and geophysical data that are used in this master thesis for the study of the deep basin and crustal configuration in the transition zone between the Vøring and Møre margins. The data include two types of marine wide-angle seismic data: expanded spread profiles (ESP) and ocean bottom seismometer (OBS) transects. In addition, we have multichannel seismic data in the form of five profiles selected for their location in relation to the ESP profiles. Figure 3.1 shows the location of these data sets. We also use gravity and bathymetry data from a satellite based gravity anomaly field and from a world wide topography data base respectively.

A number of maps presented in the following chapters have been made with the help of the Generic Mapping Tools (GMT) software (Wessel and Smith, 1998). The maps are plotted at a 1:3000000 scale, using the UTM (Universal Transverse Mercator) projection with the UTM zone 32 centered on the 9ºN meridian.

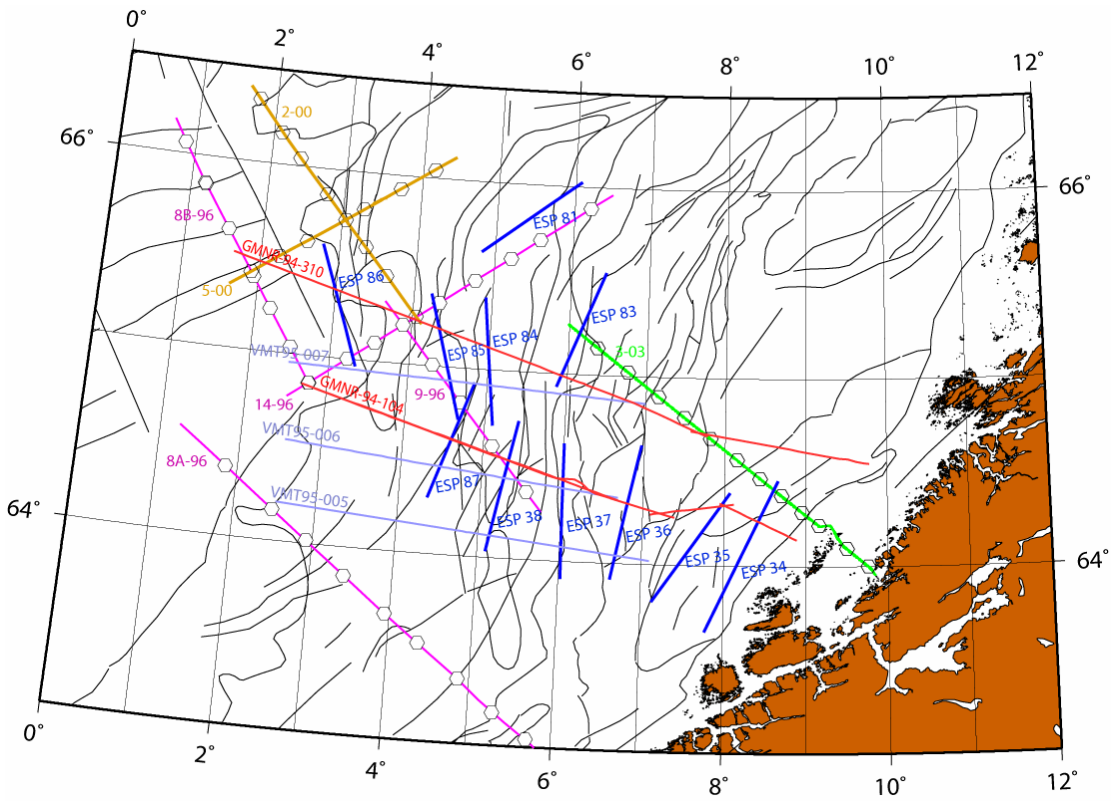

Figure 3.1. Map displaying the geographical location of the different sets of data used in this work. Colour code: ESP profiles (dark blue), OBS transects (pink, light brown and green), MCS lines (red and light blue).

3.1. ESP data

The ESP profiles used in this study correspond to a new set of data that has never been analysed before. We have had access to 11 wide-angle seismic profiles that were acquired by commercial seismic vessels during the NORMAR (joint Uio-ELF project) surveys of 1983 and 1984. The shooting vessel was equipped with a 6000 cu.inch airgun array and the recording vessel towed a 2.4 km long streamer with 96 hydrophone groups. The ESP profiles are located in a wide corridor crossing the southern part of the Trøndelag Platform and the Vøring Basin and have an orientation following the geological structural trend in this area (Fig. 3.1). The length of the ESP's varies from 50 to 100 km offset. The data are both presented in the x-t and tau-p domains. The analysis of this data set is presented in chapter 4.

3.2. OBS data

The other set of wide-angle seismic data comes from ocean bottom seismometer measurements. The relevant OBS transects in our area (Fig. 3.1); 8A-96, 8B-96, 9-96, 14-96, 2-00, 5-00 and 3-03; were acquired by the University of Bergen with the vessel Håkon Mosby. These profiles are part of regional surveys performed in the southern Vøring Margin and northern Møre Margin. The OBS transects provide estimated P-wave velocities from the seafloor to the Moho. The final velocity models were presented in different publications (Raum, 2000; Raum et al., 2002 and 2006). The final result for profile 3-03 has not been published yet (Raum et al., in prep). The 1996 and 2000 OBS transects are shown in chapter 5. The velocity information obtained from these transects helps us to depth convert the seismic data used in this study and constrain the deep structural boundaries along our key profiles.

3.3. Seismic data

The multichannel seismic data include five key profiles from two different 2-D surveys. We have two seismic profiles from the survey GMNR-94, indicated in red on Figure 3.1, shot in 1994 over the Mid-Norway region by WesternGECO. The three other lines, indicated in light blue on Figure 3.1, are a part of the VMT95 survey shot in 1995 over the Møre/Vøring

margins by TGS-NOPEC. The lengths of the VMT95 profiles vary from 200 to 225 km and the GMNR-94 lines extend over nearly 315 and 400 km. The five profiles were shot respectively down to 12 and 14 s two way traveltime (twt). They all have a NW-SE orientation and are located at the transition between the Møre and Vøring margins extending from the Faeroe-Shetland Escarpment to the Froan Basin to the east. The interpretation of these MCS data is presented in chapter 5.

3.4. Gravity data

The data, used for the gravity modelling in chapter 6, is composed by satellite based potential field data (Andresen and Knudsen, 1998) from the Norwegian Geological Survey (NGU) enhanced with ship track and land station measurements (Skilbrei et al., 2000). The data used in the marine domain corresponds to free-air gravity anomaly data. The GMT software was used to create the gravity map over our study area presented in chapter 6 and to extract the gravity anomaly values along the five MCS profiles.

3.5. Bathymetry data

The bathymetry data presented in this study derive from the world-wide topography data base described by Smith and Sandwell (1997). In the ESP data analysis (chapter 4), we used the bathymetry map to verify that the water depth has been correctly calculated at the ESP's common midpoint location. We also display a bathymetry map in the gravity modelling chapter (chapter 6) to compare the data to the free-air gravity field and show that some important changes in water depth can affect the extracted gravity data along our key seismic profiles and generate misfits between the observed and calculated gravity anomalies.

All these data are analysed and integrated in the study of the deep basin configuration and crustal structures along key profiles at the transition between the Vøring and the Møre margins.

4. ESP data analysis

In marine seismology, wide-angle data have proven to be useful in crustal and lithospheric studies; particularly in continental margin and ocean basin environments. Wide-angle profiling commonly provides highly-detailed velocity-depth information for a localized region of the crust. The obtained velocities may then be used to guide velocity analysis during multichannel seismic (MCS) processing. There are several methods for the acquisition of wide-angle data. We will here focus on the one defined as Expanded Spread Profiling (ESP). This method is characterized as a two-vessels experiment that make it possible to acquire reflected and refracted arrivals from sub-surface interfaces out to large offsets of 100km. Our data set for this study is composed by eleven expanded spread profiles that are located in a NW-SE corridor running across the Trøndelag Platform and the SW Vøring Basin (Fig. 4.1). Both of these structural elements are part of the continental margin off mid-Norway. In the following work, we will give a more detailed description of the ESP method and of our ESP data. We will explain the standard procedures for the reduction and interpretation of these wide-angle data, and present the results in form of velocity-depth diagrams. We will also see how the obtained velocity functions can be integrated with deep MCS profiles (Fig, 4.1) in our crustal study of part of the continental margin off mid-Norway.

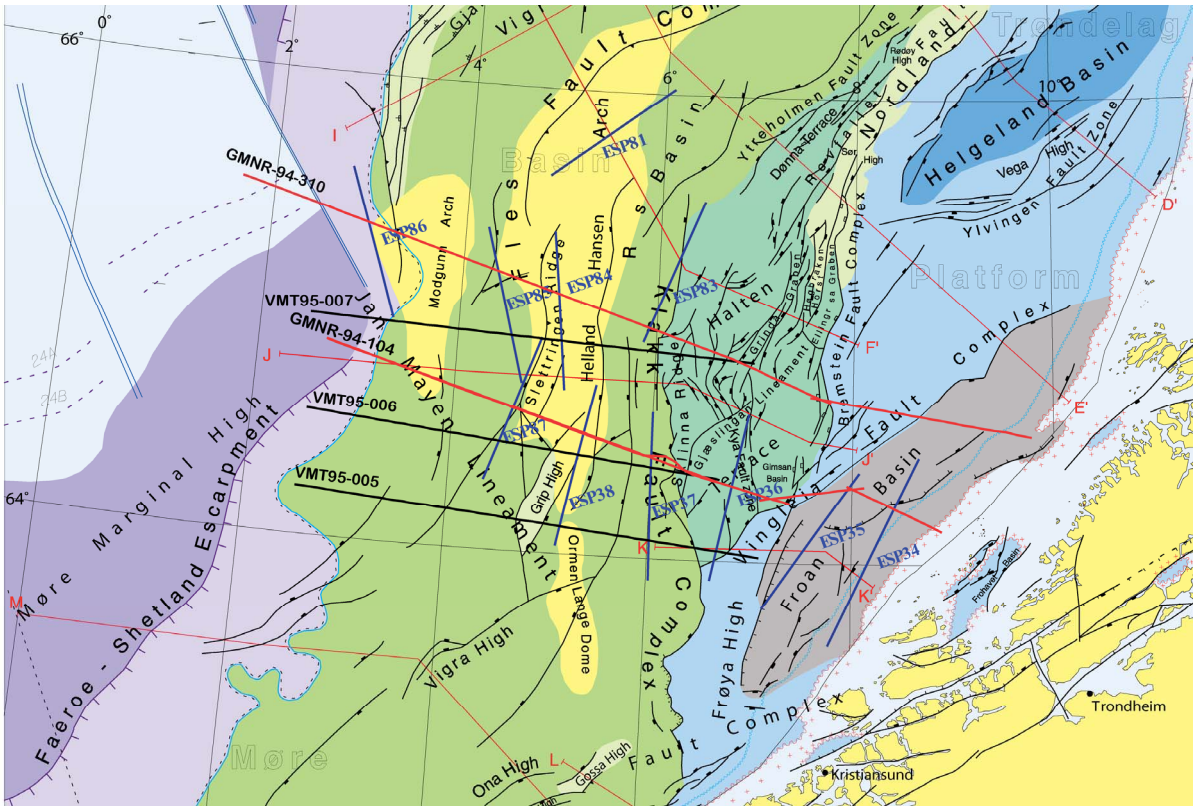

Figure 4.1. Map showing the structural elements of our study area, the location of our ESP profiles and our set of multichannel seismic lines (interpreted in chapter 5) (modified from Blystad et al. 1995). The map also shows the location of some of the profiles (thin red lines) published in the same paper.

4.1. The Expanding Spread Profiling method

The ESP acquisition technique has been developed for the detailed study of the deep structure of the crust and the upper mantle under continental margins and oceanic areas. The processing and analyzing of the acquired data allow us to produce generalized models of subsurface structure with good velocity information. The ESP method is defined as a common midpoint geometry experiment that acquires wide-angle reflection and refraction data from a common midpoint. The shooting of expanded spread profiles requires the use of two vessels that can both be equipped with an air gun array and a long multichannel hydrophone streamer. The vessels can be used in a variety of configurations to record the wide-angle data. We can have the two ships steaming apart from a common midpoint, with both ships firing their sources and recording with its multichannel streamers, producing two profiles. Another way of acquisition initially positions the two ships at the end points of the profile. These points are

usually 80 to 100 km apart. Both ships steam to the opposite end points at a constant speed of about 5 knots, crossing the midpoint at a separation of about 1km. This acquisition configuration also allows us to obtain two ESP's in one experiment, one at closing ranges and another at expanding ranges.

In the ESP experiment, the fact that each ship can be equipped with a source and a receiver makes it possible, in addition to the wide-angle data, to record near-normal incidence reflections, such as the data acquired during a conventional CMP reflection survey (Fig 4.2). The combination of these reflection and refraction data allows the derivation of a highly detailed velocity-depth structure for a localized region of the crust.

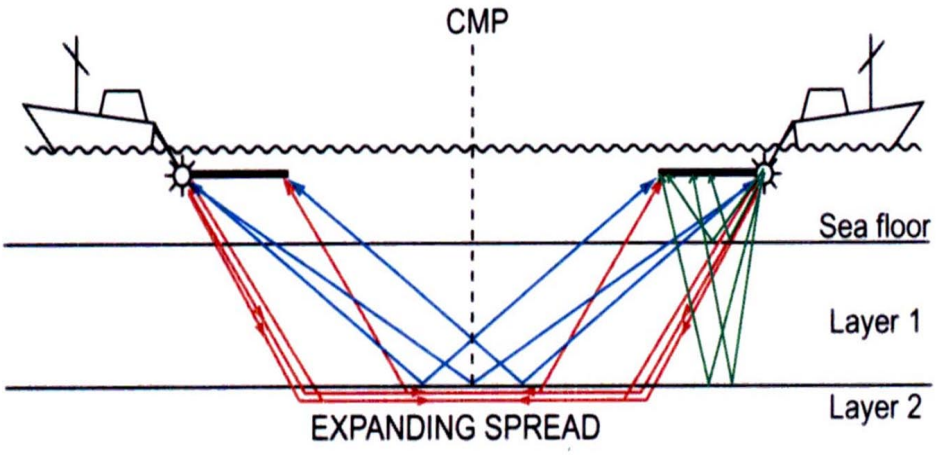

Figure 4.2. Expanding Spread Profile geometry with both vessels deploying sound sources and multichannel streamers. Consequently, both ships will record a wide-angle Common Mid-Point (CMP) profile and a standard MCS profile (Stoffa et al., 1983). In this experiment the two ships depart from a common midpoint (CMP) and steam to source-receiver offsets of 100 km or greater. Refracted and reflected wide-angle wave paths are respectively represented in red and blue. The green wave paths correspond to the MCS reflections.

In order to derive accurate velocity-depth information in deep water areas and from deep parts of continental margins, it is necessary to shoot profiles out to large offsets, usually 5 to 10 times longer than the thickness of the studied sub-surface. Large source-receiver distances are also required to make sure that the critical distance is reached. This distance is defined as the offset at and beyond which refracted energy will be returned to the surface, i.e. making it possible to record refracted arrivals from the different interfaces where we have an increase in velocity.

The acquisition of seismic data over these large offsets requires powerful sources. Nowadays, the most common sources used in marine refraction surveys are air guns which are grouped in arrays and creating high-energy seismic pulses detectable through ground waves at ranges of several hundreds of km.

The use of a multichannel streamer as the recording device enhances the signal to noise ratio. Multiple receivers can greatly reduce or eliminate spatially random (e.g. hydrodynamic noise around towed receivers) and coherent noise (e.g. multiple reflections). The signal to random noise improvement is proportional to the square root of the number of channels. We obtain data of better quality than the ones acquired in common receiver geometries like for example sonobuoy data.

One advantage of the ESP's common midpoint experimental geometry is that dipping interfaces have minor effect on the determination of interval velocities. Seismic traveltime data can be described in terms of instantaneous slope (dT/dX) and intercept time (tau-p). In a distance-traveltime (x-t) diagram, this time corresponds to the intersection of the traveltime curve for a seismic ray and the time axis at offset x=0. For CMP experiments, the instantaneous slope is the average slowness and the sum of thickness-vertical slowness products of the up- and down-going rays at the surface, and the intercept time is the sum of thickness-vertical slowness referenced to the common midpoint. The inherent averaging explains the superiority of this experiment over the sonobuoy method in the presence of dipping interfaces (Diebold & Stoffa, 1981).

The acquisition of seismic data with a source and a receiver moving symmetrically away from a midpoint produce CMP traveltime curves that are symmetric about the reference range x=0. The traveltime equation remains the same if source and receiver are exchanged as seen on Figure 4.3.

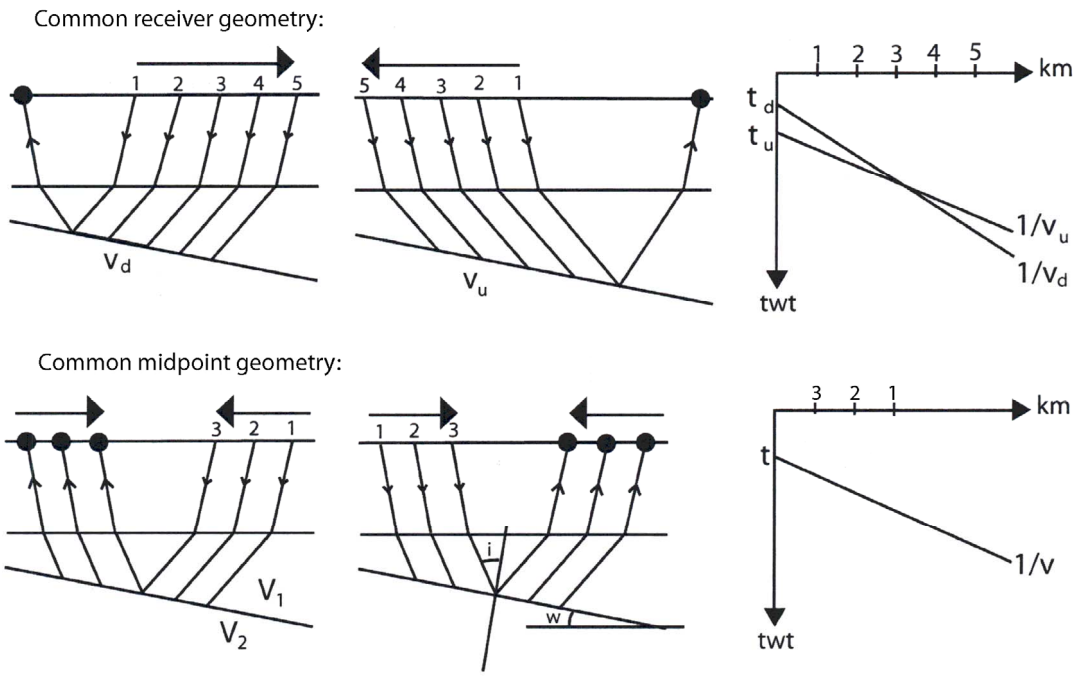

Figure 4.3. Common receiver geometry versus common midpoint geometry illustrated by ray tracing of refracted wave paths (Wilson, 2003). The black points correspond to the recording positions. In the first configuration, the receiver is a fixed hydrophone, in the second geometry; it is defined as a streamer. The shooting points are numbered and the arrows on the ray diagrams indicate the direction in which the ship(s) is (are) steaming. The numbers on the travel time diagrams correspond to the shooting points (not the distance in km). Here t_d , t_u , V_d and V_u are respectively defined as the intercept time and the velocity under the dipping interface in the down- and the up-dip shooting direction.

The fact the traveltime equation remains the same shooting a profile up-dip or down-dip with the CMP method, unable us to determine true dips and slownesses. This information can for example be obtained by measuring time dips in multichannel reflection profiles. Even though the CMP geometry minimizes the effect of dip, it is important when shooting ESP's to align the profile in the direction that shows minimum lateral variability in terms of dip and topography.

The Figure 4.4a presents a homogeneous, layered 2-D model in which velocity and density are constant within each layer but changes discontinuously across layer interfaces. This configuration allows the creation of reflected (in red) and refracted (in green) wave paths. In the case of a model with continuous increase in velocity with depth, we would also obtain diving waves which are continuously refracted and would follow a curved path from the source to the receiver. The data are first presented in the x-t domain (Fig. 4.4b).

The reflected and refracted data are plotted as a function of the offset (km) and two-way traveltime (s). The direct wave (labelled D) and the refracted arrivals (in green and labelled

H_j) are defined as linear segments. The reflected wave paths are plotted as hyperbolic curves (labelled R_j). The refracted arrivals only occur when the critical angle is reached at the respective interfaces. The refracted curves will therefore only be plotted at increasing offsets from the critical point where they are tangent to the reflection hyperbola. The first refraction will be recorded at the critical offset Xc.

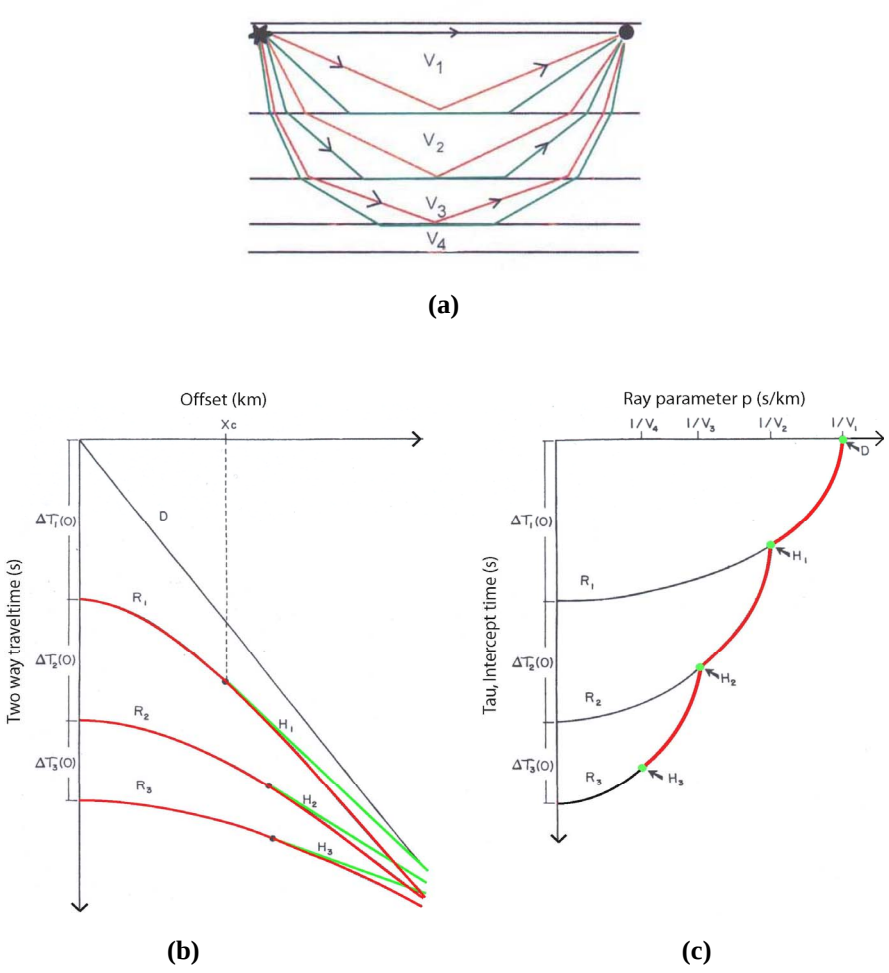

Figure 4.4. (a) Typical three-layer model with constant velocities V_j and velocity increase with depth. The model shows reflected (red) and the refracted (green) wave paths. **(b)** Travel time diagram for the reflections and refractions of the layered model. **(c)** Mapping of the traveltime data in the Tau-p domain (Diebold & Stoffa, 1981).

The seismic data can also be transformed from the (x-t) domain to the intercept time-ray parameter domain (tau-p), p being the inverse of the velocity (s/km) (Fig. 4.4c). The reflection hyperbolas are transformed to quarter ellipses and the direct and refracted arrivals are collapsed to points (in green) in the tau-p domain. These points lie at intersections of the

quarter ellipses, corresponding to both the points of critical reflection and the asymptotic approach of refracted arrivals to reflections at infinite range.

The tau-p curve between the points D and H_3, formed by the post-critically reflected arrivals (in red) and the refracted waves (green points), is defined as the 'primary tau-p path' which contains most of the energy returning to the surface. The data from the tau-p domain are well organized and the interpretation of this primary curve will provide supplemental information for the derivation of a good velocity-depth function.

4.2. ESP data

4.2.1. Presentation of the data

Available data at the Department of Geology were shot and processed during the **Normar program** in the 1980's. Our data set is composed by eleven ESP's that are localized in a corridor crossing the Trøndelag Platform and the Vøring Basin on the continental margin off mid-Norway (Fig. 4.1). The profiles were shot with an overall N-S orientation. We notice that the wide-angle profiles have similar orientations to the structures (e.g. faults). As explained earlier, even if the CMP geometry minimizes the effects of dip, it is important that the profiles are aligned in the direction that shows minimum lateral variability in terms of dip and topography.

Further details about our data set are presented in **Table 4.1**, which gathers information on the water depth and water velocity at the central position of the different profiles. The ESP's belong to two different surveys: one including ESP 34, 35, 36, 37, and 38 that are profiles shot during the ELF survey of 1983; the other with ESP 81, 83, 84, 85, 86, and 87 shot during the ELF survey of 1984.

ESP	Water depth (km)	Water velocity (km/s)	Central Position	Geological province	Survey

			(deg/min/sec)		
34	0.2	1.488	64 02 59.5N 08 12 24.7E	Froan Basin	ELF 1983
35	0.34	1.484	64 06 19.8N 07 36 30.6E	Froan Basin	ELF 1983
36	0.26	1.473	64 16 38.4N 06 47 21.0E	Halten Terrace	ELF 1983
37	0.55	1.480	64 16 36.0N 06 00 24.0E	Rås Basin	ELF 1983
38	1.369	1.465	64 23 18.0N 05 15 24.0E	Helland Hansen Arch	ELF 1983
81	0.7	1.457	65 54 55.8N 05 43 31.2E	Helland Hansen Arch	ELF 1984
83	0.5	1.462	65 08 22.8N 06 03 26.4E	Halten Terrace	ELF 1984
84	0.843	1.446	65 09 24.6N 04 58 31.8E	Slettringen Ridge	ELF 1984
85	1.113	1.446	65 10 17.4N 04 22 16.8E	Vøring Basin	ELF 1984
86	1.735	1.470	65 10 22.8N 03 09 25.2E	Vigrid Syncline	ELF 1984
87	1.550	1.440	64 31 36.0N 04 31 42.0E	Slettringen Ridge	ELF 1984

Table 4.1. Presentation of the different ESP's with the calculated water depth and water velocity at the central position and the location of the profiles on the continental margin.

The 1983 and 1984 Elf-surveys were carried out by commercial seismic vessels. The shooting vessel was equipped with a 6000 cu.inch. airgun array and the recording vessel towed a 2,4 km long streamer consisting of 96 hydrophone groups. The two ships steamed, with constant speed, on opposite bearings from a common midpoint and the maximum offset of our ESP's varies from 50 to 100 km. The profiles that were shot in 1984 are asymmetric which means that the recording vessel has not acquired data to the same offsets on each side of the common midpoint. The right side of those profiles in the x-t domain is in average twice as long as on the left side. The interpretation of the part of the ESP's with the largest offset will provide us more information about deeper refractors possibly identifying mantle refractions.

The wide-angle data of our eleven ESP's are both presented in the x-t and after transformation, also in the tau-p domain. The combined interpretation of the data in these two domains will allow the derivation of a good velocity-depth function.

4.2.2. Data Quality

ESP 34 to ESP 38 from the 1983 survey

In the x-t domain, the first seismic arrivals are clearly visible on most of the profiles and it is possible to interpret deep events at large offsets on all the ESP's apart from ESP 36 and 37. *In the tau-p domain*, it is rather easy to discern the primary curve down to at least 6 s intercept time on all the ESP's apart from ESP 34 located close to the mainland. This profile provides only velocity information from shallow depths. There are also small problems for the interpretation in the shallow part of ESP 36 and intermediate part of ESP 38 as the primary curve cannot be followed easily.

ESP 81 to ESP 87 from the 1984 survey

In the x-t domain, the data are of good quality and it is easy to identify first arrivals up to large offsets on all the profiles apart from ESP 86 where parts of the seismic data are not visible making the interpretation more difficult. *In the tau-p domain*, the primary curve is well defined down to 7 s intercept time on all these ESP's apart from ESP 86, where it is difficult to discern the curve between 2 and 4 s.

4.3. ESP analysis

After acquiring the wide-angle data, the resulting traveltime information may be processed and analyzed by a number of different procedures. In order to obtain the velocity-depth distribution and the sub-surface architecture in our survey area, we will use the so-called "integrated approach" which is defined as a do-loop-like procedure (Eldholm, 2002). This "approach" is characterized by two phases.

- First, for each individual profile, a data reduction to determine velocity-depth functions using separate methods in the x-t and tau-p domains. A more detailed presentation of those methods will be given later in this chapter. The curves that we

obtain are combined into a "common velocity-depth function" which we test and adjust by synthetic modelling.

- The second phase of the procedure is to compare this function with vertical incidence data from MCS profiles and in some cases with gravity modelled interfaces. If significant discrepancies are noted, the velocity-depth function is adjusted yielding a final "optimal function". Figure 4.5 outlines this "integrated approach".

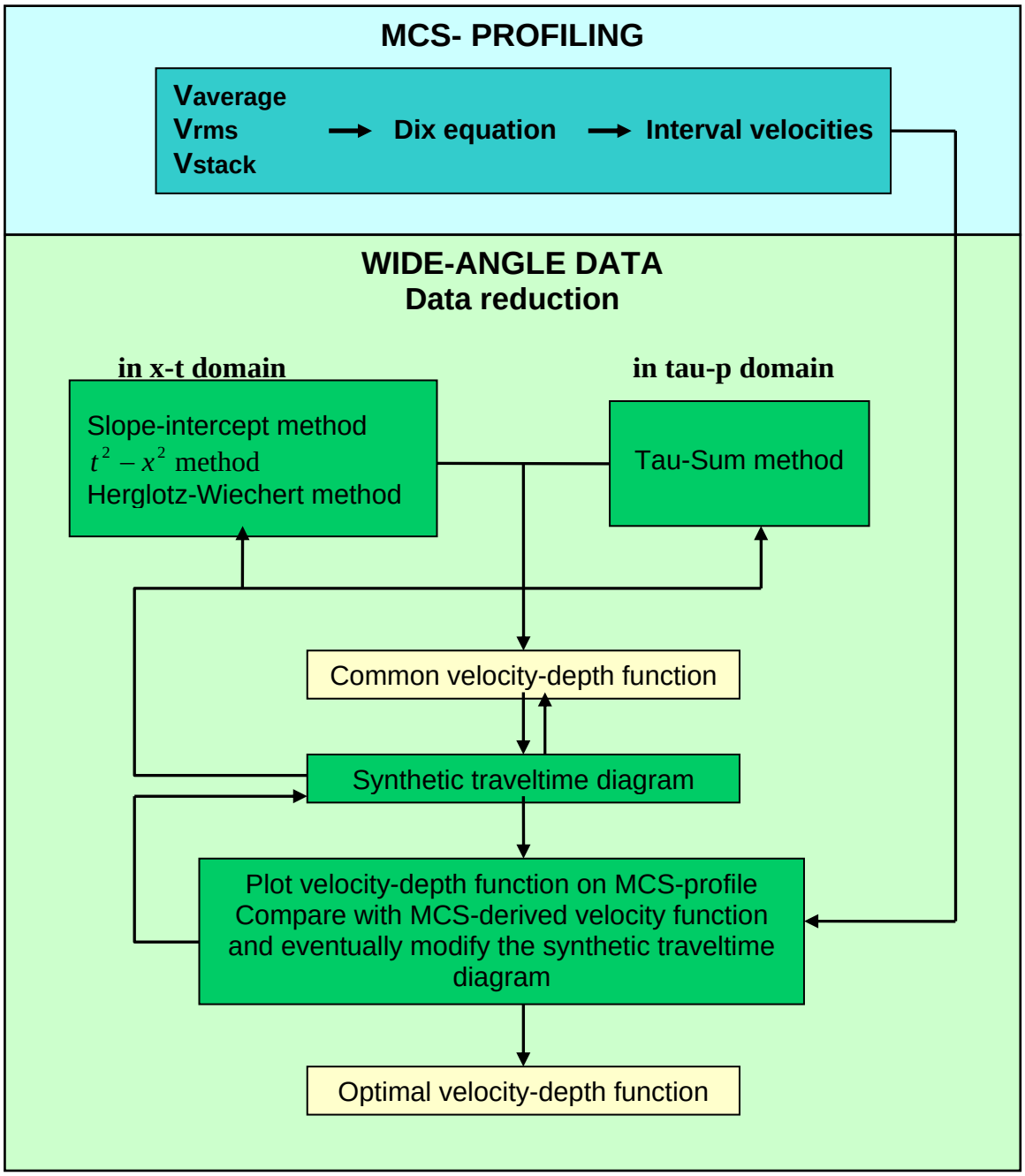

Figure 4.5. Flow-line diagram outlining the inverting and forward modelling of wide-angle data. This procedure is defined as the 'integrated approach'. The diagram has been modified from Eldholm (2002). MCS-profiling: the average velocity (Vrms) down to different reflectors can be used to compute interval velocities using the Dix formula (Keary & Brooks, 1986).

Many methods have been developed to derive a velocity-depth function V(z) from traveltime data. Each procedure is based on a set of fundamental physical assumptions and will therefore provide method-dependent V(z) curves. The inversion methods are divided into two categories depending upon whether reflected or refracted arrivals are employed. In the x-t domain, we decide to interpret the refractions, reflections and diving wave on the right side of each of our profiles as it extends to larger offsets. The inversion methods that are coupled with those different arrivals are respectively the slope-intercept, the t^2-x^2 and the Herglotz-Wiechert methods. In the tau-p domain, we interpret the primary curve and the data are reduced using the Tau-sum method. We get a common velocity-depth function by combining the different curves and this function is tested and adjusted by forward modelling. The inverse and forward modelling procedures are presented in the following sub-sections giving a general overview of the different steps in the analysis of our ESP's.

4.3.1. Inverse modelling

The goal of the inverse modelling is to build a velocity-structure model using the observational data from our wide-angle profiles. All data reduction procedures for profiles displayed in the x-t and tau-p domains include the identification of the direct wave, of the refracted and reflected arrivals. We then trace and digitize the identified arrivals and finally invert the data using several methods. Each method will give a velocity-depth function. By taking the best out of every inverse solution, we obtain a common velocity-depth function. When building this function, we have to wonder about the thickness and the velocity of the different layers or sediment packages of the sub-surface where our ESP's are located, test different solutions with constant or increasing velocities within the layers.

In the x-t domain, the identification of direct, reflected and refracted arrivals are carried out together. One main objective is to identify the onset, in traveltime, of arrivals. The procedure can be described as decomposing the 'first arrivals trajectory' into a series of straight segments that are tangent to the different arrivals. These straight segments can be enhanced by looking obliquely onto the diagram, performing a so-called 'optical stack' (Eldholm, 2002). In the tau-p domain, we have to identify the primary curve formed by the post-critically reflected and refracted arrivals. This curve contains most of the energy returned to the surface and thus contains valuable information to derive a velocity-depth function. It is sometimes difficult to

identity the tau-p curve in the deep part of the profiles and there is a risk to interpret the pre-critical reflected arrival from the deepest quarter ellipse. This part of the ellipse is difficult to define due to little energy. The inversion of the interpreted primary curve will provide the best results for shallow and intermediate depths of the crust as the inversion method in the tau-p domain also has a tendency to smooth the velocity-depth curve too much for deep arrivals (Olafsson, 1992).

For the deepest parts of the crust, it is generally the solutions from the slope-intercept and reflection hyperbola based methods that provide more accurate velocity-depth information. The solutions have a 'staircase' shape which is due to the jumps in velocity at the different layers interfaces. These velocities discontinuities are only observed at interfaces with an acoustic impedance contrast. Another solution can be obtained using the Herglotz-Wiechert method used for the inversion of diving waves. The method provides a continuous velocity curve.

The general trend is to consider that the velocity increases with depth with discontinuities over the layers interfaces. The optimal velocity-depth can then often be drawn between the slope-intercept and the Herglotz-Wiechert solutions.

To digitize the interpreted traveltime data in the x-t and tau-p domain, we use a program called **SECTION** (Planke, 1993). In the x-t domain, we digitize the direct wave and the different straight segments fitted to the refracted arrivals. We also interpret a diving wave solution by digitizing the primary arrivals trajectory in a continuous way out to large offsets. In the tau-p domain we digitalize the primary curve. The data are organized into two files for each profile, one for each domain.

These files are the input files for the traveltime inversion script 'go_inverse' (Planke, 1995) that we use to obtain our velocity-depth curves. This script can inverse both reflections and refractions in the x-t domain, together with the curve in the tau-p domain. The script will inverse the data according to the different methods presented further down and will create graphs of velocity as a function of depth in a postscript format. The information obtained about the depth to the different sub-surface layers, their thickness and additional interval velocities can be organized into a database using a program called VELO (Planke, 1993). It is

defined as a program for storage, retrieval and display of seismic refraction and wide-angle reflection derived velocities.

Slope intercept method

This method is used for the inversion of refracted waves in the x-t domain. It is based on a set of assumptions where the experimental model is homogeneous, 2-D layered in which velocity and density are constant within each horizontal layer but changes discontinuously across layer boundaries. As explained earlier, these refracted arrivals are only registered from a certain offset defined as the critical distance. These arrivals appear as linear segments in the x-t domain indicating that the traveltime of a refraction is a linear function of the offset. Each segment is defined by its intercept time on the axis x=0 and by its slope, which is the inverse of the rms-velocity of the layer along which top boundary the waves have been travelling before returning to the surface.

The slope-intercept method inverts a series of linear segments into a velocity-depth function by performing different steps. We first have to identify the direct wave which will allow us to calculate the seafloor depth and the water velocity at the location of the profile. Then we have to fit straight segment to the different refractions observed on the ESP by making sure to identify the first arrivals. It happens quite often that the amplitude of the second arrival is stronger than the first. In this situation we perform a parallel upwards shift to find the first refracted waves.

We digitize two points of each segment in order to determine pairs of apparent velocities and intercept times which will be the input parameters for the inversion, in addition with the water depth and velocity. The script ‘go_inverse’ calculates the layer thicknesses and velocities and creates a correspondent ‘stair-case’ curve.

T^2 - x^2 method

This method is used for the inversion of the reflected arrivals in the x-t domain. We work here with a model that is based on the same physical assumptions as for the slope-intercept

method. The equation for the traveltime t_{RFL} of a reflected ray from a shot point to a detector at a horizontal offset, x, is given by

$$t_{RFL} = (x^2 + 4z^2)^{1/2} / V$$

with the reflector at a depth z beneath a homogeneous top layer of velocity V (Kearey & Brooks, 1984). This equation defines the reflections as hyperbolas in the x-t domain. It is difficult to identify reflections at close offsets as the traveltime data are affected by multiples. It is though not necessary to identify the whole curve to be able to perform an inversion. At large offset, reflection hyperbolas may sometimes be detected as refracted segments as their curvature is not entirely obvious. They can possibly be interpreted as refractors, however the segment velocity will be less or greater than that of the refractor from the same interface at respectively pre- and post-critical distance (Eldholm, 2002).

The velocities and depths can be determined by plotting the reflection hyperbolas in a diagram that will express t^2 as a function of x^2. A hyperbola is then reduced to linear segment defined by its slope, which corresponds to the inverse of the square velocity above the reflector, and by its vertical reflection time at $x^2 = 0$. The parameters of this segment make it possible to calculate the layer thickness and interval velocity.

Some reflections have been identified at large offsets on a few of our profiles (ESP 34, 81, 83, 84 and 86). Strong wide-angle reflections can be associated with a mantle reflection.

Herglotz-Wiechert method

In the case of a continuous velocity increase with depth, the refracted arrivals take the name ‘diving waves’ as the rays will follow curved path until a turning point and up to the surface again. On a traveltime diagram, a diving wave is represented by a first arrival curve that does not form straight line segments but rather show a continuous gentle curvature. In order to inverse this curve we introduce the Herglotz-Wiechert method that will provide a velocity-depth function by applying an integral. Assuming we have a flat-earth model, this integral is given by the following formula:

$$Z = \frac{1}{\pi} \int_{(x=0)}^{(x=D)} \frac{1}{\cosh V_D / V_x} dx$$

where Z is the depth for a ray having apparent velocity V_D measured at the surface at a distance X=D. To obtain Z we have to determine the apparent velocities along the profile at discrete distance increments. Generally, a velocity discontinuity exists at the sea floor, violating the assumption for the method of a continuously increasing velocity with depth. The water layer is therefore removed by correcting both distances and traveltimes.

A diving wave has been interpreted on all our ESP's to which was applied the inversion method.

Tau-sum method

In the tau-p domain the post-critical reflected and refracted arrivals form a single monotonic curve defined as the primary curve. The inversion of these tau-p data is performed by the Tau-sum method which is equivalent to the standard first arrival slope-intercept method, except that it is valid for all the critical and post-critical arrivals, without distinction between reflection and refraction. The Tau-sum method is based on the assumption of a layered earth model with constant velocities within the layers, but as those are defined as rather thin, the velocity-depth will not be affected by important velocity discontinuities. This means that the method can also be applied to data arising from velocity functions containing increasing velocity gradients (Diebold & Stoffa, 1981). We have to be careful not to invert part of the deepest quarter ellipse corresponding to a pre-critical reflected arrival. If we do, a distinct 'high-velocity kink' may appear at the deepest part of the velocity-depth function (Eldholm, 2002).

The Tau-sum method gives generally good detailed velocity information with depth, but has a tendency to smooth the resulting function too much for deep arrivals (Olafsson, 1992).

4.3.2. Forward modelling

Forward modelling is defined as a standard ray-tracing technique which allows us to calculate synthetic seismograms in simple and complex 2-D geological models. The objective of this direct approach is to achieve a suitable match between synthetic and observed travel times

using kinematic ray-tracing. This match is achieved by using a 'trial-and error' approach (Eldholm, 2002), which implies numerous iterations. Forward modelling is carried out in both the x-t and tau-p domains providing a quality control of the interpretation done on our different profiles. The reduction procedure includes the following steps.

First, we select a common velocity-depth function corresponding to the best combination of the inverse solutions obtained with the slope-intercept, the $T^2 - x^2$, the Herglotz-Wiechert and the Tau-sum methods. This function represents our initial earth model. This synthetic model contains information about the velocities at the top and bottom of the different layers and the depth to each interface. We also need to consider whether the model is based on layers with constant velocity or with a velocity gradient. The most realistic solution is though to construct a model based on a combination of these two assumptions.

The next step consists of running the ray tracing program xspray (Planke, 1995) to calculate the synthetic travel time and tau-p diagram. We then run the script xsptt2ps (Planke, 1995) in order to plot the ray-traced primary events. We compare the synthetic and actual data by overlaying the ray-traced plot on the ESP. If there are significant discrepancies, the common velocity-depth function is adjusted and we calculate new synthetic diagrams. We iterate the process until we obtain a reasonable fit of the actual and synthetic data.

The last step of the forward modelling consists in a comparison and integration of the common velocity-depth function with a corresponding MCS profile. We need to transform the velocity-depth plots into velocity-two-way-traveltime curves and will plot these curves onto the MCS record at its representative location. We compare the high acoustic impedance reflectors on the MCS profile with the velocity discontinuities of our velocity-time-depth curves. The data are adjusted if there are some discrepancies and we finally obtain an optimal and final velocity-depth function. We though need to keep in mind that the important reflections from the MCS lines do not necessarily need to match the velocity discontinuities from the ESP velocity-depth function. Indeed the lateral extent of the ESP profiles and the fact that their midpoint can be located quite far from the MCS line, can create some discrepancies.

4.3.3. Examples of inverse and forward modelling

We now present three representative ESP's from our dataset to illustrate the results obtained by inverse and synthetic modelling (Figs 4.6 to 4.11). We choose ESP 35, 84 and 87.

For every chosen ESP, we will show two sets of figures. The first set presents the data from the profile before interpretation in the x-t and tau-p domain together with the inverse modelling in the form of a velocity-depth diagram. The diagram shows the solutions obtained with the different inversion methods described above. The second set of figures illustrates the forward modelling. In the velocity-depth diagram, we have added the selected common velocity-depth function representing the earth model at the location of the profile and providing the best synthetic ray-tracing plots in the x-t and tau-p domains. We show the match we obtained when overlying these synthetic data on the observed ones.

The colour code used in all the velocity-depth diagrams is the following:

- The dark blue curve gives the slope-intercept solution based on refracted arrivals
- The light blue curve gives the Herglotz-Wiecherts inverse solution for diving waves.
- The light green colour gives the T^2-x^2 solution for reflected arrivals
- The red curve gives the Tau-sum solution from the inversion of the primary curve in the tau-p domain.
- The dark green curve corresponds to the calculated common velocity-depth function obtained after forward modelling. This function gives synthetic traveltime diagram that reasonably match the observed data in the two domains.

The three ESP profiles we chose to illustrate our results (ESP 35, 84 and 87) show that the earth model giving the best synthetic ray-tracing plots to match the observed data is a combination of a model with velocity jumps across layer boundaries and of velocity gradients within layers. In our examples, the different inverse solutions on the velocity-depth plot show a rather similar shape making it easier to do forward modelling and construct a common velocity-depth curve.

We will focus on this common function giving an analysis of the velocity changes, trying to define the depth to the main interfaces such as base Tertiary, base Cretaceous, top of crystalline basement and Moho. A closer look at the interpretation done on the MCS lines can help us in this attempted identification of these different horizons. Raum et al. (2002) summarized the velocities that have been calculated from wide-angle seismic in the sedimentary and crustal sequences of the southern part of the Vøring Basin (Table 4.2)

Sea water	**1.5 km/s**
Quaternary and Tertiary	**from 1.7 km/s to 2.5-2.8 km/s**
Cretaceous	**2.5-4.8 km/s**
Pre Cretaceous	**5.4-5.6 km/s**
Crystalline basement	**6.1-6.8 km/s**
Lower crustal high-velocity body	**7.0-7.4 km/s**
Moho	**Over 8 km/s**

Table 4.2: Overview over chosen sequences and their respective velocity range

ESP 35

This NE-SW oriented ESP profile is located across the southwestern part of the Froan Basin (Fig. 4.1). This basin is defined as a Permo-Triassic structural element (Blystad et al., 1995) composed by half-grabens and by a thick sedimentary infill of Late Permian-Early Triassic age. The southwestern part of the basin was uplifted and deeply eroded during Late Jurassic and moderately active during Cretaceous times, which explains that older sediments are located at shallower depths than for the two other example profiles.

Figure 4.6 shows the wide-angle seismic data in the x-t and tau-p domains and the velocity-depth plot obtained by inverse modelling. In the x-t domain, we clearly see the direct wave which corresponds to a straight line starting at zero offset and tangent to the sea bottom reflection hyperbola. We also distinguish the first arrivals of seismic energy that represent the refracted waves from the different interfaces encountered in the subsurface at this location. These first arrivals form a succession of linear segments with different slopes. We can also identify reflection arrivals, but they do not appear as clearly as the refractions.

For ESP 35, we interpreted refraction arrivals and diving waves in the x-t domain and the primary curve in the tau-p domain. The results from the inverse modelling are given in Figure 4.6 in the form of a velocity-depth plot. There is a rather good match between the different inverse solutions making it easy to construct a common velocity-depth function in thick dark green colour in Figure 4.7.

Figure 4.7 illustrates the forward modelling results. The synthetic ray-tracing results are plotted on the top of the observed data, and we obtain a good match in both domains. In the x-t domain, the first arrivals in the shallow part of the data form a gentle curvature. A diving wave solution (in dark blue) is matched to this part of the seismic. The sedimentary layers are here defined by velocity gradients. In the deeper parts, synthetic refracted arrivals provide the best results (in light blue) with a change to a velocity gradient at a certain depth (dark blue). In the tau-p domain, the observed primary curve is matched by synthetic quarter of ellipses (light blue colour).

We now focus on the common velocity-depth function in Figure 4.8. The first thing catching our eye is the fact that the velocity increases quite rapidly and we reach values of 6 km/s at shallow depths of 6-7 km. This is explained by the location of the ESP 35. The thicknesses of the Cretaceous and Late Jurassic sediments are not very large over the southern Froan Basin. Triassic sediments are at rather shallow depths explaining the higher velocities and the relative shallow depths of top crystalline basement.
There is a small velocity jump from 2.9 to 3.2 km/s around 1.8-2 km depth, which could be associated with the base of the Tertiary sedimentary sequence. Other clear velocity jumps, from 4.1 to 4.9 km/s and from 5.2 to 6.0 km/s, are seen at 4.5 km and 6 km depths respectively. The second one could indicate that the crystalline basement is found at a depth of about 6.5 km. The Tau-sum solution shows a ‘high-velocity kink’ in the deepest part, which may be due to the inversion of a pre-critical reflected arrival at the deepest level in the Tau-P domain.

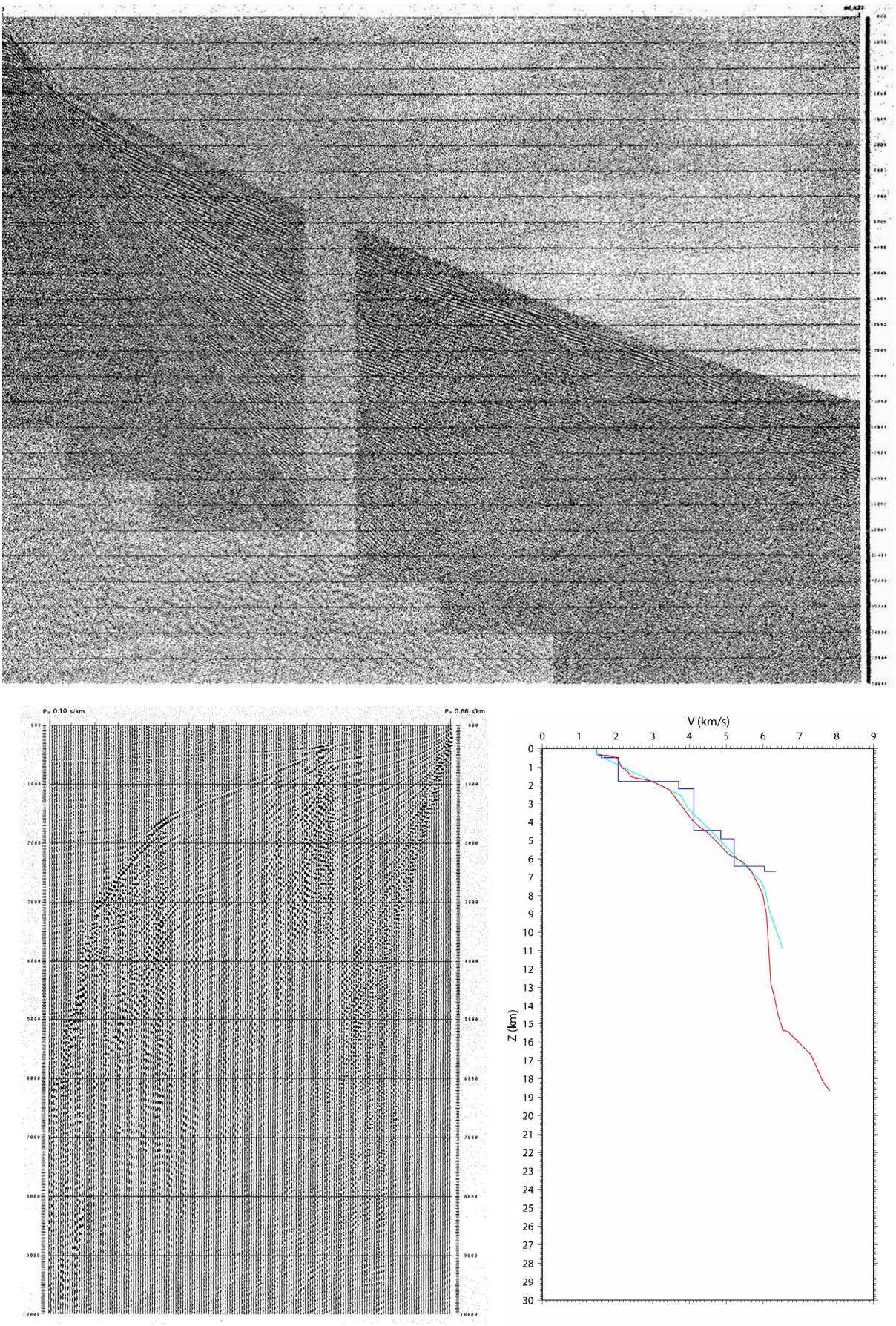

Figure 4.6. ESP 35 and velocity-depth functions obtained by inverse modelling.

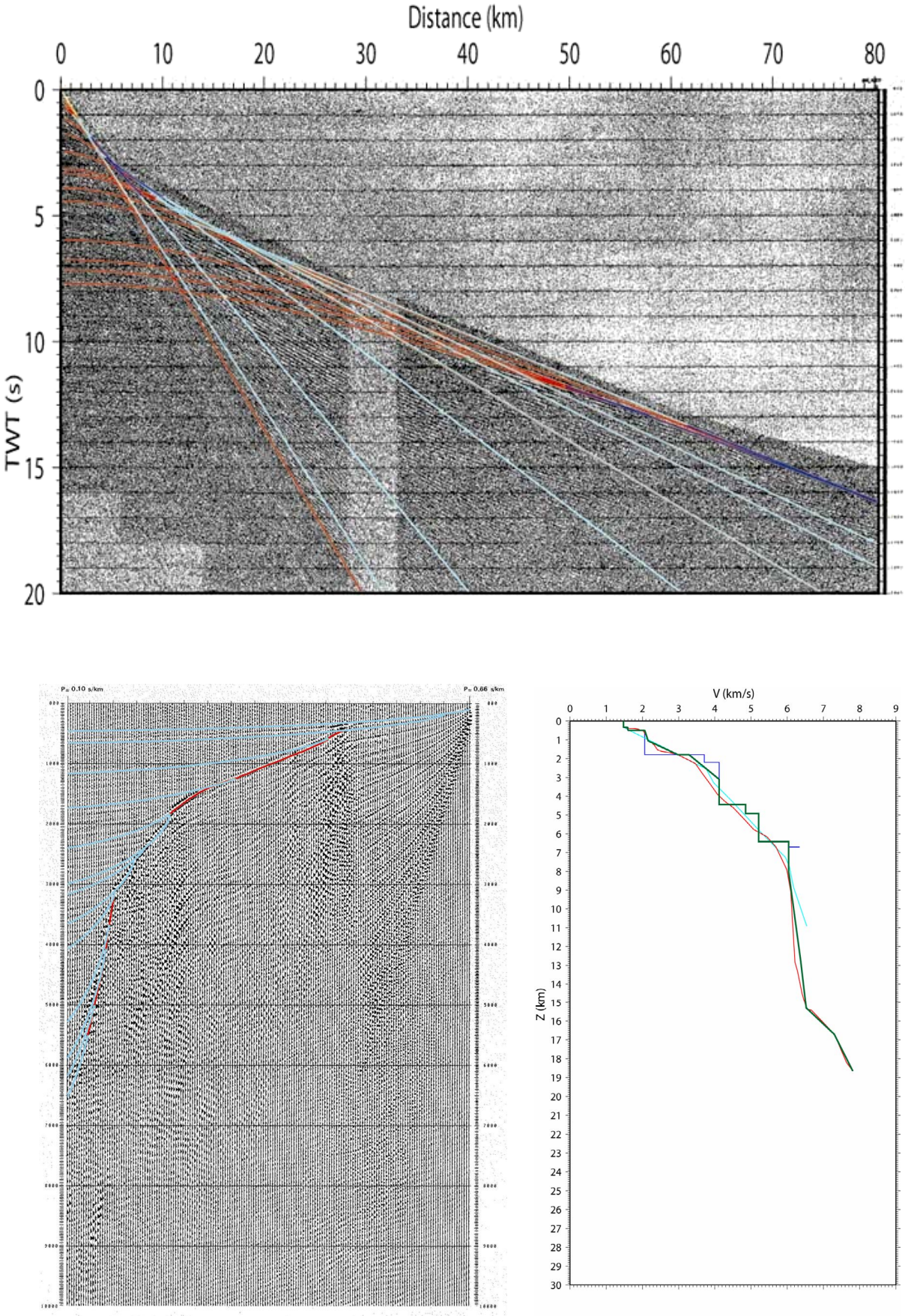

Figure 4.7. ESP 35 with synthetic ray-tracing plots overlaying the original data and corresponding common velocity-depth function

ESP 84

ESP 84 has a N-S orientation and is located across the Helland Hansen Arch and the Slettringen Ridge (Fig. 4.1). The Helland-Hansen Arch is defined as a Tertiary structural element and was developed during Eocene-Oligocene and Late Miocene. The Slettringen Ridge is developed below the southern part of the Tertiary arch and is defined at the base Cretaceous unconformity as a set of N-S trending rotated fault blocks (Blystad, 1995).

Figure 4.8 shows the wide-angle seismic data in the x-t and tau-p domains and the velocity-depth plot obtained by inverse modelling. In the x-t domain, we can easily see the direct wave and the first arrivals of seismic energy. Unlike ESP 35, it is possible to identify refraction arrivals at greater depths. In the tau-p domain, the primary curve is well defined. The velocity-depth plot shows homogeneous inverse solutions making the construction of a common velocity-depth function easier, in thick dark green colour on Figure 4.9. Figure 4.9 also presents forward modelling results. The common velocity-depth function allows us to calculate the synthetic travel times, and these are overlain over the observed data in the x-t and tau-p domain, showing a good match. For this ESP, we chose an earth model with a rather continuous velocity increase with depth and small velocity jumps across some interfaces. In the x-t domain, the observed data are matched with the synthetic diving wave solution (in dark blue) on the first diagram of Figure 4.9.

The common velocity depth function shows a velocity jump from 2.6 to 2.9 km/s at about 2 km depth, and this could be interpreted as the base Tertiary. The interpretation done on our seismic lines give that interface at a similar depth. Another velocity discontinuity from 4.7 to 5.0 km/s is located around 9.3 km and could correspond to the base Cretaceous. Between 2 and 9 km depth, the velocities range from 2.9 to 4.7 km/s which are characteristic of Cretaceous sediments velocities (Table 4.2). 6 km/s velocities are found at about 15 km depth and these are assigned to the top of the crystalline basement.

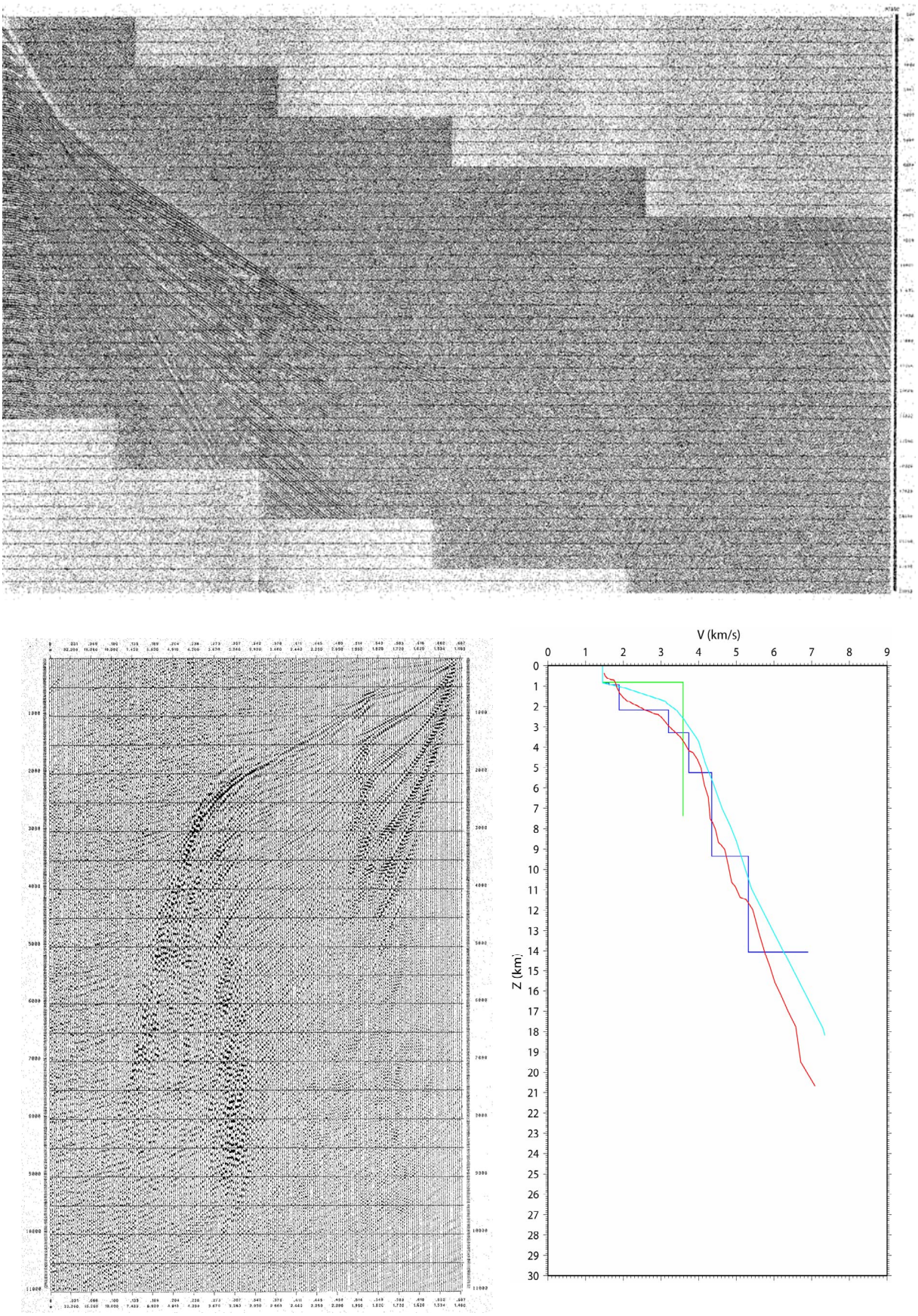

Figure 4.8. ESP 84 and velocity-depth functions obtained by inverse modelling.

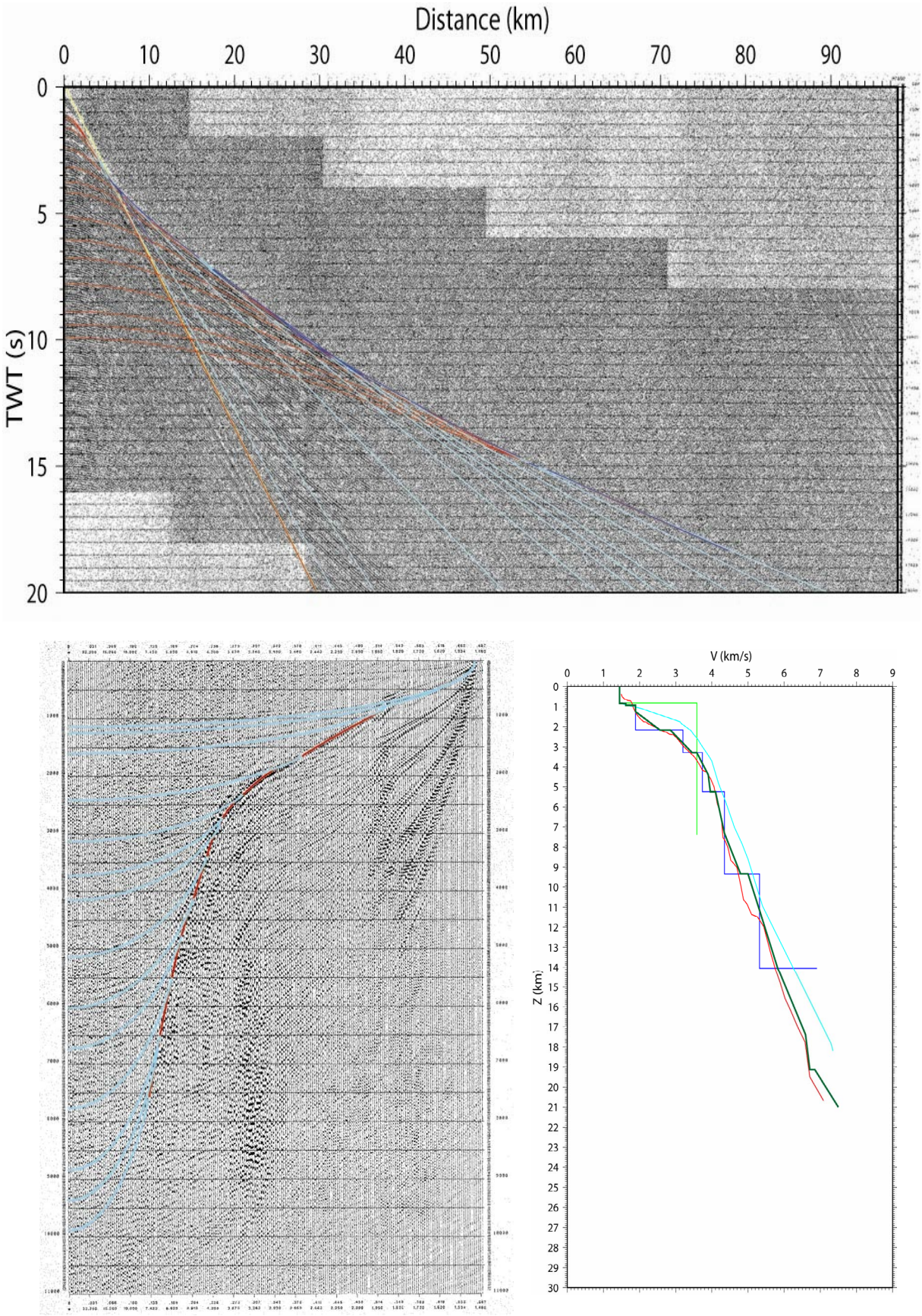

Figure 4.9. ESP 84 with synthetic ray-tracing plots overlaying the original data and corresponding common velocity-depth function

ESP 87

This NE-SW trending ESP profile is located at the south western boundary of the Helland Hansen Arch across the southern part of the Slettringen Ridge (Fig. 4.1). The common mid-point of the profile is located very close to the MCS line GMNR-94-104 (in red), it is therefore interesting to have a look at the seismic interpretation of this line when analyzing the common velocity-depth function of this ESP.

Figure 4.10 shows the wide-angle seismic data and the results of the inversion of the first arrivals curve in both domains. In the x-t domain, we notice that the depth to the sea bottom is quite important. The quality of the data is good making the interpretation of the first arrivals easy. The inverse solutions from the velocity-depth plot present a similar trend allowing us to construct a satisfying common velocity-depth function, in dark green colour on Figure 4.11.
The forward modelling provides a very good match between the synthetic ray-tracing plots and the observed data (Fig. 4.11).

The common velocity-depth function does not show the rather continuous velocity increase with depth as for the previous profile. The function has two segments with high velocity gradients respectively around 4 and 9 km depth. The starting points of these segments could correspond to main interfaces in the sedimentary sequence. We have a velocity jump from 2.4 to 2.9 km/s at about 3.7 km just before the first high velocity gradient segment. The MCS interpretation indicates that this discontinuity could represent the base Tertiary. The second important change in velocity gradient is observed around 9.5 km and could be interpreted as base Cretaceous. Velocities of 6 km/s and over indicates that the top crystalline basement is located at depths of 12 km, shallower than that the ESP 84.

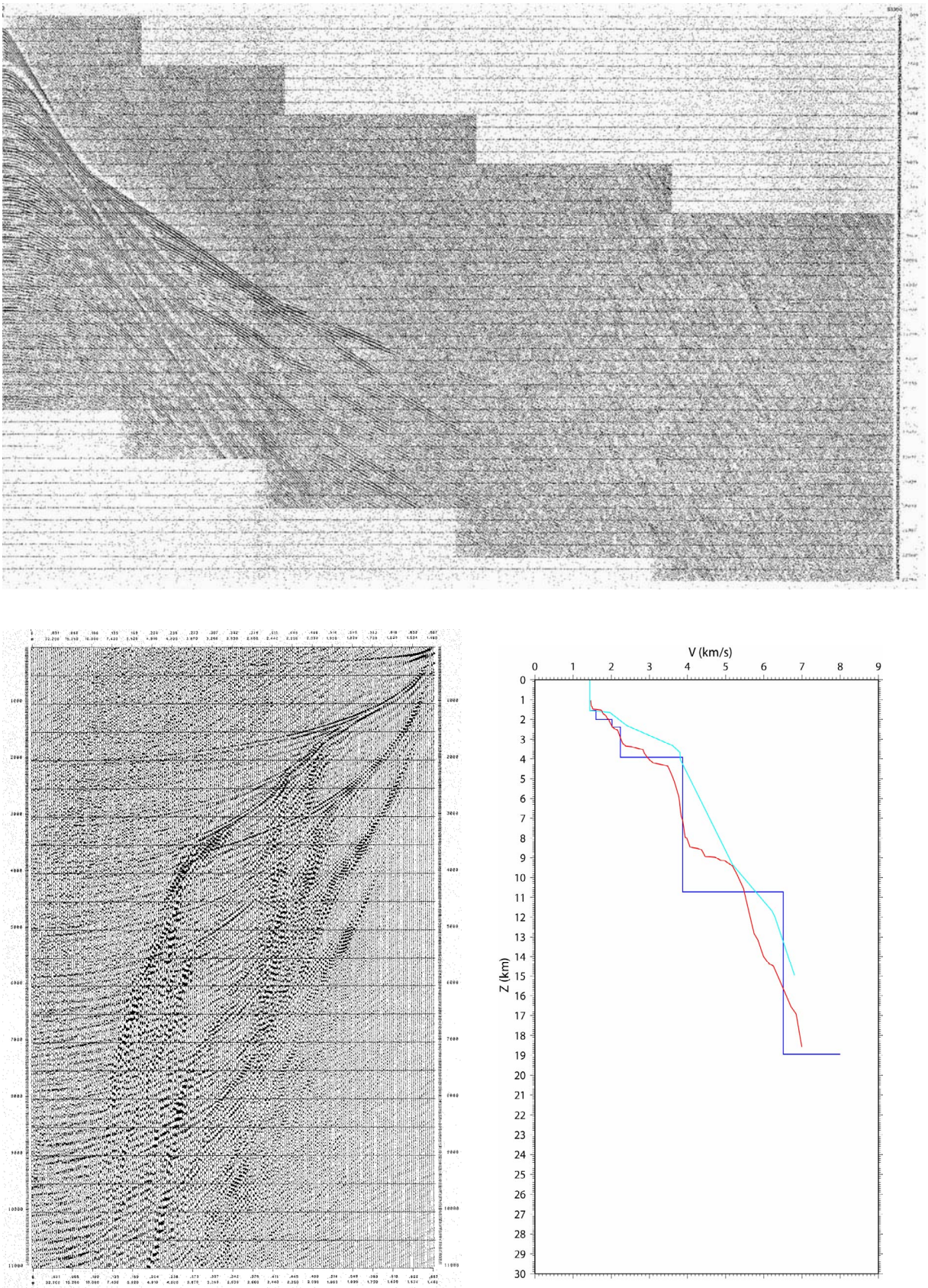

Figure 4.10. ESP 87 and velocity-depth functions obtained by inverse modelling.

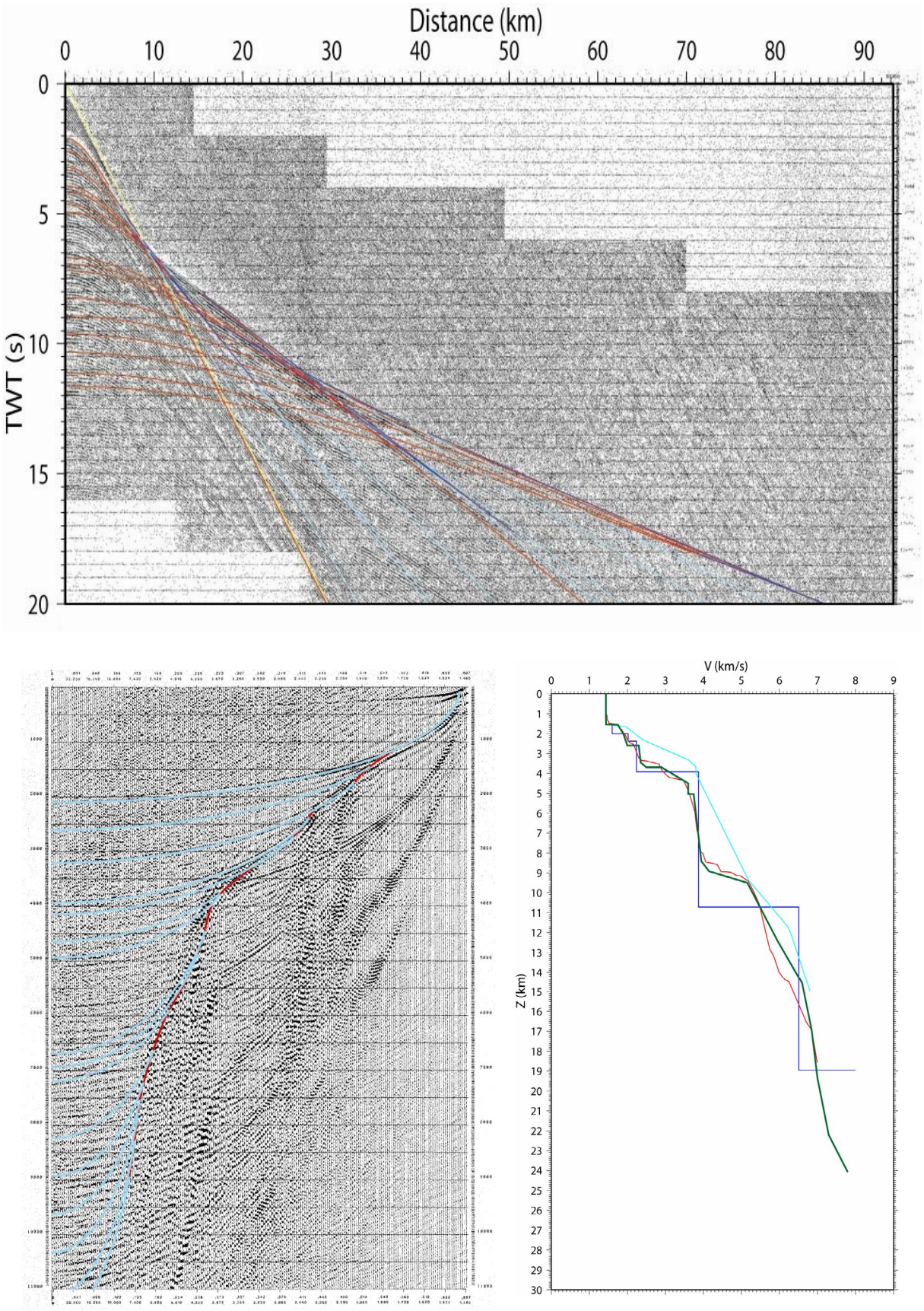

Figure 4.11. ESP 87 with synthetic ray-tracing plots overlaying the original data and corresponding common velocity-depth function

4.4. Special features and problems

Throughout the wide-angle data analysis, we face some problems due to data quality and derivations from the simple earth models assumed in data reduction. Problems can rise from the identification of the first arrivals and the positioning of the critical point. The data can be affected by lateral velocity discontinuities and anisotropy as well as by dipping and irregular interfaces. The problem of the hidden layer also needs to be taken into consideration.

4.4.1. Identification problems

During the analysis of our data set, we may encounter problems to identify the first arrivals. They are sometimes only partly visible or only interpretable over a very short offset interval. These identification problems may be caused by low signal strength and interference phenomena. Interference is amplified if the different seismic arrivals have similar frequency content. At large offsets it may be difficult to differentiate refracted and reflected arrivals. The curvature of deeper reflections is not entirely obvious and the seismic arrivals can be interpreted as refracted arrivals.

The use of the complementary data set in the x-t domain can minimize these identification problems. We interpret the data on the left side of the zero offset axis which will help us to verify the interpretation on the right side. In case of errors, we proceed with the necessary changes. We notice though that the complementary data set for the ESP 81 to 87 is not of great use to verify the interpretation of deeper arrivals. Indeed for these profiles the offset axis is one third shorter than on the right side.

4.4.2. Critical point

Refracted arrivals need to be interpreted in the vicinity of the critical distance which is defined as the distance within which refracted energy will not be returned to surface (Keary & Brooks, 1984). The critical point corresponds to the tangent point between the reflection hyperbola and the refraction segment.

As the refracted waves are only detected as first arrivals at critical distance and beyond, they have to be identified at critical or post-critical energy. If the interpretation is done at pre-critical energy, the seismic arrival is then part of the reflection hyperbola. This will induce some errors in velocity and depth calculations.

As mentioned previously, there are some uncertainties concerning the interpretation of deep refractors like the one that could be associated with the Moho discontinuity. At greater depths, it may be difficult to differentiate a refracted from a reflected arrival as the curvature of a deep reflection will flatten and appear as a straight segment characteristic of refraction arrivals. However, the error will not be significant if the interpretation is done close to the critical point.

4.4.3. Lateral velocity discontinuities

Lateral velocity discontinuities and anisotropy are deviations from the simple earth models assumed in reduction of wide-angle data. The data acquisition is however designed to minimize their effects. Lateral velocity discontinuities can be related to facies changes or structural setting, but they may be difficult to determine in a single wide-angle profile. As for the anisotropy, it is most pronounced in laminated rocks, such as shale, where the velocity changes relative to the strike of the rock unit.

4.4.4. Dipping/Irregular interfaces

According to Diebold and Stoffa (1981), dipping interfaces have minor effect on the determination of interval velocities in the case of an ESP geometry seismic experiment. The ESP profiles are shot with the same orientation as the structural elements of the area minimizing also the impact of dip on the seismic data. Still we should keep in mind that our study area is characterized by complicated structural settings and that some dip-induced errors can be found. This means that refracted and reflected arrivals can respectively have incorrect slope and curvature.

Reflected and refracted arrival can also be perturbed by irregular non-planar interfaces. The perturbations are usually associated with diffraction phenomena and focusing/defocusing effects. In this work, we have assumed that the earth models, chosen in the wide-angle data reduction, are composed of planar refracting interfaces.

4.4.5. The hidden layer problem

One special problem in the data analysis is the hidden layer or “blind zone” problem.
This type of layer is undetectable by refraction surveying. The velocity and thickness of the layer, compared to those of the adjacent layers, will induce a ray path which does not allow the refracted wave at the top of the layer to arrive as first arrival. If such layer is not detected, we will have an underestimation of the depths to the deeper refractors.

Firstly, a layer may simply not be detected as seismic arrivals critically refracted on deeper interfaces may arrive before the refracted waves from the layer in question. This can result from the thinness of the layer, or from the fact that the velocity contrast between the layers and our layer is very small.

Another type of hidden layer problem is associated with low-velocity layer which cannot be detected by refracted arrivals. The top of this layer will not give rise to refracted waves and it will induce overestimated depths to the underlying layers. A low-velocity layer may be found below a local high-velocity layer within a sequence in which the velocity increases gently with depth.

4.5. Velocity-depth curves

This part of the chapter presents the results of the inverse and forward modelling for each ESP profile not presented in detail above (Figs. 4.12 to 4.19). The colour code for the velocity-depth curves is given page 43 and the geographical location of the profiles is shown in Figure 4.1. Table 4.3 gives an overview of the ESP analysis. The first four rows indicate which inversion methods have been used for each profile. The fifth row shows the ESP for which we performed forward modelling to obtain a common velocity-depth function giving the best match between synthetic and observed data.

ESP	34	35	36	37	38	81	83	84	85	86	87
Slope-int.	x	x	x	x	x	x	x	x	x	x	x
$t^2 - x^2$	x					x	x	x		x	
Herg. Wiech.	x	x	x	x	x	x	x	x	x	x	x
Tau-Sum	x	x	x	x	x	x	x	x	x	x	x
Common vz function		x	x	x	x			x	x	x	x
Good match		x	x	x	x			x	x	x	x

Table 4.3: Overview over the analysis of the ESP profiles from our data set

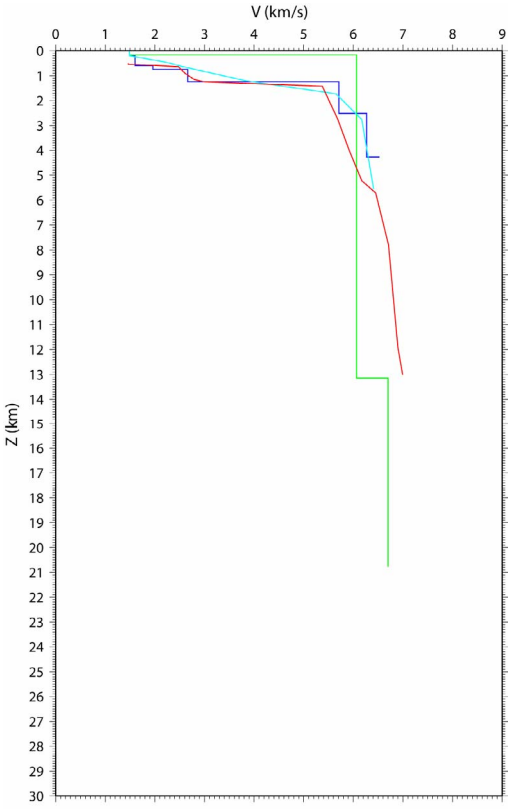

Figure 4.12: ESP 34

This profile is located at close to the mainland, in the Froan Basin (Fig. 4.1).
The inverse solutions show a very rapid increase in velocity at shallow depth with an important velocity jump from values of 2.65 to 5.4-5.7 km/s at around 1.3 km
The slope-intercept and Herglotz. Wiechert. solutions give a 6 km/s velocity at a depth of 2.5 km which could place the top crystalline basement at a rather shallow depth. The interpretation of this ESP in the x-t domain does not give much velocity information at great depths. We reach velocities of 7 km/s at 13 km with the Tau-sum solution.
This ESP has not been taken into consideration for a synthetic modelling as we did not have the ESP 34 scan in the x-t domain.

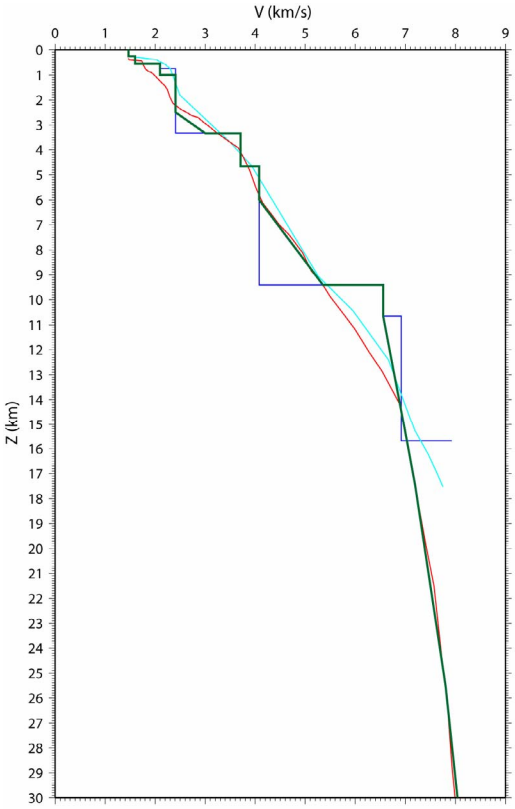

Figure 4.13: ESP 36

This profile is located in the southern part of the Halten Terrace (Fig. 4.1)
This plot shows a good correspondence between the solutions of the different inversion methods. The slope-intercept. and the Herglotz Wiechert solutions provide velocity information down to about 16 km.
The Tau-sum solution can be traced down to 30 km where we observe a 8 km/s velocity which is characteristic of the Moho.
The common velocity-depth function defines the earth model at the ESP location as a succession of constant velocity layers in the first 6 km of the sedimentary sequence.
A velocity gradient solution is then preferred down to 9 km depth, where we have an important velocity jump from 5.3 to 6.5 km/s. This could be interpreted as the top of the crystalline basement. Below this point, the velocity gradient remains rather constant down to 30 km depth.

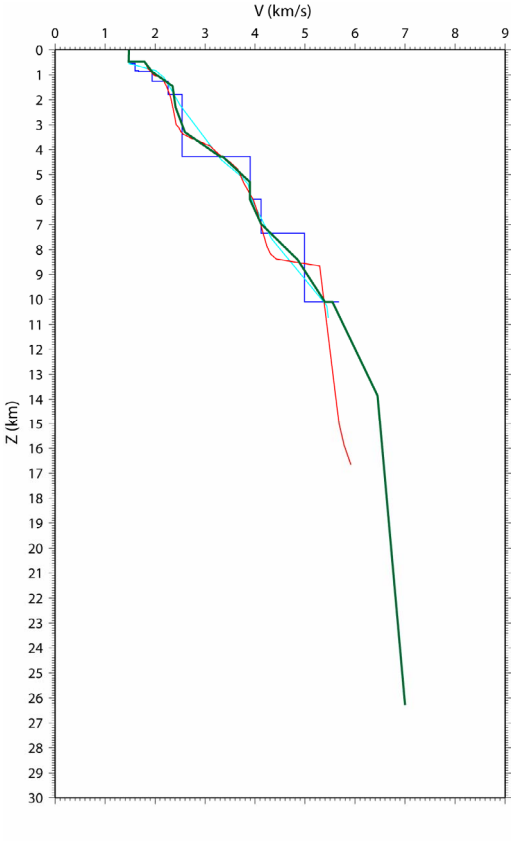

Figure 4.14: ESP 37

This ESP profile has a N-S trend and is located along the Klakk Fault Complex (Fig. 4.1)
The common velocity-depth function is defined here by a succession of segments with different velocity gradients.
There is a notable change in gradient around 3.5 km depth where we have velocities of 2.5-2.6 km/s. These are characteristic velocity values for the lower Tertiary sediments and we assume that this change defines the base Tertiary. At a depth of 8.5 km, the Tau-sum solution shows an important velocity jump from 4.4 to 5.1 km/s. This could be interpreted as the Base Cretaceous. The interpretation done on the MCS line crossing this profile indicates a similar depth to this interface.
The common function places velocity of 6 km/s at a depth of 12 km, but it is difficult to correlate to top crystalline basement as we do not have a marked increase in velocity.

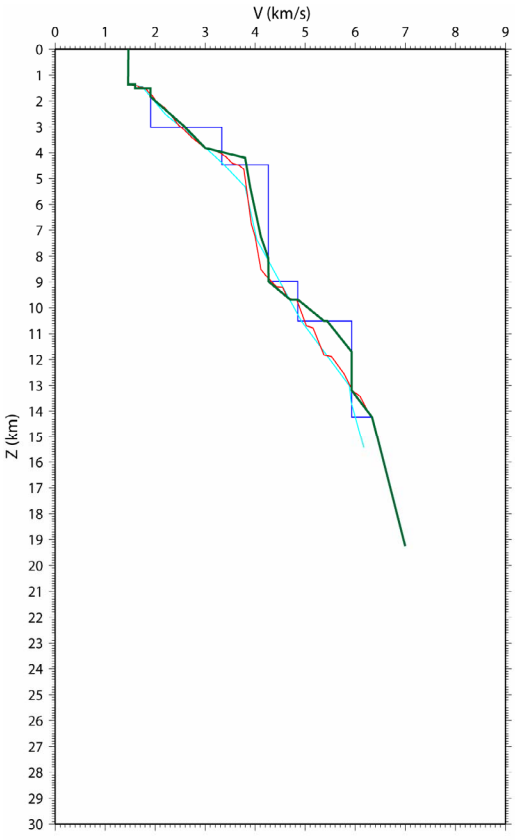

Figure 4.15: ESP 38

This N-S trending profile is located in the southern part of the Helland Hansen Arch and crosses the northern part of the Grip High (Fig. 4.1)
The inverse solutions give velocity information down to around 15 km, but after forward modelling, we reach depths of 20 km.
The common function shows important changes in velocity gradient at depths of 3.7, 9 and 19 km. At 3.7 km we observe a high velocity gradient where the velocity increases from 3 to 3.8 km/s over a thin interval. These values are representative of Cretaceous sediments, and the base Tertiary could maybe be placed around 3 km where we observe an important velocity jump in the slope-intercept solution.
A significant change in gradient is also seen at 9 km depth where we have velocity of 4.3 – 4.7 km/s and this could be interpreted as been the depth to the base Cretaceous unconformity. 6 km/s values are found at about 11.5 km and we notice a higher velocity increase around 19 km.

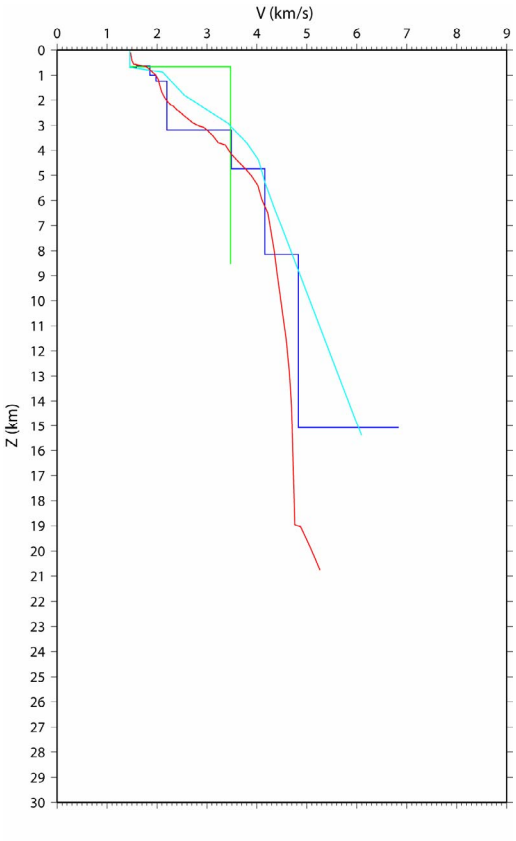

Figure 4.16: ESP 81

The ESP 81 is the profile located furthest north in our data set. It has a NE-SW orientation and covers the northern part of the Helland Hansen Arch (Fig. 4.1). We present here the results of the inverse modelling but we decided to skip the forward modelling as the velocity-depth information for this profile cannot be projected on any of our MCS lines.
The slope-intercept solution shows an important velocity jump around 3 km depth and this could be interpreted as the base Tertiary. The other significant feature is observed at an approximate depth of 15 km where the velocity increases from about 5 to 7 km/s and it could represent the crystalline basement or an intrusive body.

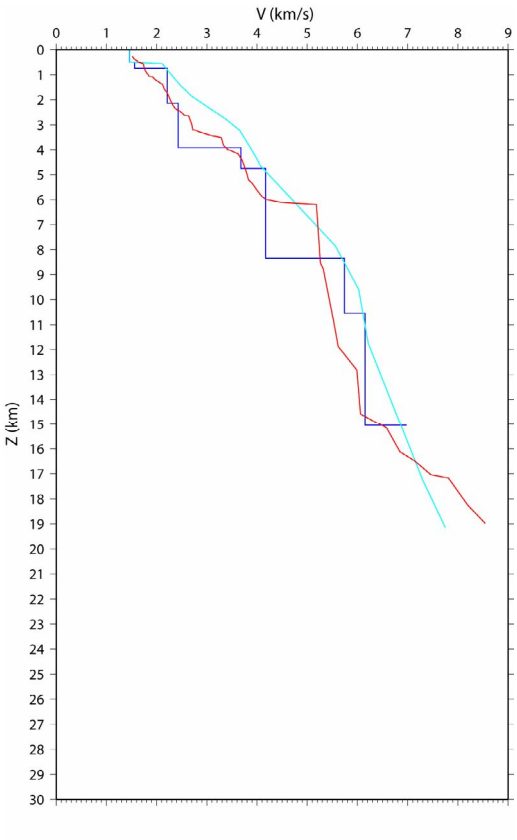

Figure 4.17: ESP 83

The NE-SW trending profile is located along the western boundary of the Halten Terrace across the Klakk Fault Complex (Fig. 4.1). The velocity-depth plot shows the inverse solutions. We tried to perform forward modelling for this profile, but it was very difficult to construct a common velocity-depth function providing a good match between the synthetic and observed data.
The Tau-sum and Herglotz.-Wiechert solutions give information down to about 19 km where we reach 8 km/s velocities characteristic of the Moho.
The Tau-sum solution presents a ‘high-velocity kink’ at 6 km and could be due to interpretation of pre-critical arrivals.
The slope-intercept solution shows an important velocity jump from 4 to 5.8 km/s that could be generated by refraction at the top crystalline basement around 8.5 km.

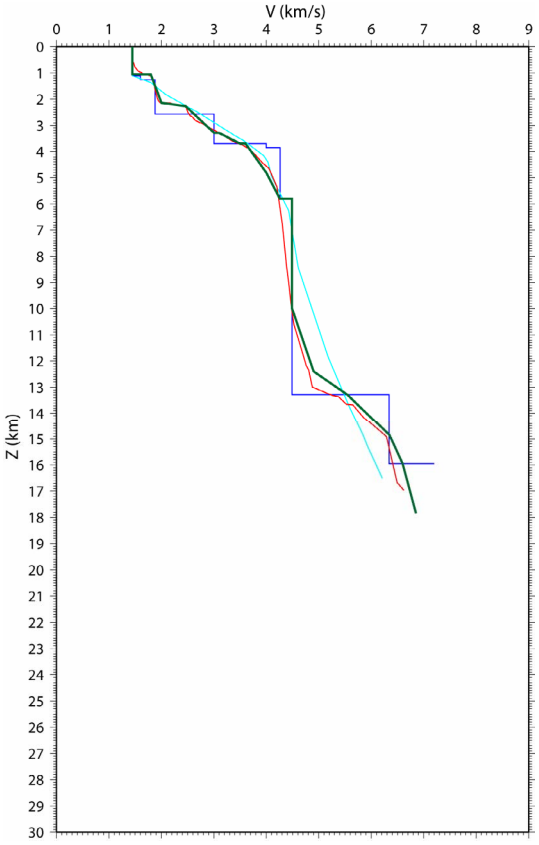

Figure 4.18: ESP 85

This ESP has a NW-SE orientation and spreads along the western boundary of the Helland Hansen Arch (Fig. 4.1).
The plot shows a good correspondence between the inverse solutions. The common velocity-depth function provides information down to 20 km depth. The sedimentary sequence, down to 5.5 km, is defined by a high velocity gradient, followed by a thick layer with a constant velocity of 4.5 km/s which could be associated with Cretaceous sediments. The slope-intercept solution indicates a significant velocity jump around 13.5 km and we reach values higher than 6 km/s characteristic of crystalline basement.

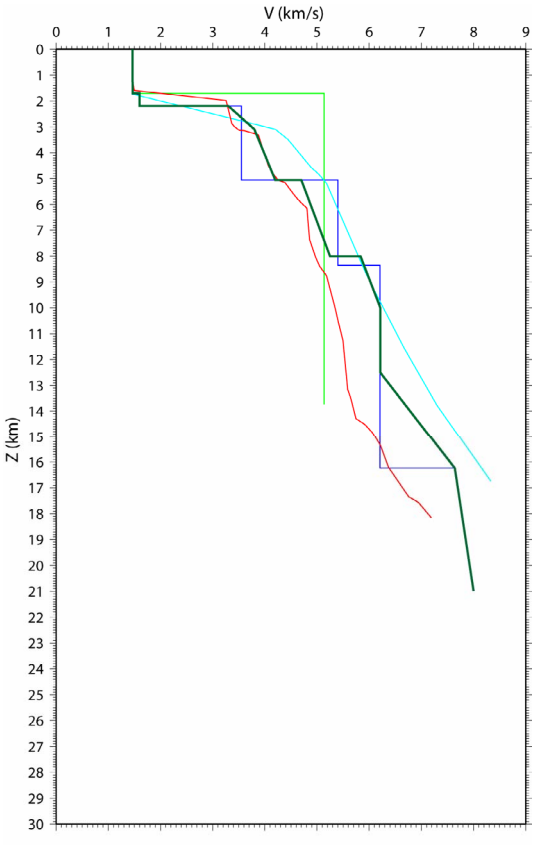

Figure 4.19: ESP 86

This NW-SE trending ESP is located close to the southern part of the Jan Mayen Fracture Zone (Fig. 4.1) and within an area covered by Palaeogene volcanic.
The common velocity-depth function was difficult as the inverse solutions do not show a good correspondence. This could be explained by the location of the profile and the fact that the seismic response is affected by the volcanics.
The shallow sedimentary sequence is characterized by a very high velocity gradient. This feature can be interpreted as Tertiary lavas.
We reach Moho velocities at 21 km depth.

5. MCS lines

This chapter presents the results of the interpretation of five multichannel seismic (MCS) lines crossing the transition between the Møre and Vøring margins. These lines have a NW-SE orientation and extend from the northern part of the Faeroe-Shetland Escarpment, crossing the Vøring Basin, the Halten Terrace and ending in the Froan Basin to the east (Fig. 4.1).The selection of key profiles for this study is based on the fact that they cover the main part of the continental margin in this area. The selected seismic lines are also crossing the ESP profiles analyzed in the previous chapter and a number of OBS crustal transects. The velocity information obtained from the ESP's together with OBS and sonobuoys data will allow us to depth convert our seismic lines. The depth converted profiles are then used as input for gravity modelling in chapter 6.

5.1. Presentation of the MCS data

The interpreted data set includes two multichannel seismic lines from the 2D survey GMNR-94 shot in 1994 at the Mid-Norwegian margin for WesternGECO. We also have three lines from the 2D survey VMT95 shot in 1995 over the Møre/Vøring margins for TGS-NOPEC. The profile length varies from about 200 to 225 km for the VMT95 profiles and the two lines from the GMNR-94 survey, indicated in red on Figure 4.1**,** extend over nearly 315 and 400 km respectively. The depths in two-way traveltime of the VMT95 and GMNR-94 lines are 12 and 14 seconds respectively.

Each MCS line is actually composed by a number of segments but as these are closely connected and have similar orientations, we consider them as five continuous seismic lines. Our key lines are migrated and of general good quality which means that there is a good correlation between the seismic traces and that we have continuous reflectors with strong contrasts. This implies also that we have good horizontal and vertical resolution. The continuous prominent reflectors observed on the seismic lines do usually belong to the Tertiary and Cretaceous sedimentary sequences. Though, in the western part of the lines, the

presence of igneous intrusions and extrusions that follow the stratigraphy make it difficult to correlate the seismic reflectors. It also happens that some of horizons from the Cretaceous sequence disappear or become chaotic in some areas along the lines. Problems in the seismic interpretation can also rise from the complex structural configuration in our study area. Structural highs and fault complexes mask geological information and can create seismic noise which adds some difficulties to the correlations of the horizons in the deeper parts of the profiles.

Attempts have been made to identify the top of the basement within which we do not observe seismic reflections. The basement is usually defined as a strong reflector due to high velocity contrast between the overlaying sedimentary layers and the crystalline crust. In very deep sedimentary basins this contrast is reduced due to compaction of the deep sedimentary fill resulting in high velocities approaching those of crystalline basement rocks. Strong reflections, possibly identified as top basement, can be observed along the profiles, but it is rather difficult to constrain this boundary with only MCS data. Therefore, we need gravity and refraction data to position the top of the crystalline crust on our profiles.

5.2. Interpretation and digitalization of the seismic profiles

We introduce here the interpretation procedure for the five multichannel seismic lines that compose our data set. A number of chosen reflectors are identified on all the profiles and this task was executed by tying the lines to the large seismic database available at the University of Oslo. We used information from crossing MCS lines, from wells located in our area and from profiles published in earlier works (Blystad et al. 1995).

The aim of this chapter is the interpretation of our key profiles with emphasis on the sedimentary sequences down to the base Cretaceous. We will also focus on identifying the main faults and deeper structures in order to get a good overview of the basin structure along the profiles. The seismic interpretation was done on paper with the sections in two-way traveltime. Finally, the interpreted seismic lines were depth-converted using the velocity-depth information from different data sets.

5.2.1. Interpretation procedure

The seismic interpretation was carried out based on:

- information provided by profiles and the structural map from Blystad et al. (1995) (Figs. 4.1 and 5.1)
- information from wells located in the area
- correlation of the interpreted horizons between the key profiles using tie lines

Profiles JJ' and KK' from Blystad et al. (1995) (Fig. 5.1) provide useful information about the stratigraphy at their tie points with lines GMNR-94-104 (west of the Modgunn Arch) and VMT95-005 (west of the Vingleia Fault Complex) respectively (Fig. 4.1). We also had a closer look at the southern part of profile FF' over the Halten Terrace as it is located north and parallel to the line GMNR-94-310. It provides relevant information about the succession and age of the main sedimentary sequences in the Halten Terrace area.

Two wells are of particular importance for our seismic interpretation. Well 6406/03-2 can be projected on the two northern profiles: GMNR-94-310 and VMT95-007. This well was drilled by Statoil in the Haltenbanken area and its completion log gives us information about the depth in twt to a number of key sedimentary horizons such as base Pliocene, base Eocene, base Paleocene, top Coniacian and base Cretaceous. The other well, 6406/11-1, ties the seismic interpretation on line VMT95-005. This well was drilled by SAGA Petroleum down to Late Triassic strata and is located near the southern end of the Halten Terrace on the western slope of the Frøya High. Additional MCS lines and wells, as well as interpreted seismic profiles from Flakstad (1998), were used for the correlation between our lines. Using these information, we have been able to correlate the interpreted horizons down to base Cretaceous between all our key profiles.

Figure 5.2 shows the interpretation of part of one of the key profiles with the names of all interpreted horizons from the sea floor to the base Cretaceous, and the abbreviations are explained in the figure caption. A geological time scale is also shown to remind the stratigraphic succession and age of the sediments.

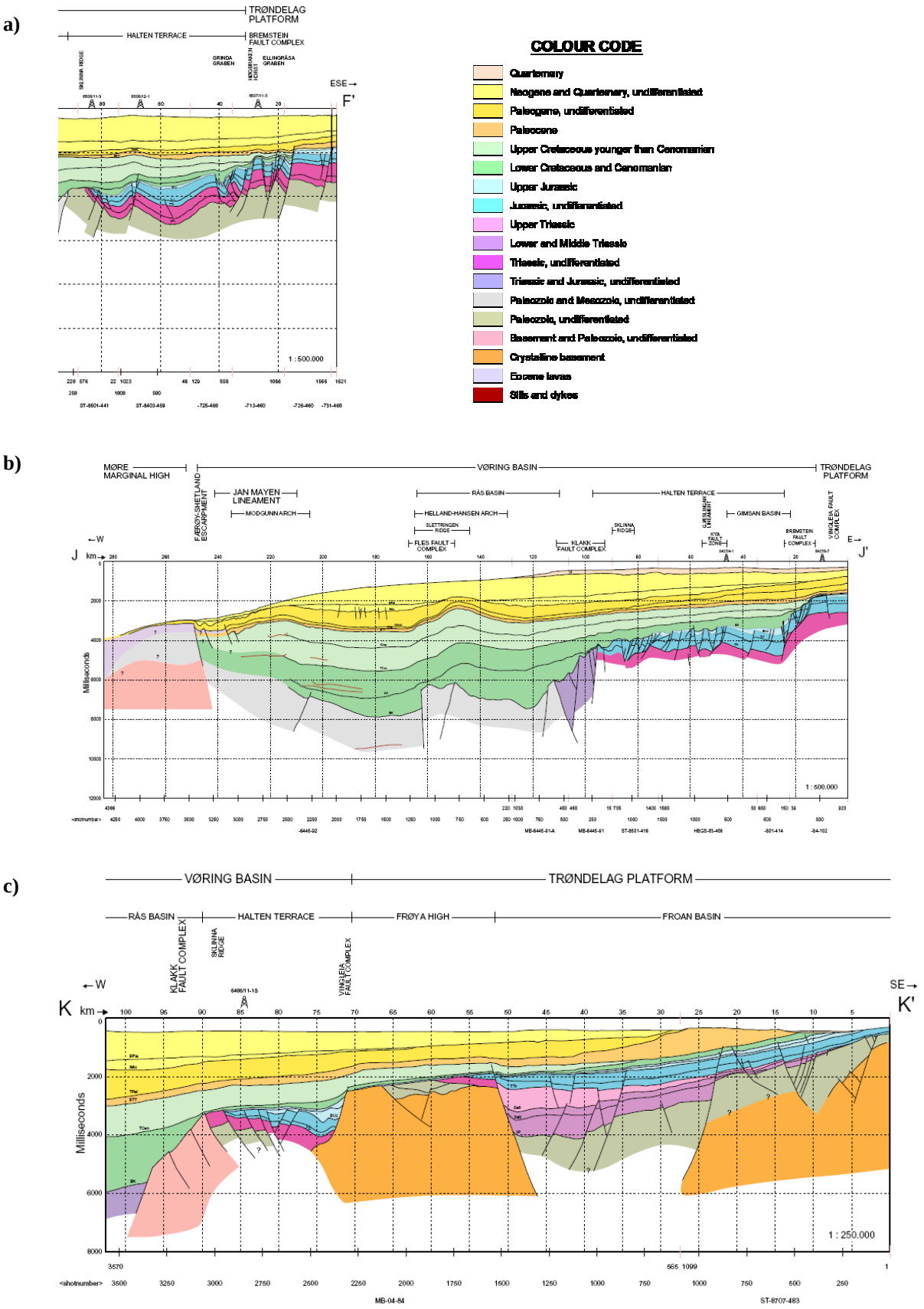

Figure 5.1. Figure presenting selected profiles from Blystad et al. (1995) that provided information for our seismic interpretation. a) Southern part of profile FF' over the Halten Terrace, it is located north of the MCS line GMNR-94-310. b) and c) Profiles JJ' and KK' have tie points with 2 of our key profiles (see Figure 4.1 for the location of the lines)

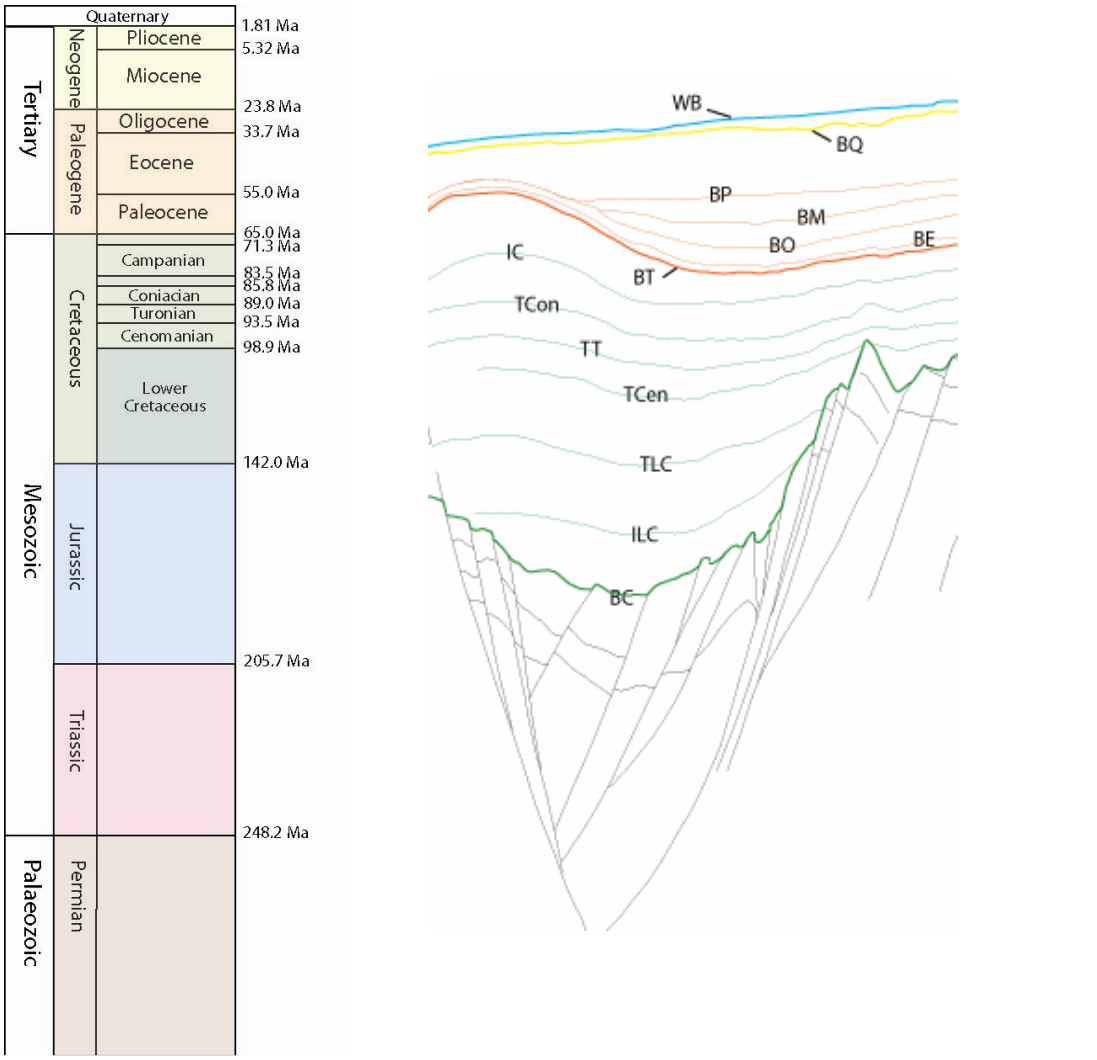

Figure 5.2. Figure showing a geological time scale together with the interpretation of one of the key seismic lines with its identified horizons: WB, water bottom; BQ, base Quaternary; BP, base Pliocene; BM, base Miocene; BO, base Oligocene; BE, base Eocene; BT, base Tertiary; IC, intra Campanian; TCon, top Coniacian; TT, top Turonian; TCen, top Cenomanian; TLC, top Lower Cretaceous; ILC, intra Lower Cretaceous; BC, base Cretaceous.

5.2.2. Seismic profiles in two-way travetime (s)

After finishing the interpretation of our key profiles on paper, we digitized them using the program SECTION (Planke, 1993). This program is used for digitizing and display of seismic sections

The plots from SECTION were modified a little by adding some colours, names of structural elements and abbreviations for the different interpreted horizons (Figs 5.3 to 5.5).

The colour code for the profiles is the following:

- **Blue**: water bottom
- **Yellow**: base Quaternary
- **Orange**: Tertiary, from base Pliocene to base Tertiary (indicated in thick orange)
- **Green**: Cretaceous horizons with the base Cretaceous in thick green.
- **Red**: Igneous intrusions (sills)

5.3. Depth conversion

The interpreted key profiles (Figs. 5.3 to 5.5) were then depth converted using velocity information from the wide-angle ESP, OBS and sonobuoys. Wide-angle seismic data limit some of the uncertainties for the positioning of deep interfaces such as the top crystalline basement, the top of the lower crustal body and the Moho. Gravity modelling (chapter 6) further constrain the deep crustal structures. The upper part of the transects shows many details whereas the lower part of the models is smoother.

5.3.1. Selection and projection of seismic velocities

In order to perform depth conversion, we had to find the velocity information available close to the location of our seismic lines. We used the program VELO (Planke, 1993) to list the velocity-depth profiles inside the study area. We retrieved with VELO seismic refraction and wide-angle reflection derived velocities, i.e. ESP and sonobuoys data. These data were then projected on the MCS lines following the structural trend. We also projected velocity information from published OBS transects (Fig. 5.6). We put more value on the ESP and OBS data as the sonobuoys in this area only provide velocity information down to shallow depths. Figure 5.6 shows the velocity-depth profiles that were used for the depth conversion.

We selected a number of velocity stations along each MCS line in order to perform depth conversion. The velocity stations were chosen among the available ESP, OBS and sonobuoys data. Their positions along the MCS lines corresponded to the crossing point of the velocity-depth profile with the seismic line or projected velocity stations. The projection of the velocity-depth functions was done along the structural trend and based on a study of the regional geology.

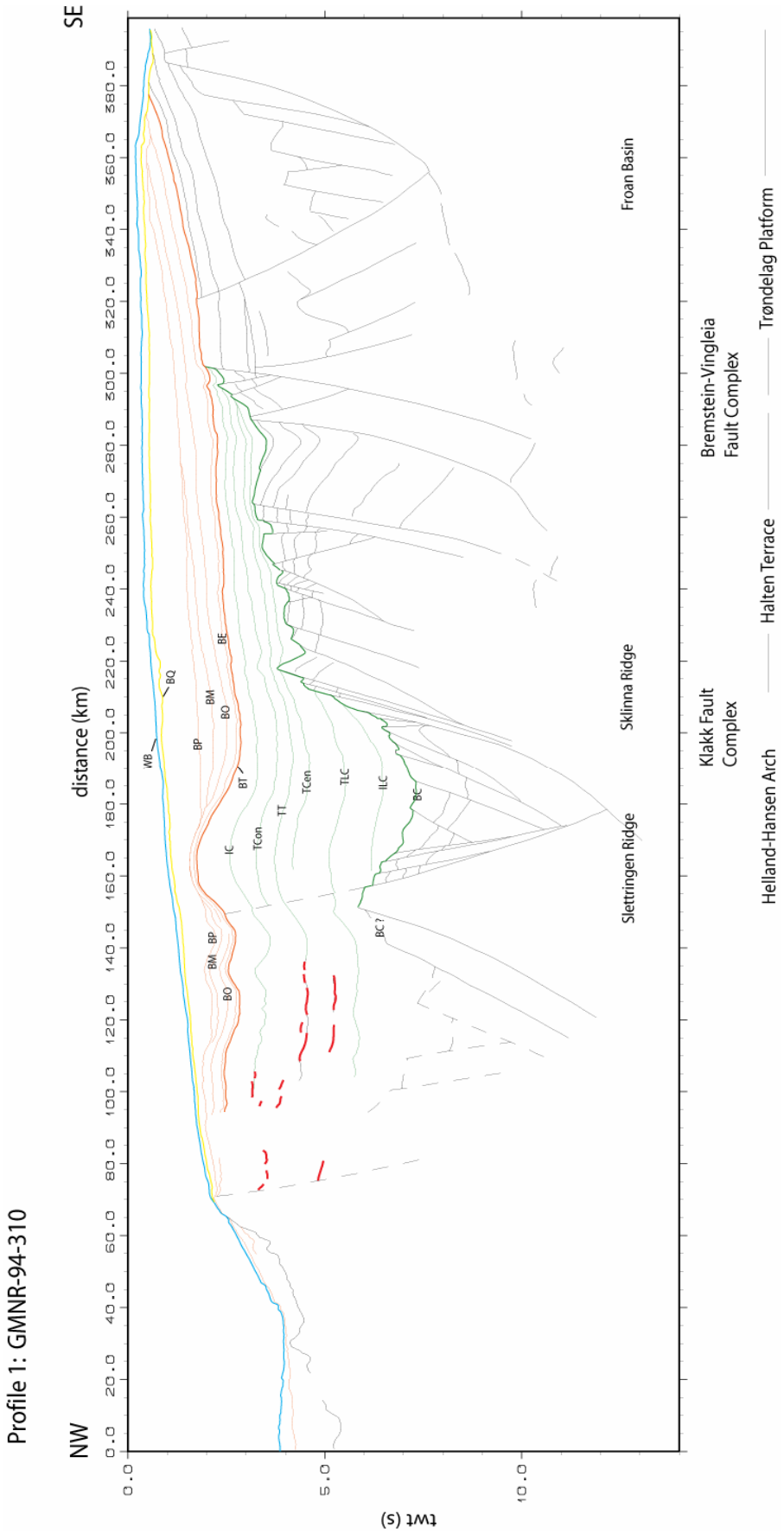

Figure 5.3. Interpretation of the seismic profile GMNR-94-310 in twt (s). Location of the profile in Figure 4.1.

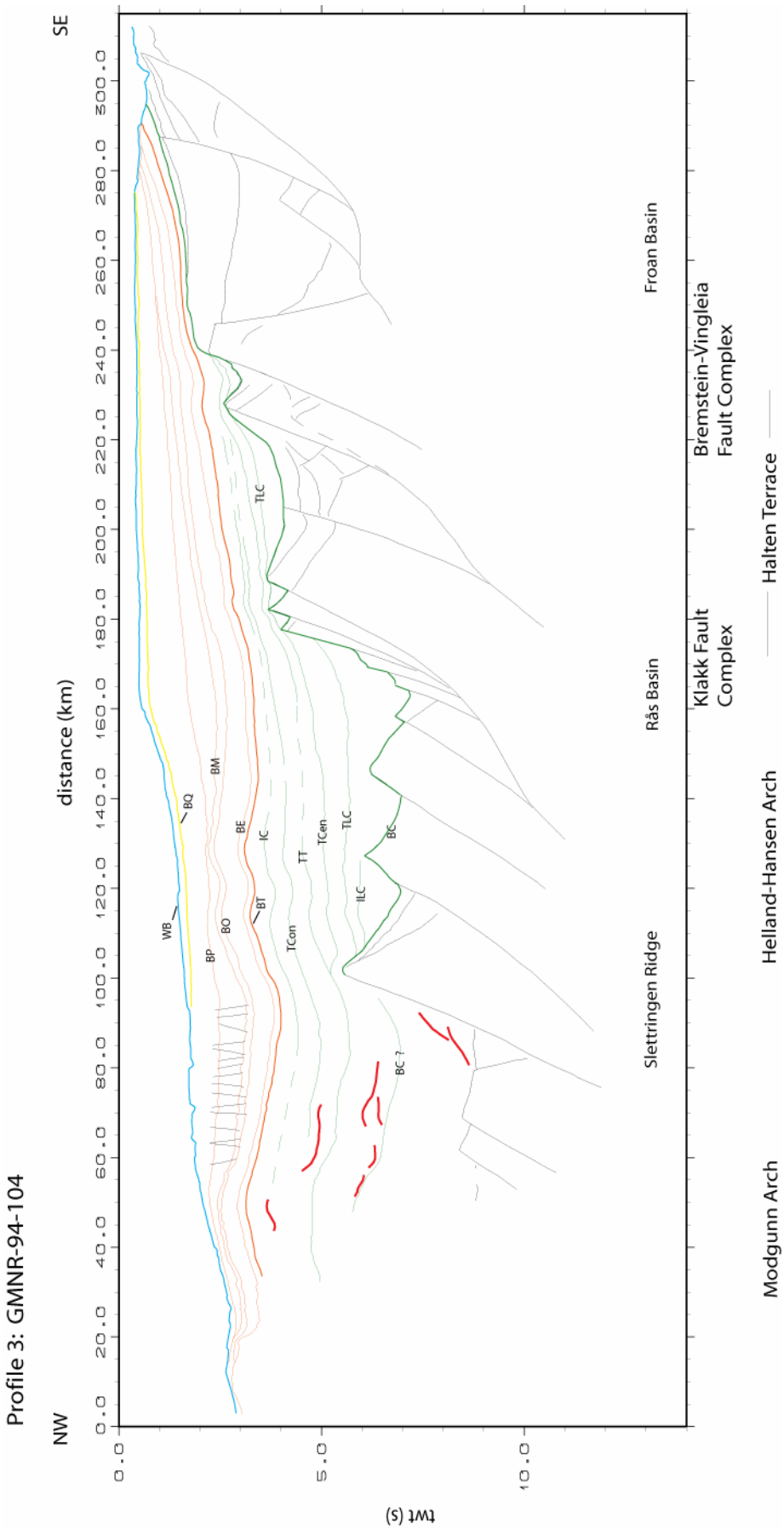

Figure 5.4. Interpretation of the seismic line GMNR-94-104 in twt (s). Location of the profile in Figure 4.1.

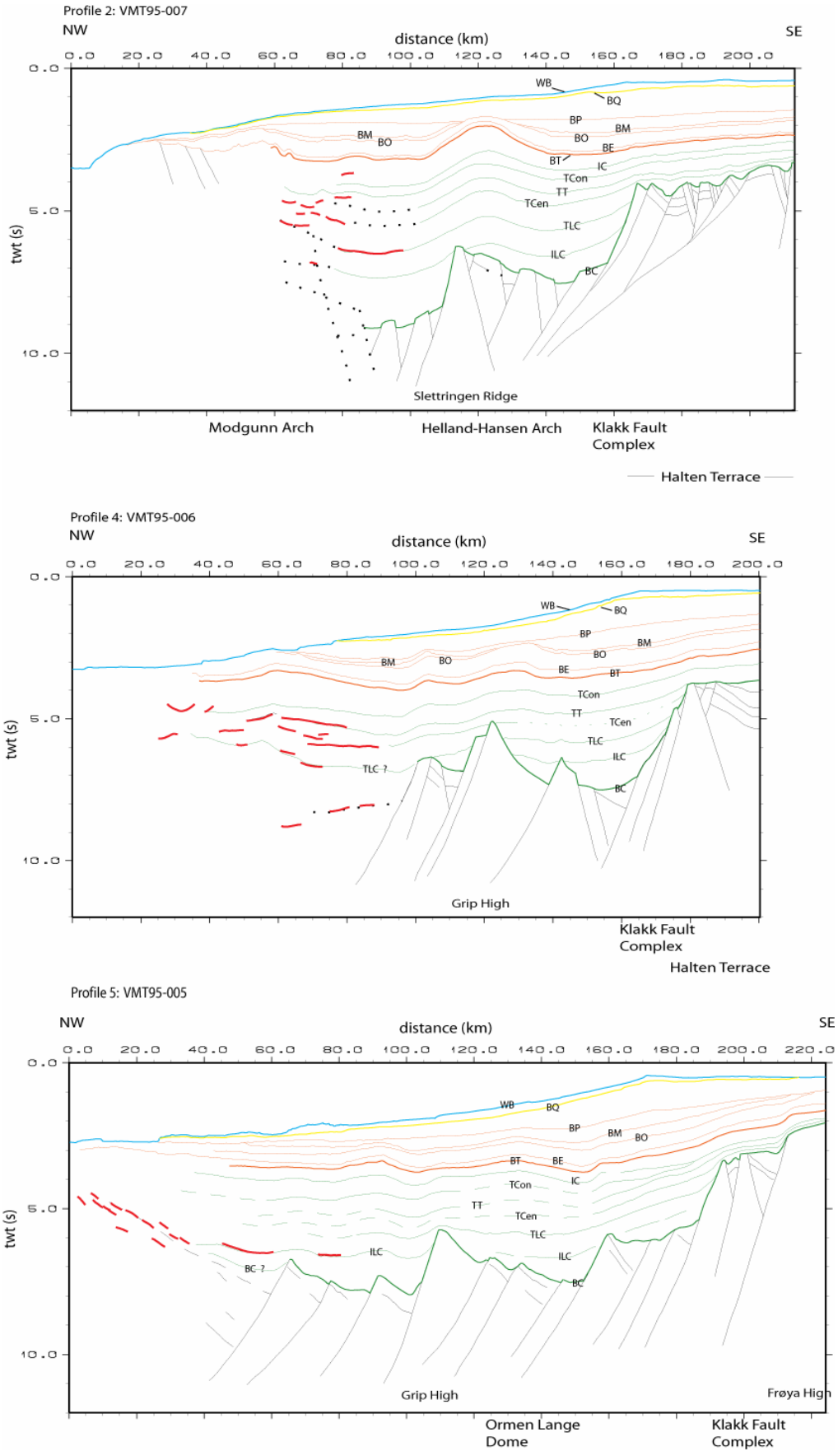

Figure 5.5. Interpretation of the three VMT95 lines from north to south: VMT95-007, VMT95-006, VMT95-005. Location of profiles in Figure 4.1.

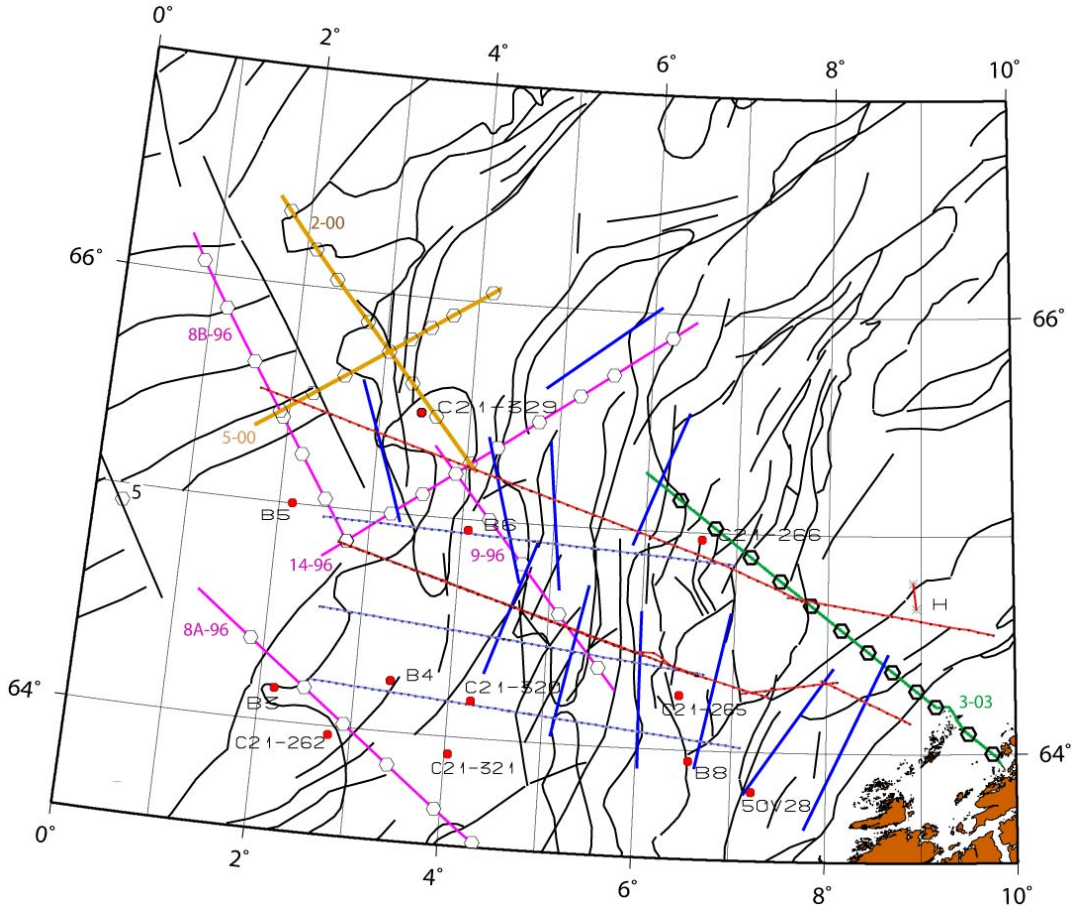

Figure 5.6. Map indicating the location of the velocity information used for the depth conversion of our interpreted profiles. The red and light blue lines correspond to the MCS lines. The dark blue segments indicate the location of the ESP profiles. The pink, light brown and green lines are the useful OBS transects and the red points show the position of the different sonobuoys.

The OBS data provide very useful and reliable velocity information down to greater depths. In our study area, we have 7 OBS transects, and five of them are presented in the next section of this chapter. The latest one (3-03) is not published yet (Raum et al., in prep). OBS profiles constitute very good velocity stations at the locations where they intersect the MCS lines.

The ESP velocity-depth functions documented in chapter 4 were also used. As these profiles often have offsets up to 100 km, we have to be careful where to position the ESP velocity stations. If the ESP profile follows the structural trend, the corresponding velocity-depth function is plotted at the crossing point of the profile and the MCS line. In the opposite case, we project the midpoint of the ESP profile along the structural trend onto the seismic line.

5.3.2. ESP data

In this section, we present our interpreted seismic profiles on which we project the ESP velocity-depth functions that we have selected for the depth conversion (Figs. 5.7 to 5.11). On these figures we have also indicated the location of the other types of velocity stations that we have along the profiles. The small legend below explains the symbols that we have used on top of each line:

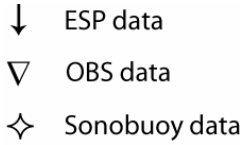

A general observation for all profiles indicates that the velocity jumps or changes in velocity gradient with depth tend to match the main reflectors we have interpreted. Even if we do not have a good match in some cases, the velocity information projected on the profiles shows reasonable values compared to the typical velocities for the different sedimentary sequences at these locations and depths.

Inconsistencies between the seismic reflectors and the velocity jumps from the projected functions are mainly due to the distance of the ESP's midpoint from the MCS line. The depth to important reflectors can be modified over short distances by complex geology and bathymetric changes

Profile 1: MCS line GMNR-94-310

The ESP's midpoint are located south of the MCS line. The depth to the sea floor from the velocity-depth functions matches the seismic data (Fig. 5.7). We have velocities down to a depth of 10 s (twt). Basement velocities, typically 6+ km/s, are observed below or rather close to the interpreted pre-Cretaceous reflections. We notice that the velocities increase faster for ESP 86 located to the west on the profile.

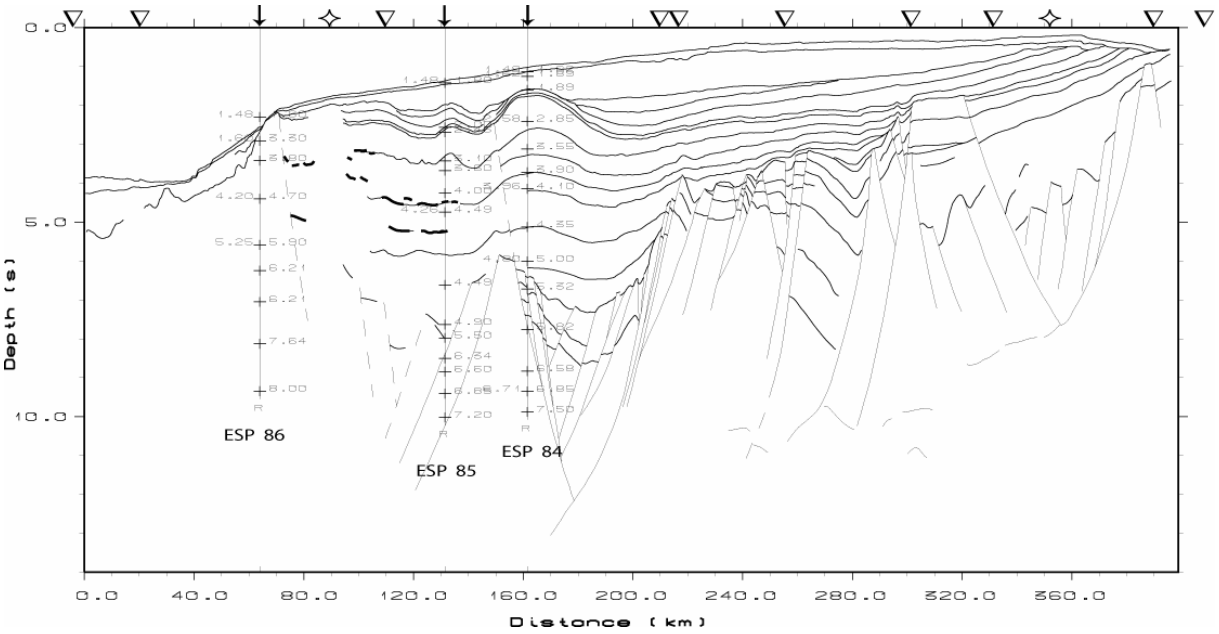

Figure 5.7. Profile 1: GMNR-94-310 in twt (s) with projected ESP velocity-depth functions

Profile 2: MCS line VMT95-007

This profile has only one projected ESP velocity-depth function (Fig. 5.8). The velocity stations along the line are mostly from OBS data. We notice that the velocity changes with depth do not really match the interpreted reflectors. The ESP's midpoint is not located too far from the MCS line but the ESP profile is located across the Slettringen Ridge making it difficult to project the data.

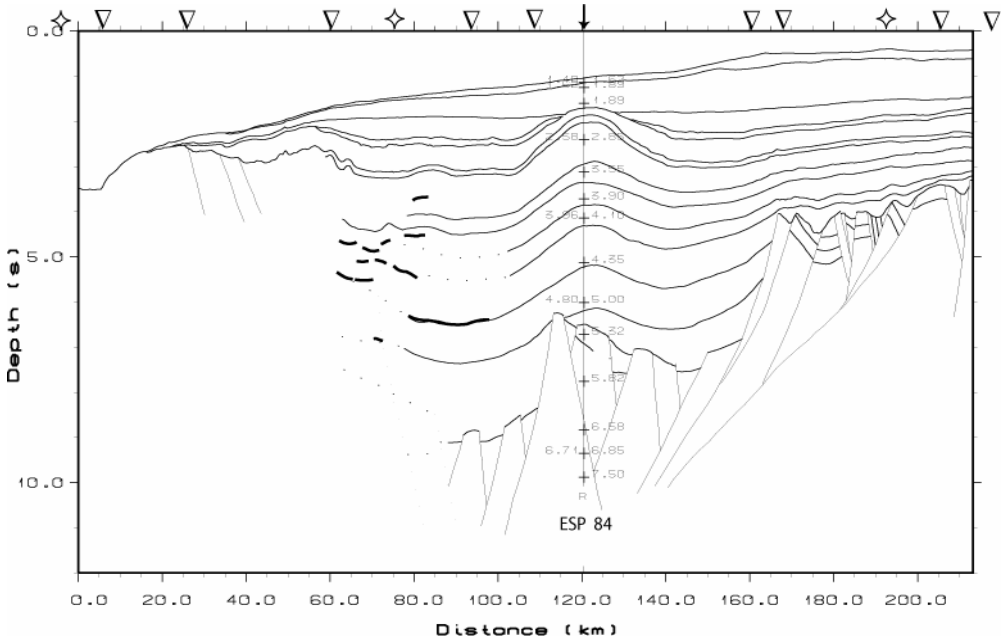

Figure 5.8. Profile 2: VMT95-007 in twt (s) with projected ESP velocity-depth functions.

Profile 3: MCS line GMNR-94-104

Five ESP velocity-depth functions have been projected on this profile (Fig. 5.9). We observe important discrepancies in the depth to the sea floor for ESP 87 and ESP 34 which can possibly be related to important bathymetric changes along the ESP profiles. The three other projected velocity-depth functions show a good match between the data sets.

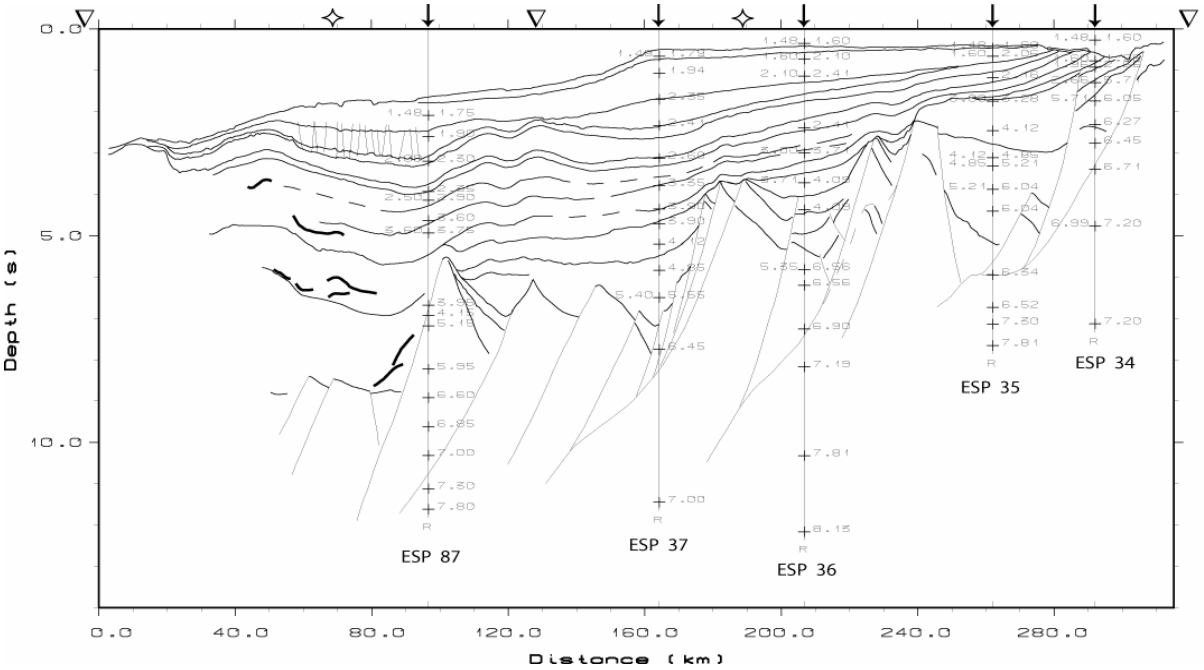

Figure 5.9. Profile 3: GMNR-94-104 in twt (s) with projected ESP velocity-depth functions

Profile 4: MCS line VMT95-006

This profile has many sonobuoy data associated velocity stations which provide bad velocity information at greater depths (Fig. 5.10). This will leave us a certain liberty for the modelling of the deeper structures to the west of the profile. The ESP projected data matches very well the seismic and similar velocities can be correlated along the same sedimentary sequences.

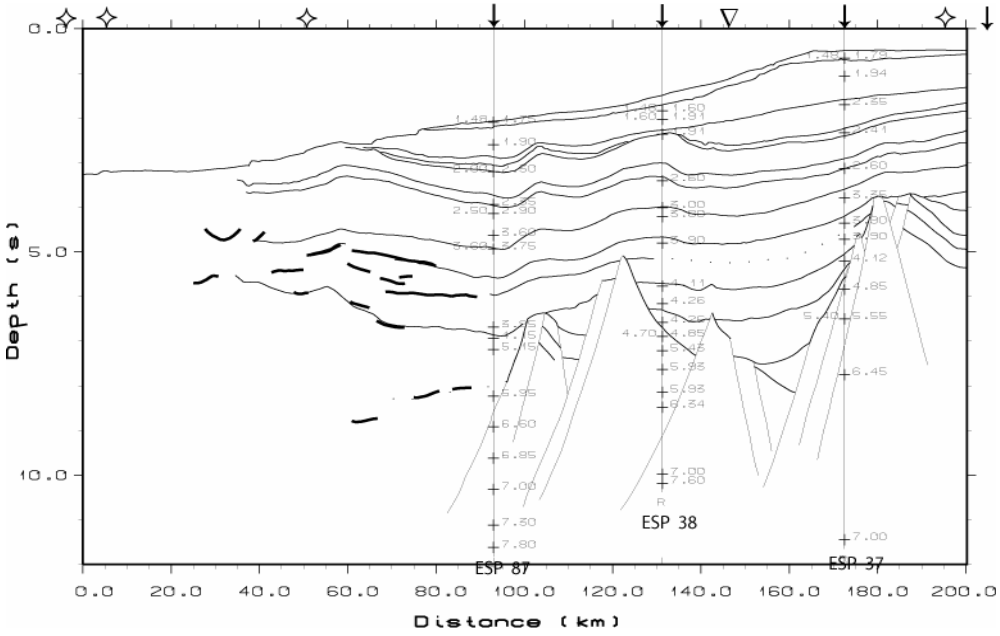

Figure 5.10. Profile 4: VMT95-006 in twt (s) with projected ESP velocity-depth functions

Profile 5: MCS line VMT95-005

As for profile 4, we have an important number of sonobuoy related velocity stations especially to the west of the profile. The ESP projected velocities are all located to the east and give information down to 12 s (twt). The ESP's midpoints are located north of the seismic line, which can explain the small discrepancies for the depth to the sea floor and to the main reflectors, but we still achieve a rather good match between the two data sets.

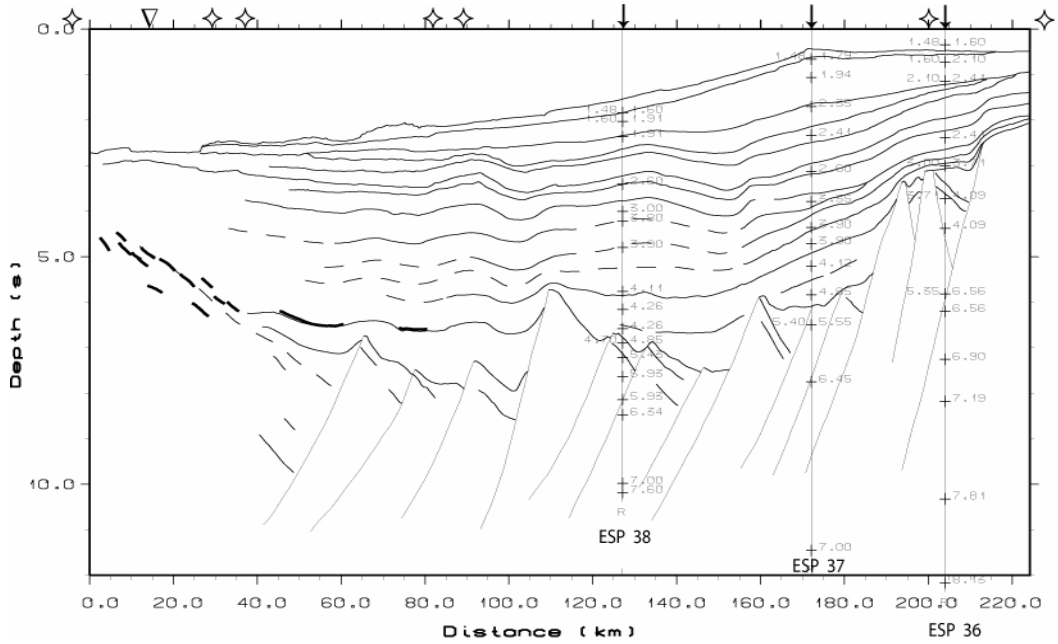

Figure 5.11. Profile 5: VMT95-005 in twt (s) with projected ESP velocity-depth functions

5.3.3. OBS data

The OBS transects that are located within the study area, in the vicinity of the interpreted MCS lines, comprise profiles 8A-96, 8B-96, 9-96, 14-96, 2-00, 5-00 and 3-03 (Fig. 5.6). The seven profiles were acquired respectively in 1996, 2000 and 2003 by the University of Bergen using the vessel *Håkon Mosby*. The profiles from 1996 are part of a regional survey performed in the southern Vøring Margin and northern Møre Margin. The articles from Raum et al. (2002 and 2006) present the final velocity models for the OBS profiles 8B-96, 9-96, 14-96, 2-00 and 5-00 (Figs. 5.12 The velocity model for the OBS transect 8A-96 (Raum, 2000) is shown in chapter 7 (Fig. 7.7). The final results for the profile 3-03 have not been yet published (Raum et al., in prep). The OBS transects have 2 different orientations: one group of lines with a NW-SE trend (8A-96, 8B-96, 9-96, 2-00 and 3-03) and another group where the profiles have a SW-NE orientation and perpendicular to the first group of transects.

The OBS transects gives us estimated P-wave velocities from the seafloor to the Moho. OBS data were modelled by a combination of inverse and forward modelling. Though, we should be careful when using OBS transect 14-96. On the SW side of the profile, we see that the Moho is very shallow as expected for normal oceanic crust, but the profile terminates landward of the continental-ocean boundary. So to infer that the Moho is at a depth of about 12 km would be incorrect (Asbjørn Breivik, personal communication). Table 5.1 indicates the velocity information from the OBS transects that are used for the depth conversion of our profiles

OBS transect	Position (OBS profile)	Velocity station on profile
8A-96	90	VMT95-005
8B-96	90	GMNR-94-310
	160	VMT95-007
9-96	60, 80	VMT95-007
	120	GMNR-94-104
	130	VMT95-006
14-96	10	GMNR-94-104
	30, 80	VMT95-007
2-00	160	GMNR-94-310
5-00	30	GMNR-94-310
3-03	10, 20, 60	VMT95-007,
	10, 20, 60, 100, 130, 180	GMNR-94-310
	190	GMNR-94-104

Table 5.1: Table indicating the position of velocity-depth functions from the OBS transects and the corresponding seismic profiles they have been projected onto.

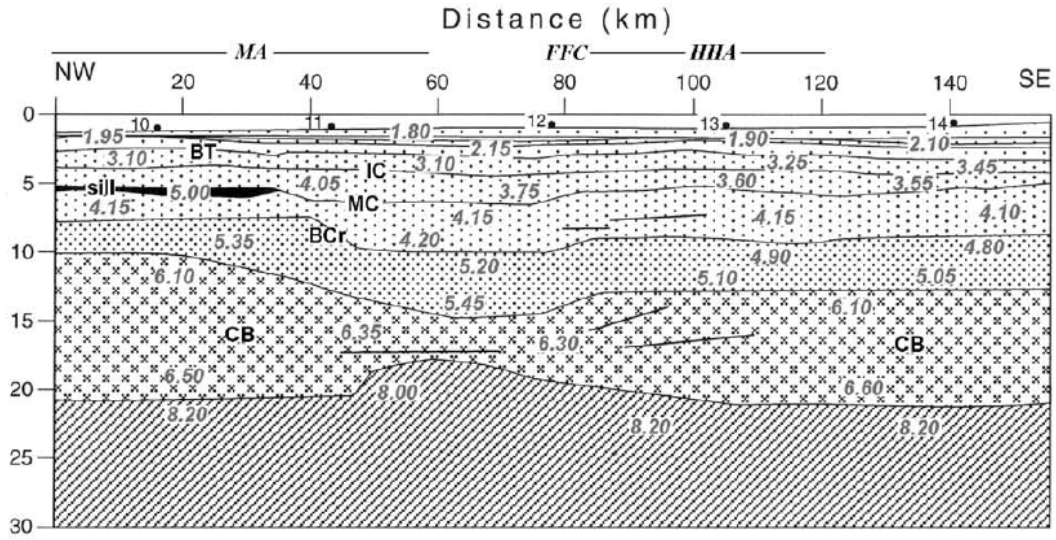

Figure 5.12. Final velocity model for OBS transect 9-96 (Raum et al., 2002). The profile intersects nearly all the MCS lines and we use the velocity information at the offsets 60, 80, 120, and 130. OBS are shown at the seafloor. FFC, Fles fault complex; JMFZ, Jan Mayen Fracture Zone; HHA, Helland-Hansen Arch; MA, Modgunn Arch; MMH, Møre Marginal High

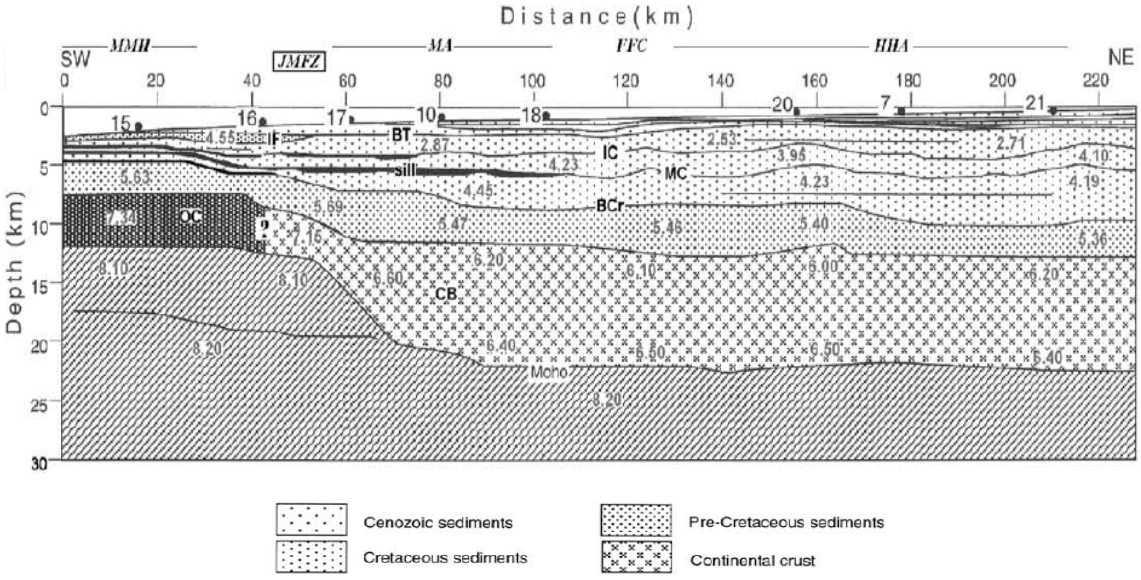

Figure 5.13. Final velocity model for OBS transect 14-96 (Raum et al., 2002). We use the velocity information at the offsets 10, 30, 60, and 80. OBS are shown at the seafloor. FFC, Fles fault complex; JMFZ, Jan Mayen Fracture Zone; HHA, Helland-Hansen Arch; MA, Modgunn Arch; MMH, Møre Marginal High

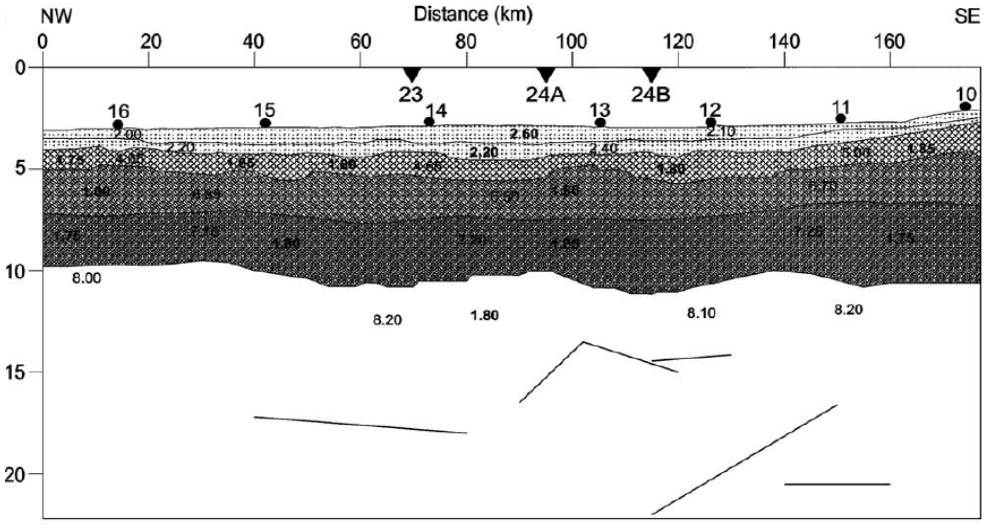

Figure 5.14. Final velocity model for profile 8B-96 (Raum et al., 2006) that provides a velocity station western end of MCS lines GMNR-94-310 and VMT95-007(at the respective offsets 90 and 160). P-wave velocities are shown in small numbers and bold numbers represent the Vp/Vs ratios. OBS positions are shown at the seafloor.

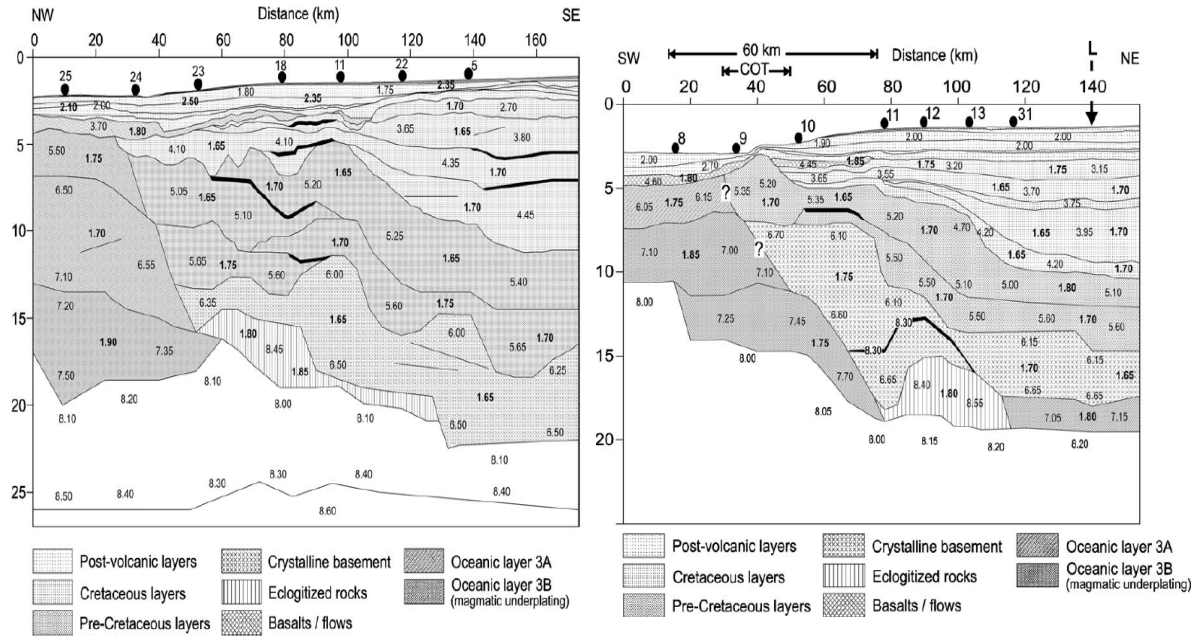

Figure 5.15. Final velocity models for profiles 2-00 and 5-00 (Raum et al., 2006). The velocity information at offset 160 on the profile 2-00 and at the offset 30 on the profile 5-00 provides two velocity stations for our MCS line GMNR-94-310. P-wave velocities are shown in small numbers and bold numbers represent the Vp/Vs ratios. OBS positions are shown at the seafloor. COT (continental-ocean transition)

5.3.4. Depth conversion procedure and resulting profiles

To depth convert our interpreted seismic profiles, we use the option ‘depth convert x-y section’ from the program SECTION. The input files are the section digitized file from the previous step and a parameter file containing the velocity-depth information for all the velocity stations along the profiles. The first and last stations need to be left and right of the minimum and maximum x-value of the seismic section. This x-axis has to be in kilometres and not in shotpoint numbers. As the velocity-depth functions have to go through the whole section, we indicate that the deepest velocity value stays the same all the way down to 99 km.

Each digitized point is depth converted separately using a linearly interpolated velocity-depth function at the given location. The two closest velocity stations are used for the interpolation. We then use the option ‘plot section’ and we obtain the depth converted profiles shown the Figures 5.16 to 5.18. The location of the velocity stations is indicated along the x-axis of each profile. The symbols are the same as used previously. These depth converted profiles are the input for the gravity modelling presented in the next chapter.

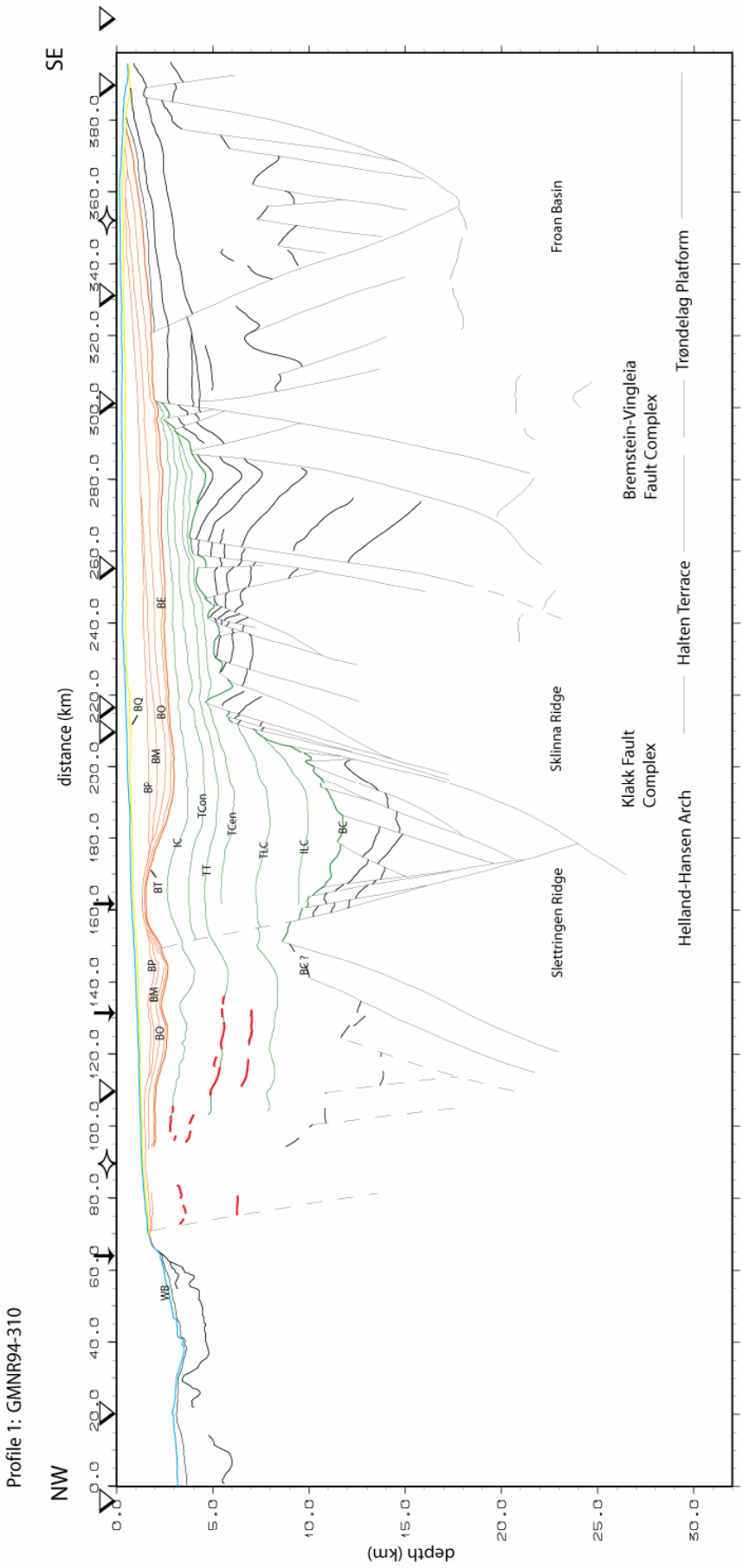

Figure 5.16. Depth converted interpretation of the seismic profile 1. Location of profile on Figure 4.1.

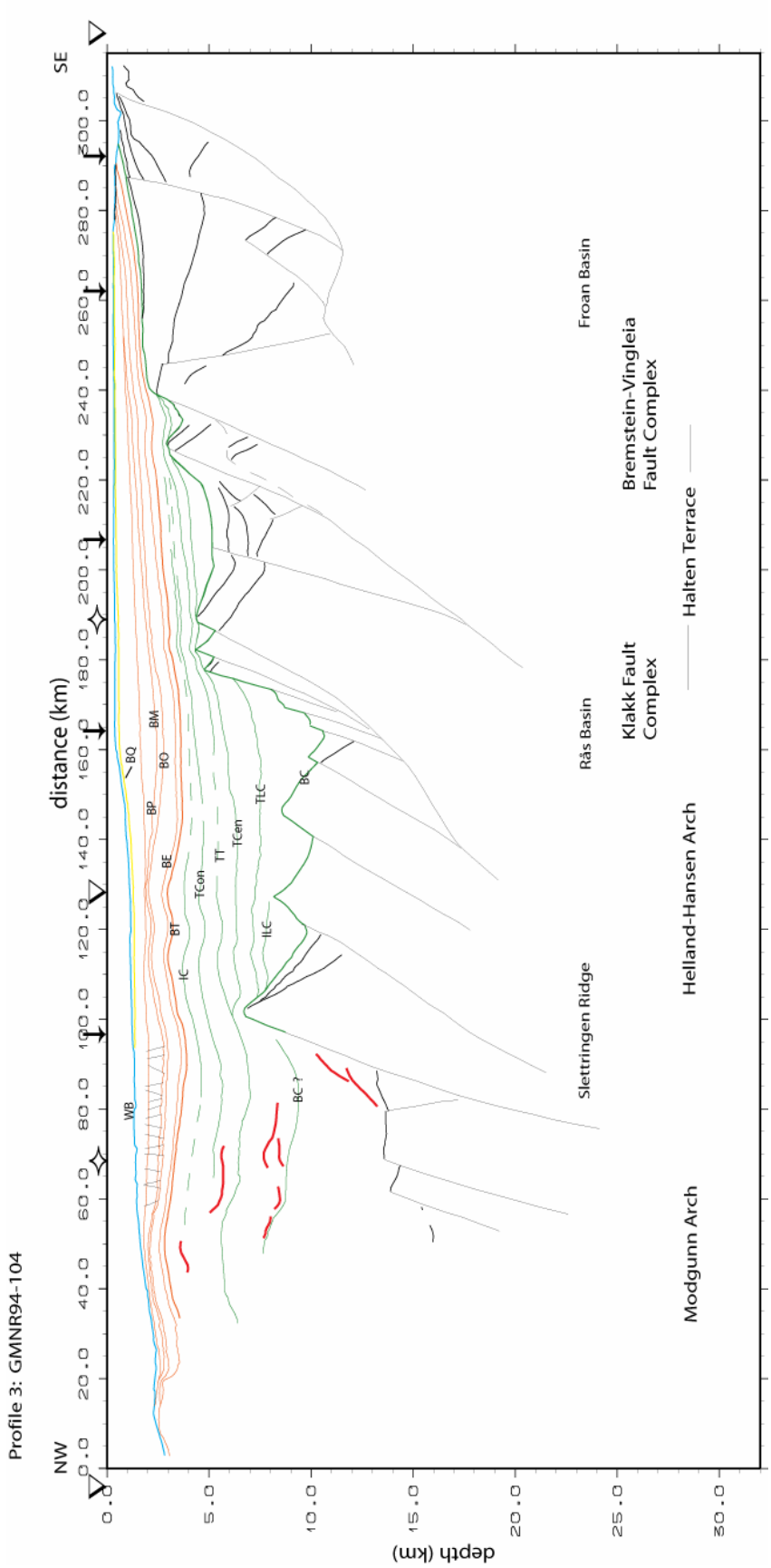

Figure 5.17. Depth converted interpretation of the seismic profile 3. Location of profile on Figure 4.1.

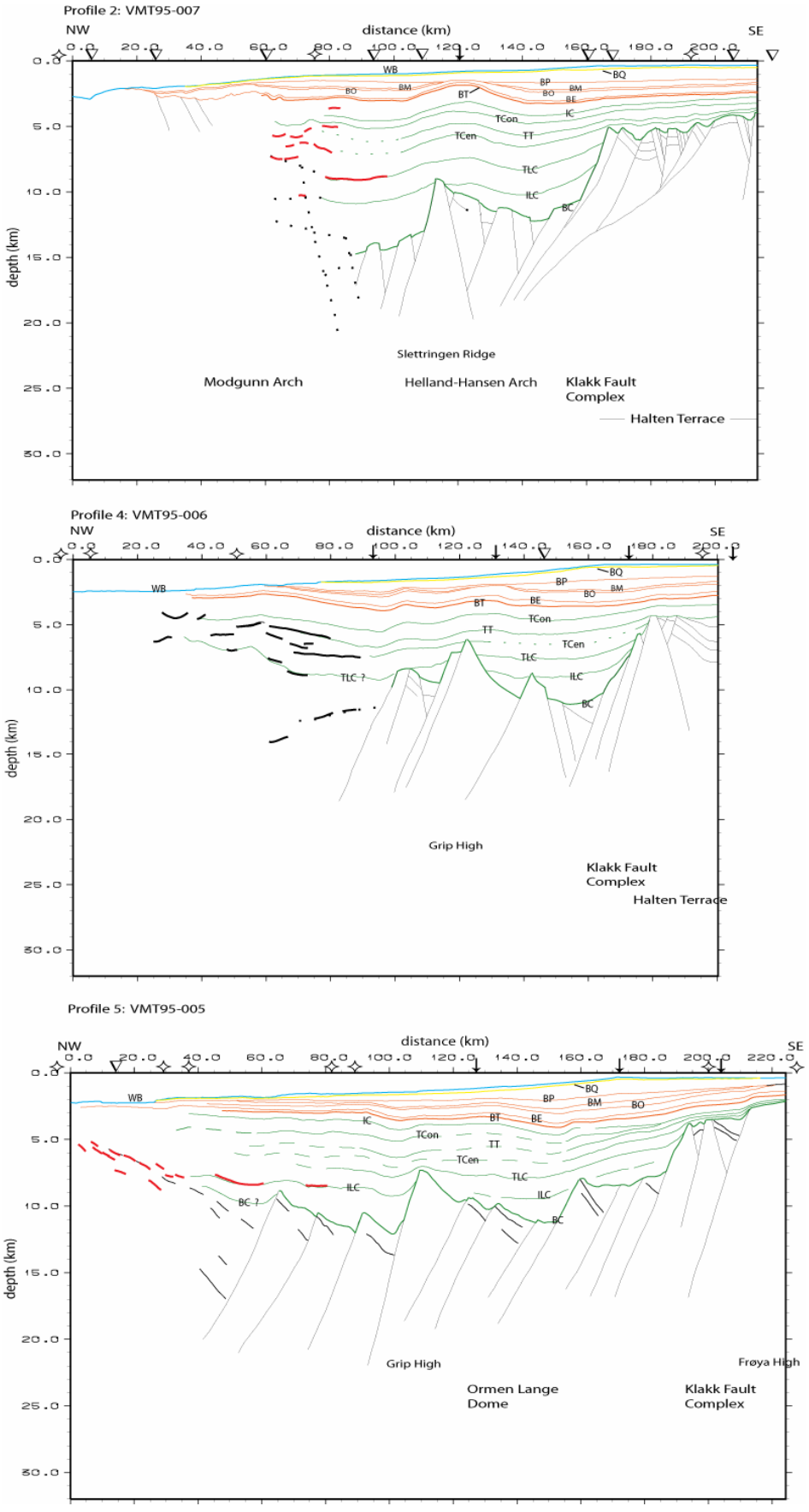

Figure 5.18. Depth converted interpretation of the three VMT95 profiles from north to south: VMT95-007, VMT95-006, VMT95-005. Location of profiles on Figure 4.1.

6. Gravity modelling

The aim of this chapter is the gravity modelling of the key profiles interpreted and depth converted in chapter 5. The gravity data help us to further constrain the main deep features that could not be determined by the use of MCS data only. It allows us to correlate some of the interpreted horizons towards the west of the profiles where the seismic data is masked by igneous material. The gravity modelling also provides a good test of the velocity models derived from the wide-angle seismic data. Using the MCS interpretation results with the final gravity models for each seismic line, we will then be able to construct deep crustal transects across the southern Vøring Margin along our key profiles.

6.1. Data

6.1.1. Potential field data

Our data set for the gravity modelling is composed by satellite based potential field data (Andresen and Knudsen, 1998) from the Norwegian Geological Survey (NGU) enhanced with ship track and land station measurements (Skilbrei et al., 2000). The data, in the marine domain, correspond to free-air gravity anomalies and have been interpolated using a 2x2 km grid. Figure 6.1 shows a free-air gravity anomaly map for the study area together with the geographical location of the key profiles. We also display the bathymetry for the same area (Fig. 6.2) as it might be relevant to do some observations when presenting the final gravity models for our profiles.

The gravity modelling is carried out using the GMSYS software (Northwest Geophysical Associates, Inc., www.nga.com). This program is an interactive modelling program that calculates the gravity and magnetic response of a geological model and tests its accuracy by comparing the calculated data to observed gravity and magnetic measurements. The model volume is divided into blocks shaped like tabular prisms and each block is associated with an average density value. The user-friendly interface makes the modelling fast and easy and provides many opportunities to constrain the model variables.

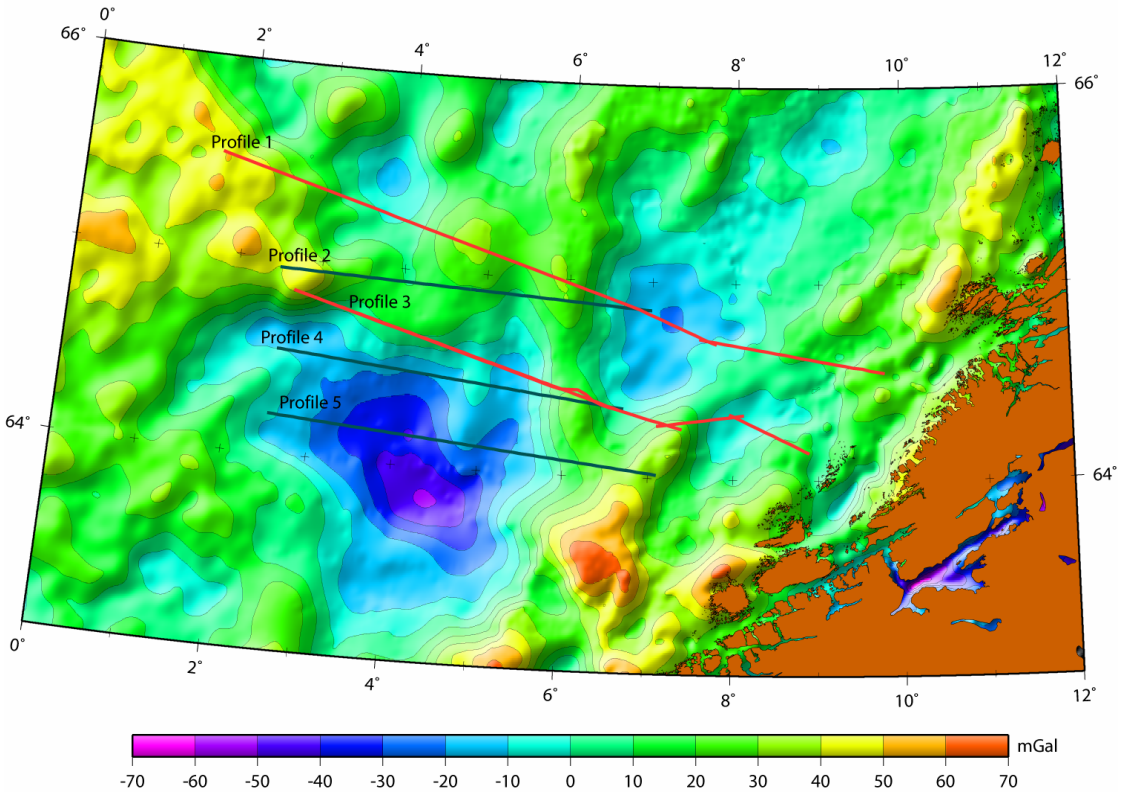

Figure 6.1. Free air gravity anomaly map for the study area. The figure also shows location of the five key profiles. [2]

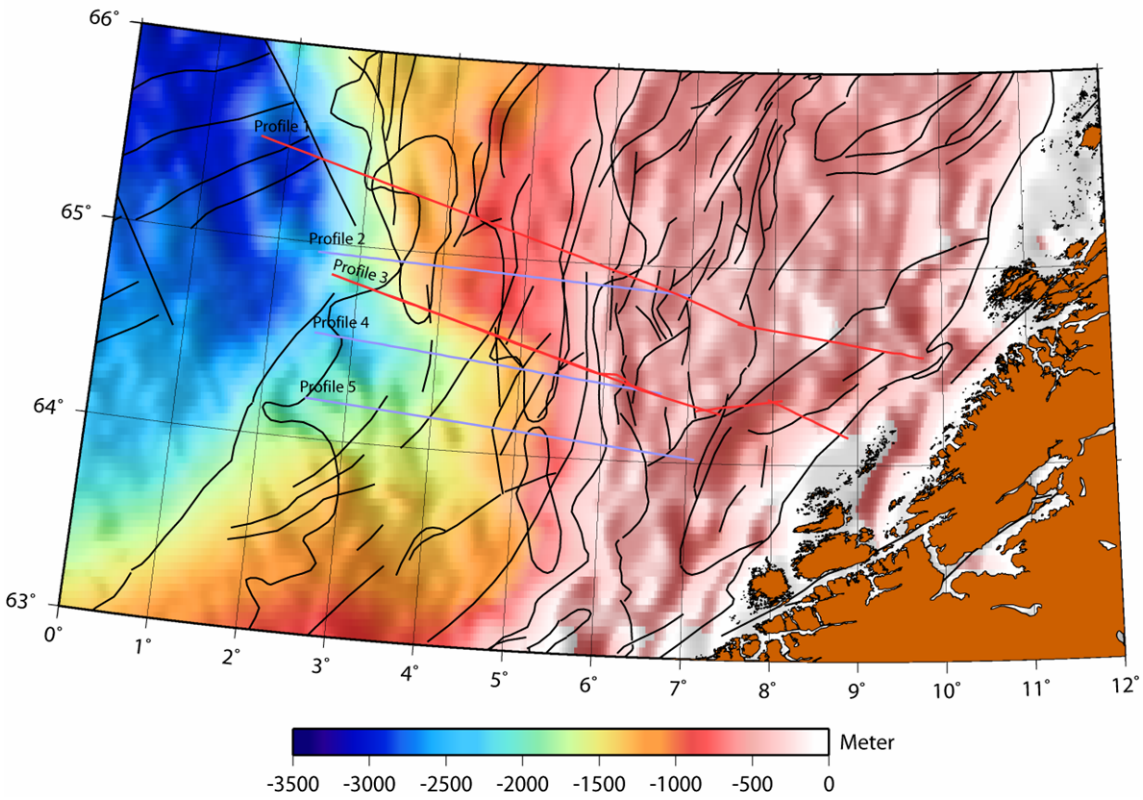

Figure 6.2. Map showing bathymetry and structural elements in the study area. Location of the key profiles is also shown.

6.1.2. Extracted gravity data along our key profiles

Figure 6.3 shows the extracted gravity data along the five profiles. The data were imported in GMSYS during the model build-up phase. More about the data extraction method is explained in the gravity modelling procedure below.

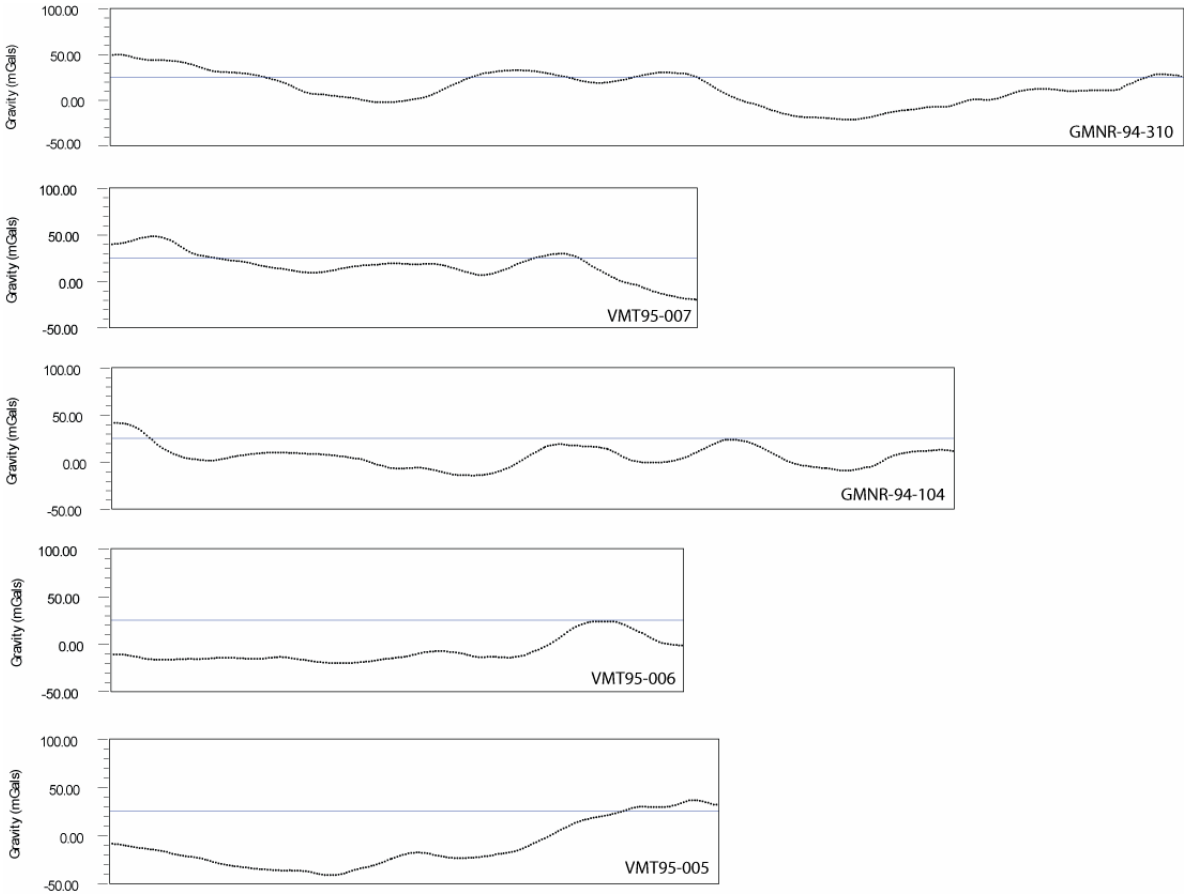

Figure 6.3. Extracted gravity data along each of the key profiles.

6.2. Gravity modelling procedure

The modelling procedure is divided into two stages:

- The first stage (model build-up) is the creation of the model by importing observed gravity data and a background image corresponding to the depth-converted seismic section. We then digitize the different interpreted horizons within GMSYS defining the model geometries.

- The second stage of the procedure is the model editing; repositioning of the horizons, testing of different densities based on velocity information, in order to obtain the best fit possible between the observed data and the model based gravity response.

6.2.1. Model build-up

Observed gravity anomaly

The curves from figure 6.2 are obtained using a script that extract, from the NGU potential field data, the observed gravity anomaly along each seismic profile. These observed curves are imported into GMSYS.

Block geometry

The creation of a new model into the gravity modelling software also implies the import of a background image. This image is here the digitized depth converted seismic section corresponding to the line along which we have extracted the gravity anomaly curve. The geological model is extended to infinity to remove the edge-effects in our gravity response calculations. The isostatic compensation depth is fixed at 100 km. The digitizing the model geometry is performed by adding, moving points and splitting blocks. At the end of this process, the original input section is divided into a number of blocks delimited by the interpreted horizons from the MCS data. The deeper layers of the model, i.e. top basement, top lower crystalline crust and Moho, with boundaries that are not observable in the multichannel seismic data, are positioned according to velocity information from ESP and OBS data.

Velocity to density conversion

The model is now divided into blocks following stratigraphic horizons for the upper crustal structure and constrained by velocity information for the deeper blocks; i.e. continental crust and upper mantle. The next step in the gravity modelling is to assign a certain density value for each of these blocks. The densities are chosen based on the velocities used in the depth conversion of the imported seismic section and on velocity ranges determined in our area of interest by Raum et al. (2002) for sedimentary units, crystalline crust and Moho. The

velocities are converted to densities using the Nafe-Drake relationship (Ludwig et al., 1970) averaging the velocity over individual blocks. The Nafe and Drake velocity-density empirical curves are shown in Figure 6.4.

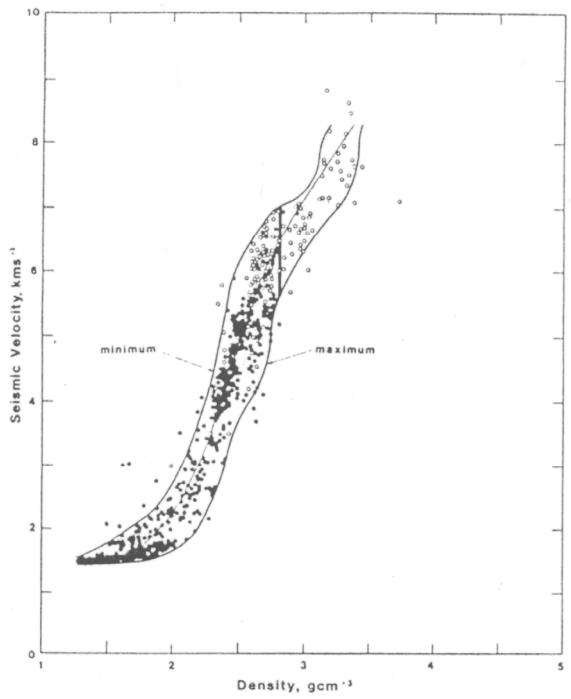

Figure 6.4. Laboratory measurement of P-wave seismic velocity and density in rocks (from Ludwig, Nafe and Drake, 1970). The thin line in the centre is the mean velocity density relationship commonly used for gravity calculations on seismic models.

Table 6.1 summarizes the velocity intervals and corresponding densities for the individual blocks composing the five gravity models presented in this chapter. The sedimentary units down to Upper Cretaceous are defined by the same density in all the models. The lower Upper Cretaceous, Lower Cretaceous and pre-Cretaceous density values vary from one model to the other. These variations are justified by the fact that equivalent sedimentary units can be buried to different depths in the five models and density is increasing with depth due to mechanical and/or chemical compaction. It is sometimes necessary to create sub-blocks with different density values within thick sedimentary units. Giving the same density to the whole block would not be a reasonable solution for the model.

Sedimentary sequence	Velocity interval	Density
Water layer	1.48 km/s	1.03 g/cm³
Pleistocene-Pliocene	1.7 to 2.3 km/s	2.05 g/cm³
Tertiary	2.3 to 3.0 km/s	2.2 g/cm³
Upper Cretaceous	3.2 to 3.8 km/s	2.35 g/cm³
Lower Upper Cretaceous	3.8 to 4.5 km/s	2.4 to 2.43 g/cm³
Lower Cretaceous	4.5 to 4.9 km/s	2.49 to 2.55 g/cm³
Pre-Cretaceous	4.6 to 5.5 km/s	2.5 to 2.63 g/cm³
Upper Crystalline crust	6.0 to 6.6 km/s	2.75 g/cm³
Lower Crystalline crust	6.6 -6.9 km/s	2.85 g/cm³
Moho	> 8km/s	3.25 g/cm³

Table 6.1. Table summarizing the velocities and corresponding densities for the sedimentary units, basement and Moho blocks composing our gravity model.

6.2.2. Model editing

We need to refine our initial gravity model to reduce the estimated error between the calculated gravity response and the observed anomaly. This can be done quite easily in GMSYS by performing reasonable changes in density values and block geometries without violating the seismic interpretation. The geometry changes are performed by selecting individually the points/blocks and moving them to a new position with a drag of the mouse. As they move, the gravity response of the model is automatically recalculated. GMSYS displays the new and former calculated gravity curves. This allows us to see if a better fit between the observed and calculated data has been achieved. We re-calculate the model until we obtain a satisfying fit between the two gravity anomaly curves.

6.3. Final gravity models for our key profiles

6.3.1. General observations

Figures 6.5 to 6.10 display both the modelled geological cross section, down to 40 km depth, and the gravity observed (dotted line) and calculated (black line) gravity anomalies. In addition to these curves, we also show the estimation of the error (red line) defined as the

difference between observed and calculated gravity data. The five models are divided into main blocks which are the following: water layer, Pleistocene-Pliocene, Tertiary, Upper Cretaceous, Lower Upper Cretaceous, lower Cretaceous, pre-Cretaceous, upper and lower crystalline crust and Moho. We have kept the same colour code for all the models. In addition to these pre-defined blocks, we have included, to the west, oceanic crust and inner flows block in the modelling of profile 1 (Fig. 6.5) and an inner flow (basalts) block in western part of the profile 2 (Fig. 6.6). We have attributed a density to each block of our models based on velocity information from ESP, OBS data (Raum et al. 2000, 2002, and 2006) and using the Nafe-Drake relationship (Ludwig et al., 1970) to convert the velocities into densities, averaging the velocity over individual blocks (Table 6.1). A sedimentary unit can be divided into several blocks with different densities. This is mainly a feature characterizing the pre-Cretaceous units.

The crystalline crust is divided, in all models, into two blocks defined as upper crystalline and lower crystalline crust. Their associated density values are 2.75 and 2.85 g/cm³ respectively. The top of the lower crystalline crust is positioned where we have velocities of 6.6 + km/s. The upper mantle is assigned a density of 3.25 g/cm³.

The upper crustal model, down to base Cretaceous, is constrained by the depth-converted MCS data whereas we have a greater degree of freedom for the positioning of the deeper boundaries. The ESP and OBS velocity stations along the profiles provide constraints for these deeper interfaces. The basement is defined by 6 + km/s velocities and the Moho is located at depths where the velocities reach 8 + km/s. We have tried to place the three deepest boundaries of the gravity models at the same depths at the tie points between the profiles (see figure 4.1 for the location of these points).

The top basement, the lower crustal and Moho boundaries are the three interfaces with the highest uncertainties that went through the biggest modifications in order to obtain a good match between the observed and calculated data. Reasonable fits are achieved for our models in which the Moho and the top lower crystalline crust follow the same trend. We did not try to ‘over’ improve the estimated error for our models; i.e. try to achieve a ‘perfect’ match between the data; by introducing density variation. The misfits can results from important changes in bathymetry and 3-D density variations along the margin.

6.3.2. Profile 1: GMNR-94-310

The depth-converted GMNR-94-310 profile was imported in GMSYS to perform gravity modelling. The extracted gravity anomaly along the profile matches quite well the geological structures. We notice two positive gravity anomalies at the geographical locations of the Slettringen Ridge and the Sklinna Ridge at distances of about 130 and 200 km respectively (Fig. 6.5). We only obtained a good fit between the observed and calculated data by thinning the continental crust at these locations. The Moho boundary is there placed at about 20 km depth. The Moho boundary shallows up to 11 km towards the oceanic domain. To the east of the profile, we place the interface at approximately a 30 km depth.

An important feature of this model is the great misfit to the west of the profile. The GMNR-94-310 seismic line is the only profile from our data set that extends into the oceanic domain crossing the Jan Mayen Fracture Zone (JMFZ) (Fig. 6.5). We have tried to build a reasonable model to the west based on information from the OBS transect 5-00 (Raum et al. 2006) (Fig. 5.15) that helps us to position the COT and constrain the Moho boundary. The OBS transect introduces a two-layer oceanic crust. In the model, we have indicated a continental-oceanic transition (COT) at 50 km distance, and included an upper and lower ‘oceanic crust’ block with densities of 2.8 and 2.95 g/cm³ respectively. A closer look at the interpreted seismic sections crossing the southern most part of the Vøring Transform Margin in the article published by Berndt et al., 2001 gives an idea about the geological configuration in the area west from the JMFZ. We adopt this configuration in our gravity model for the profile 1.

In this study, we focus on the deep structural basin and crustal configuration landward of the COT and do not put too much weight on the misfit between the observed and calculated gravity data in the oceanic domain west of the JMFZ. The misfit can be the result of an important increase in the depth to the sea floor. The effect of the bathymetry was tested by replacing the extra thickness of water by sediments and we observed a reduction of the misfit. Though, the important estimated error to the west would be rather attributed to a warmer and shallower mantle in the oceanic domain characterized by lower densities. The final model for profile 1 is shown in Figure 6.5.

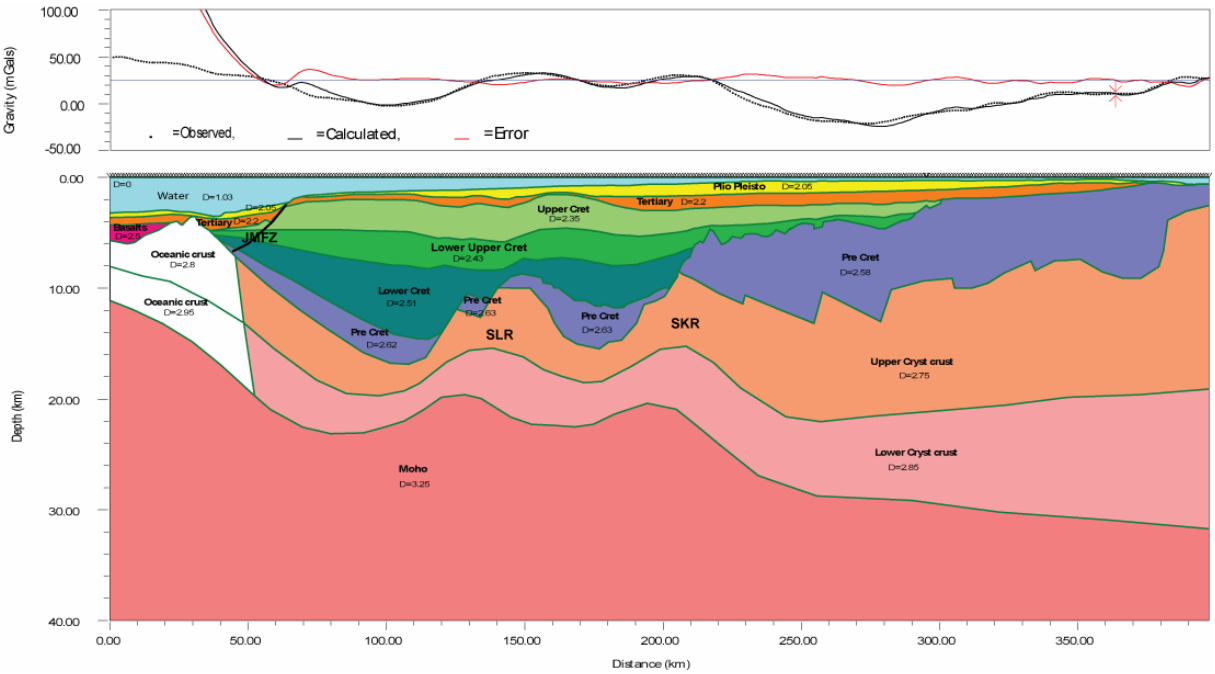

Figure 6.5: Final gravity model profile 1. Location in Figure 4.1. JMFZ, Jan Mayen Fracture Zone; SKR, Sklinna Ridge; SLR, Slettringen Ridge.

6.3.3. Profile 2: VMT95-007

The final gravity model for the profile 2 is presented in Figure 6.6. We have obtained a rather good match between the observed and calculated anomalies. The lower and pre Cretaceous blocks were divided internally as the sedimentary units are much shallower to the east of the profile, i.e. less dense, on the Halten Terrace. The thickness of the continental crust is varying quite considerably along the profile: from about 7 km in the west to approximately 18 km landwards. The crust is thicker under the Halten Terrace area and drastically thins to less than 10 km when crossing the Klakk Fault Complex defining the western boundary of the Halten Terrace. As seen in the previous model, the Moho is shallower under the deep basins and its shallowest position along the profile is at about 18 km depth under the deepest Cretaceous basin. We also observe that the crystalline crust is very thin, less than 4 km, in the deep basin area west of the Slettringen Ridge. Despite the elevation of the Moho boundary to shallower depths, we did not manage to match the observed and calculated anomalies at this location. The free-air gravity anomaly map (Figure 6.1) indicates a positive anomaly high of this location which can affect the observed gravity along profile 2.

We have added an 'inner flow' block to the west in an attempt to match the positive gravity anomaly as the end of our profile extends over the Møre Marginal High (Fig. 6.6), which is defined as a province capped by Palaeogene volcanics (Blystad et al. 1995).

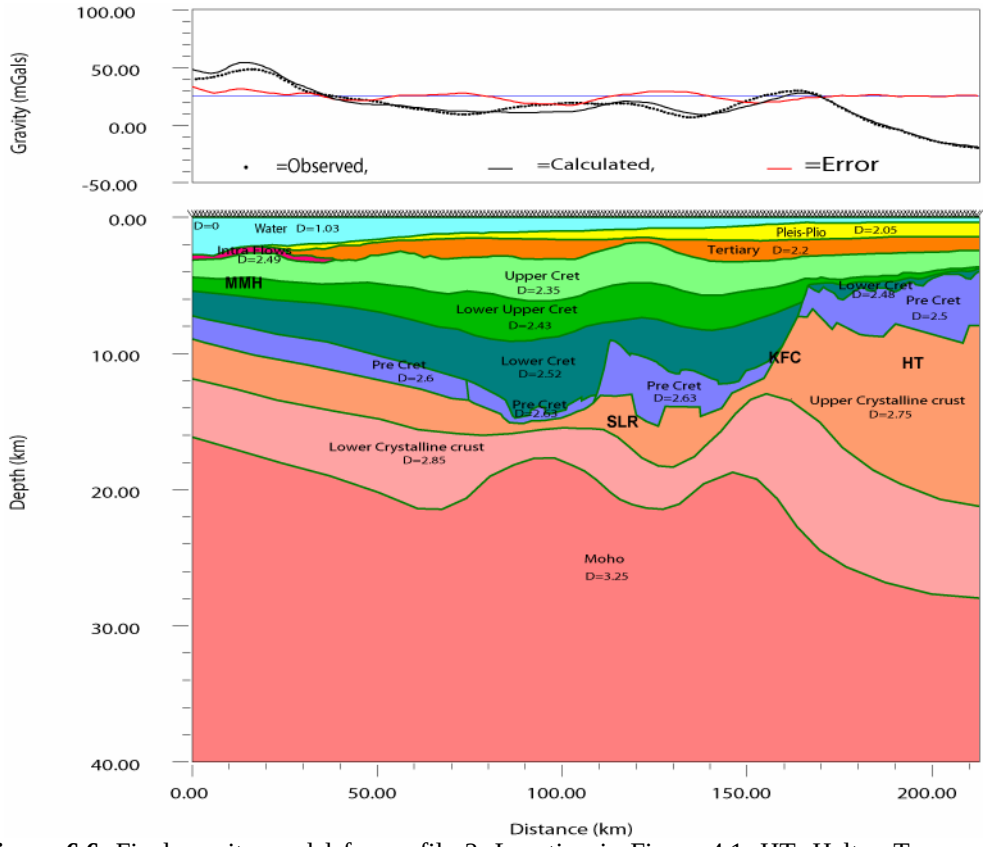

Figure 6.6. Final gravity model for profile 2. Location in Figure 4.1. HT, Halten Terrace, KFC, Klakk Fault Complex; MMH, Møre Marginal High, SLR, Slettringen Ridge.

6.3.4. Profile 3: GMNR-94-104

The gravity modelling of profile 3 (Figure 6.7) presents a good match between the observed and calculated data. The observed data show two positive anomalies at about 160 and 230 km along the x-axis of the model. These anomalies are the gravity response of the two fault complexes bounding the Halten Terrace; the Klakk and the Breimstein-Vingleia Faults Complexes (KFC and BVFC) (Fig. 6.7). It has been difficult to achieve a very good match at these locations, which we infer to be a result of 3-D density variations. In the BVFC area, we had to place the basement at about 4 km and position the top lower crystalline crust at 18 km. At the KFC location, west of the BVFC, the two deepest interfaces have been moved a few kilometres upwards.

The misfit towards the end of the model is justified by bathymetric effect and due to the important density contract between the two shallower blocks; from 1.03 to 2.6 g/cm³. The pre-Cretaceous sediments are located in the vicinity of the sea floor. The thickness of the crust varies greatly along the profile: from about 6 km to the west to approximately 30 km landwards. The model shows lateral variation in depth to Moho; from 16 km to the west to about 32 km landwards with a shallowing of this boundary under the deep sedimentary basins along the profile.

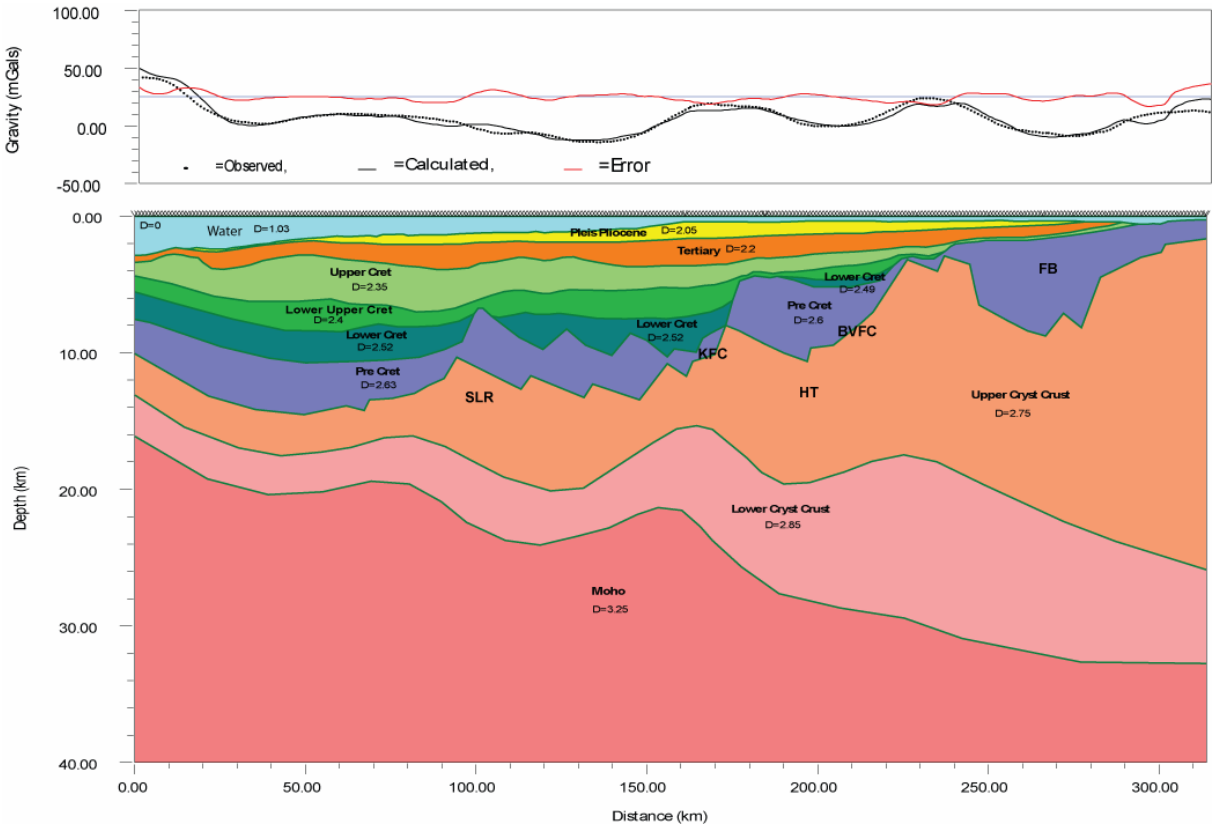

Figure 6.7. Final gravity model for profile 3. Location in Figure 4.1. BVFC, Bremstein-Vingleia Fault Complex; FB, Froan Basin; HT, Halten Terrace; KFC, Klakk Fault Complex; SLR, Slettringen Ridge.

6.3.5. Profile 4: VMT95-006

The observed gravity anomaly along the profile 4 does not show important variations. The small positive anomaly high at about 120 km is associated with the Grip High and the important anomaly to the eastern end of the profile is attributed to an effect of the Klakk Fault Complex (Fig. 6.8). A reasonable fit has been achieved to the east by sub-dividing the pre

Cretaceous sedimentary unit in two with respectively 2.5 and 2.62 g/cm³ for the upper and lower block. The thickness of the crystalline crust does not vary as greatly as in the previous models. It ranges from 10 km in the west to about 16 km landwards. The model displays important lateral variations in depth to top lower crystalline crust and Moho. These boundaries have been changed simultaneous by plus or minus 5 km. As observed in the other models, the Moho is shallower under the deep sedimentary basins.

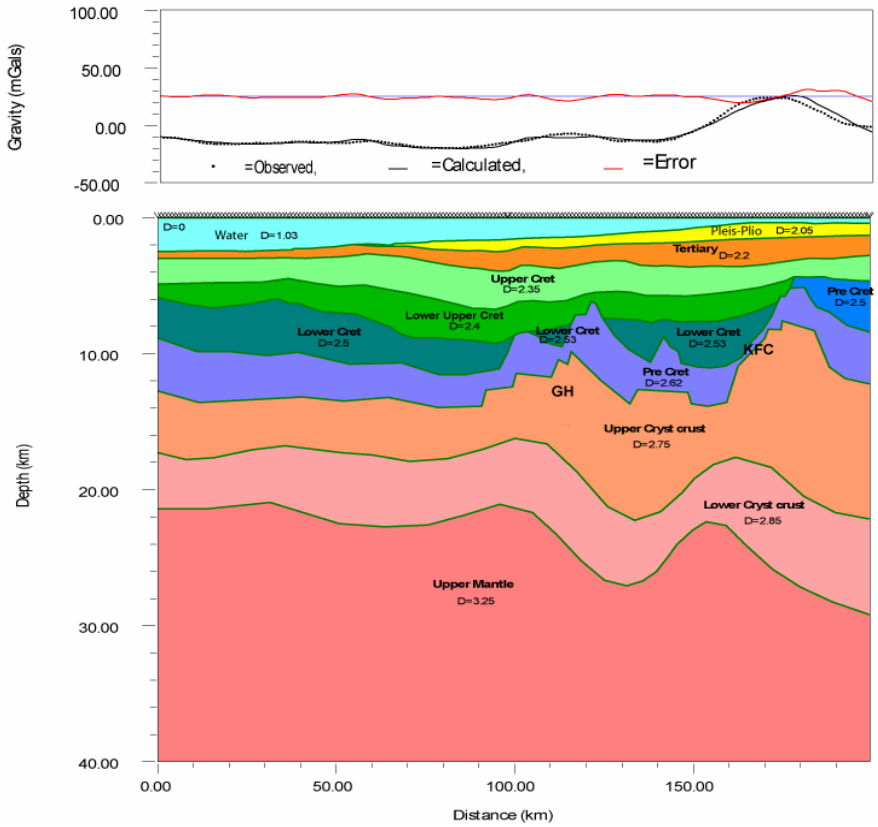

Figure 6.8. Final gravity model for profile 4. Location in Figure 4.1. GH, Grip High; KFC, Klakk Fault Complex.

6.3.6. Profile 5: VMT95-005

This last gravity model, for the profile (Fig. 6.9), presents the best match between observed and calculated anomalies. At about 115 km distance along the line, we find the Grip High (Fig. 6.9) which produces a positive gravity anomaly. In order to obtain a reasonable fit in this area, we elevated the top lower crust and Moho boundaries. Though, the model does not display very important lateral variations in depth to Moho as for the other profiles. It is

positioned at about 22 km depth in the west and at 30 km in the eastern end of the model. The top of the lower crystalline crust follows the trend of the Moho boundary with exception in the east where we needed to place that interface at a shallower depth to get a better fit to the observed gravity anomaly. The thickness of the crystalline crust varies from about 11 km in the west to 25 km landwards.

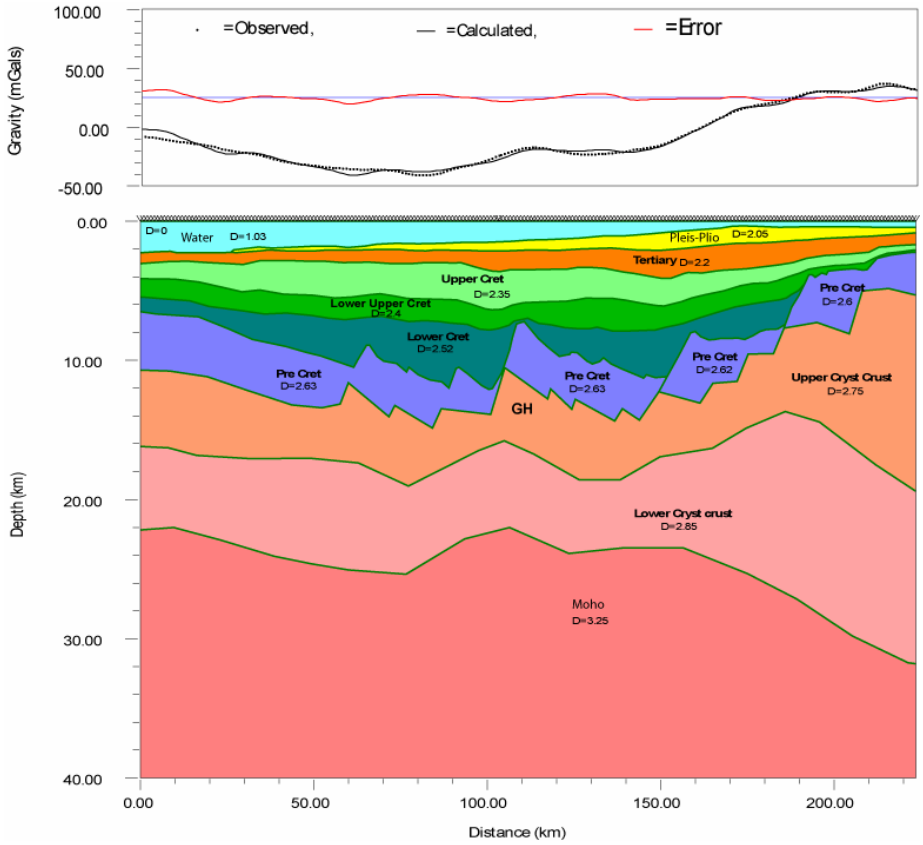

Figure 6.9. Final gravity model for profile 5. Location in Figure 4.1. GH, Grip High.

The gravity models provide improved constraints for the deeper basin and crustal configuration. The upper crustal structure of the profiles is more detailed whereas the lower part is much smoother. The gravity modelling combined with results from previous chapters allow us to construct deep crustal transects along our five regional profiles. These transects are presented and discussed in the next chapter.

7. Discussion

In this chapter we will integrate and discuss the deep basin and crustal configuration in the transition zone between the Møre and Vøring margins. By putting together the results from the ESP analysis, the interpretation of the MCS data set and gravity modelling of the key seismic profiles, we are able to construct deep crustal transects across the study area (Fig. 4.1). The transects reveal the relationships between the deep-seated geological structures and the shallower sedimentary layers. By comparing our results with earlier works, the faults geometries and basin configuration can be discussed in relation to tectonic models for crustal stretching and thinning. In addition, some important observations are made about the lower crustal body characteristic of the Vøring and Møre margins.

7.1. Crustal transects – key observations

This section presents the five deep crustal transects that are constructed along the representative key seismic profiles we selected for this study (Figs. 7.1 to 7.3). The construction of these transects was based on the results obtained in the previous chapters. Our geological models give an overview of the crustal structures, down to 40 km depth. This enables us to discuss the sedimentary and crystalline thicknesses along the transects as well as the topography and the depth to the Moho. We will later compare the two GMNR-94 profiles with geological models along the same lines published by Osmundsen et al. (2002) (Fig. 7.4). The models are displayed with a horizontal to vertical ratio of 1:2. As they are exaggerated two times vertically, the faults in our transects are steeper than they are in nature. The main observations made from the study of the geology along our models are summarized below, from the sea floor to Moho discontinuity.

7.1.1. Cenozoic

The Quaternary sedimentary layer is very thin and therefore difficult to observe on our transects at this scale. The thickness of these sediments is in the order of several tens of meters.

The thickness of the Tertiary layers ranges from a few hundred meters to 2-3 km with the largest thicknesses observed in the basin southwest of the Helland Hansen Arch. The sediments are thinning seawards and landwards over the Halten Terrace and the southern part of the Trøndelag Platform. Early Eocene basalts are inferred to the west of our two northernmost transects. This western area is defined as the Møre Marginal High and the thickness of the basaltic layers varies from 0.2 to 1.5 km, though there are some uncertainties in these estimations as they were modelled by gravity; the seismic data being difficult to interpret in these areas masked by igneous material.

7.1.2. Cretaceous

The thickness of the Cretaceous sedimentary layers vary greatly along the crustal transects from its absence over the southern part of the Trøndelag Platform to approximately 12 km west of the Helland Hansen Arch and the Slettringen Ridge. In this deep basin area, the base Cretaceous was inferred from gravity modelling and OBS data as igneous intrusions masks the seismic data in the western part of the transects.

The general trend indicates that the Cretaceous units are shallowing towards the Helland Hansen Arch, where they have a thickness of about 8.5 km, and they decrease both landwards and seawards to less than 5 km. The deep Cretaceous depocentres are located east and west of the Slettringen Ridge and the Grip High. In the two northernmost profiles (Fig. 7.1), the base Cretaceous is observed at 12 and 14.5 km depth in the eastern and western basins respectively. These basins are not so deep on the southern transects, though the Cretaceous succession reaches depths of 11-12 km.

7.1.3. Pre-Cretaceous

The pre-Cretaceous layer also varies greatly in thickness, ranging from 1 to 10 km. The thickest sections are found in the Halten Terrace and the southern Trøndelag Platform on the northernmost transect. The thinnest pre-Cretaceous sequence is observed to the west of the Slettringen Ridge with a thickness of 1 km. Seawards the layer is relatively constant in thickness with approximate values of 2.5 to 3 km. One exception is observed on profile 1 where the layer pinches out towards the continent-oceanic transition.

Though there are uncertainties for the thickness evaluation of the pre-Cretaceous sedimentary strata. The lower boundary of the unit, also defined as top crystalline crust, is constrained by seismic velocities at scattered location along the profiles and 6 km/s is usually used as a criteria to position this interface.

7.1.4. Crystalline crust

The variations in thickness of the crystalline crust along the crustal transects indicate that the area has experienced important extension and rifting over a long period of time. Along the profiles, the basement shallows and thickens landwards, while we observe crustal thinning towards the deep basins west of the Klakk Fault Complex. The thickest crystalline crust is observed under the Trøndelag Platform, close to the mainland; on transect 1 and 3, where it reaches values of 30 km. The top crystalline basement is found here at the shallowest depths of 1 to 2.5 km. This horizon drops down to about 15 km under the deep sedimentary basins to the west where we also observe the maximum crustal thinning of the crystalline crust.

The minimum thickness of the crystalline crust is observed under the deep basin areas east and west of the Slettringen Ridge. On transect 1 and 2, it is inferred from gravity modelling a crystalline crust of 3 to 5 km under these basins. On the three southern profiles, the crystalline crust also thins under the same structural elements, but the thinning is not as important as for transects 1 and 2. The general trend observed is a thickening and thinning of the basement under respectively the highs and basins along our crustal models.

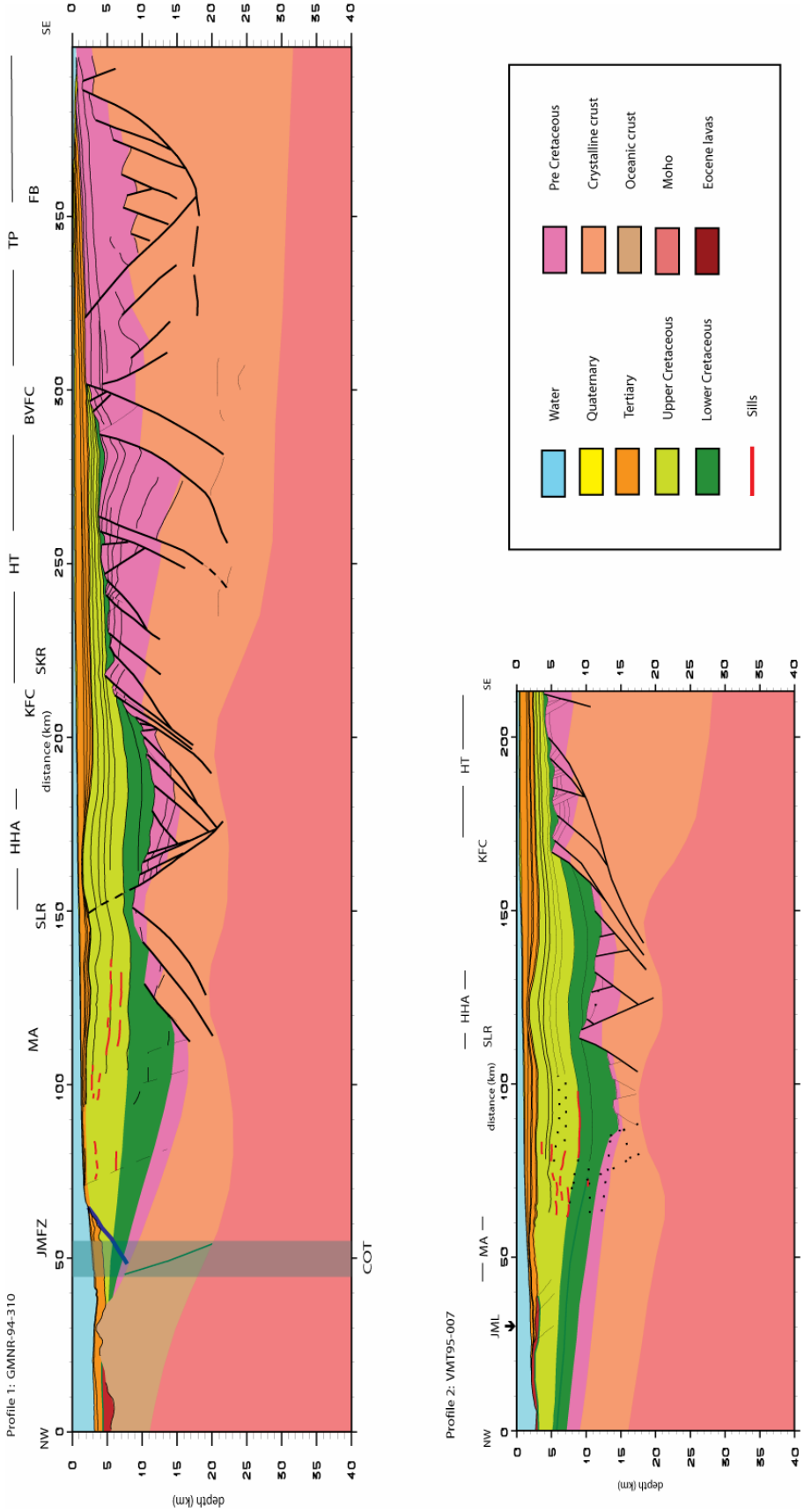

Figure 7.1. Crustal transects along the seismic lines GMNR-94-310 and VMT95-007. BVFC, Bremstein-Vingleia Fault Complex; KFC, Klakk Fault Complex; FB, Froan Basin; HHA, Helland Hansen Arch; HT, Halten Terrace; MA, Modgunn Arch; SLR, Slettringen Ridge; TP, Trøndelag Platform; COT, Continent-ocean transition; JML, Jam Mayen Lineament; JMFZ, Jan Mayen Fracture Zone.

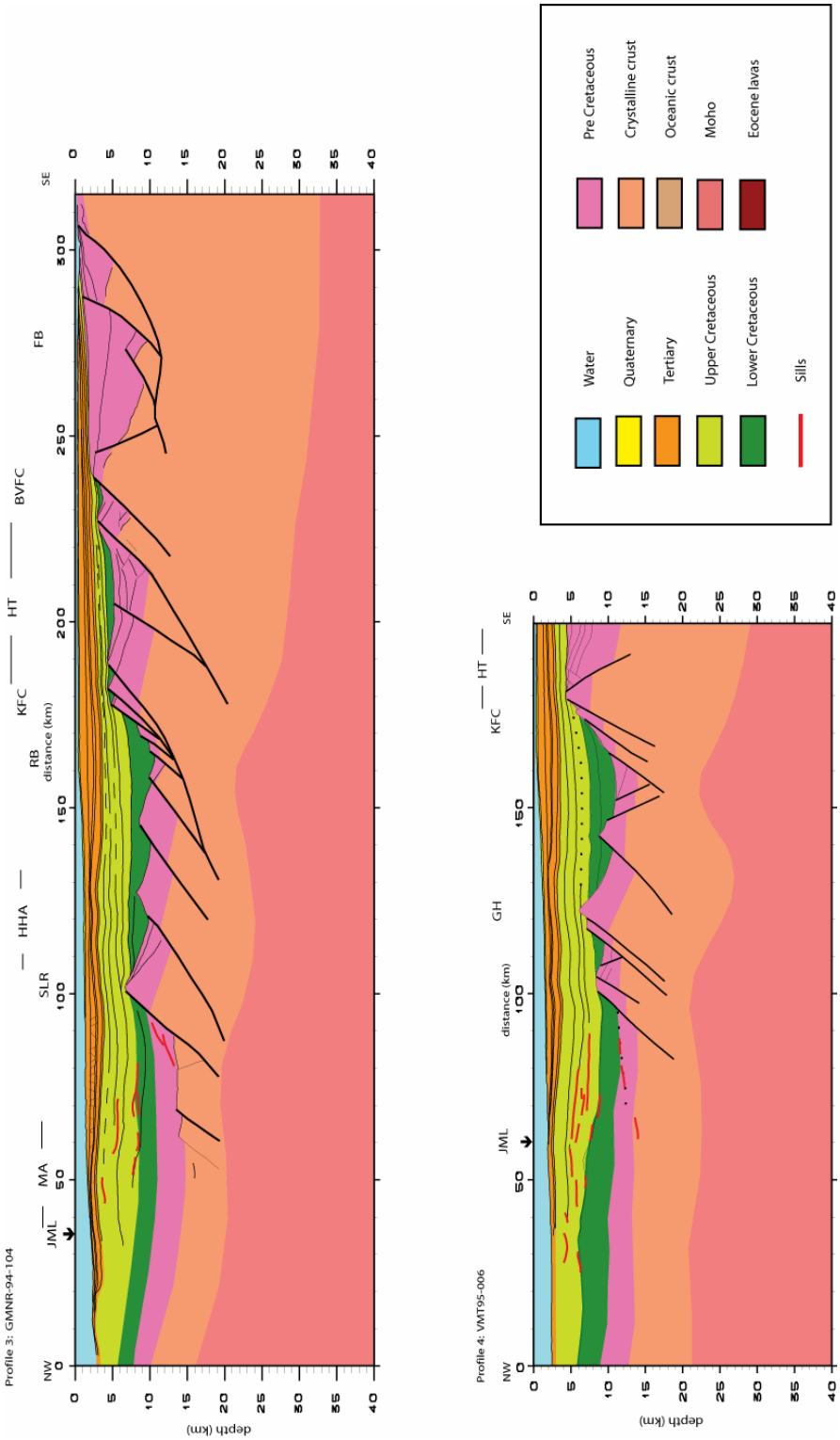

Figure 7.2. Crustal transects along the seismic lines GMNR-94-104 and VMT95-006. BVFC, Bremstein-Vingleia Fault Complex; KFC, Klakk Fault Complex; FB, Froan Basin; GH, Grip High; HHA, Helland Hansen Arch; HT, Halten Platform; Modgunn Arch; RB, Rås Basin; SLR, Slettringen Ridge; JML, Jan Mayen Lineament.

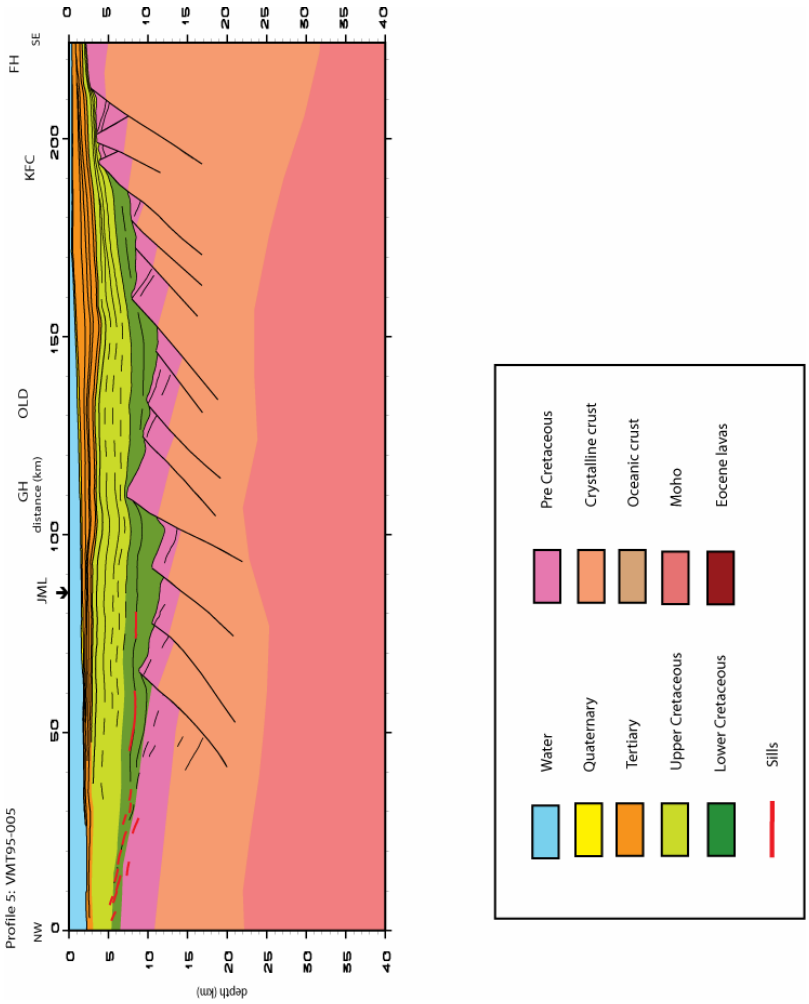

Figure 7.3: Crustal transect along the seismic line VMT95-005. KFC, Klakk Fault Complex; FH, Frøya High; GH, Grip High; OLD, Ormen Lange Dome; JML, Jan Mayen Lineament.

7.1.5. Moho relief

The Moho relief has been positioned on our profiles based on velocity information from ESP/ OBS and gravity modelling. The topography of this boundary varies significantly along our profiles. The Moho is observed at depths of about 32 km under the southern part of the Trøndelag Platform and at approximately 28 km under the Halten Terrace. All profiles indicate a similar topography of this deep boundary. The Moho shallows towards the Klakk Fault Complex and, deepens under the Slettringen Ridge and shallows again under the deep basin areas west of this structural high. The variation in Moho uplift in the area between the western boundary of the Slettringen Ridge/Grip High and the Klakk Fault Complex is in the order of plus or minus 5 km. Further west, towards the Møre Marginal High, the Moho shallows up to respectively 11 km for the transect 1 and 16 km for the transects 2 and 3. This is due to the fact that we enter or are at close distance from the oceanic domain where the Moho is usually observed at depths of 8 to 10 km.

7.1.6. Comparison with earlier works

There is an interesting comparison to make between our two profiles (1 and 3) based on the GMNR-94 lines and the interpretation of the same lines published by Osmundsen et al. (2002) (Fig. 7.4). These profiles are in two-way traveltime (twt) and in order to compare the two sets of lines, we reduced our time-depth interpreted seismic profiles presented in chapter 5 to the same scale. The profiles showed a similar interpretation of the seismic data except for the western part of the GMNR-94-310 line in the Helland Hansen Arch area. In our crustal transect, we interpret some E-dipping normal faults at the eastern boundary of the Slettringen Ridge, whereas Osmundsen et al. (2002) do not define this structural element as a horst and only indicate W-dipping faults. In the northern profile (Fig. 7.4), a common level of detachment is defined in the Trøndelag Platform at c. 6 s twt under the Froan Basin. This detachment is observed at about 17 km depth to the west of our profile 1 (Fig. 7.1). The second profile in Figure 7.4 shows a basinward dipping detachment at 5 s twt under the Trøndelag Platform. In our interpretation of the same line (Fig. 7.2), this feature is seen under the Froan Basin at an approximate depth of 11 km.

The results from our crustal transects present advantages to address the deep structures of the study area. The published profiles (Fig. 7.4) are in twt which makes it difficult to quantify the amount of thinning of the crust and the sedimentary thicknesses. Displaying a geological

section in twt does not bring out the topography of the Moho; which appears then as a relatively flat boundary. Our models (Figs 7.1 to 7.3) were constrained by velocity control from the ESP analysis and the OBS data and depth-converted. Furthermore the depth-converted profiles were taken through gravity modelling. We have thereby been able to add deeper structures in our crustal transects that reduce the uncertainties for the deeper parts of the profiles from Osmundsen et al. (2002)

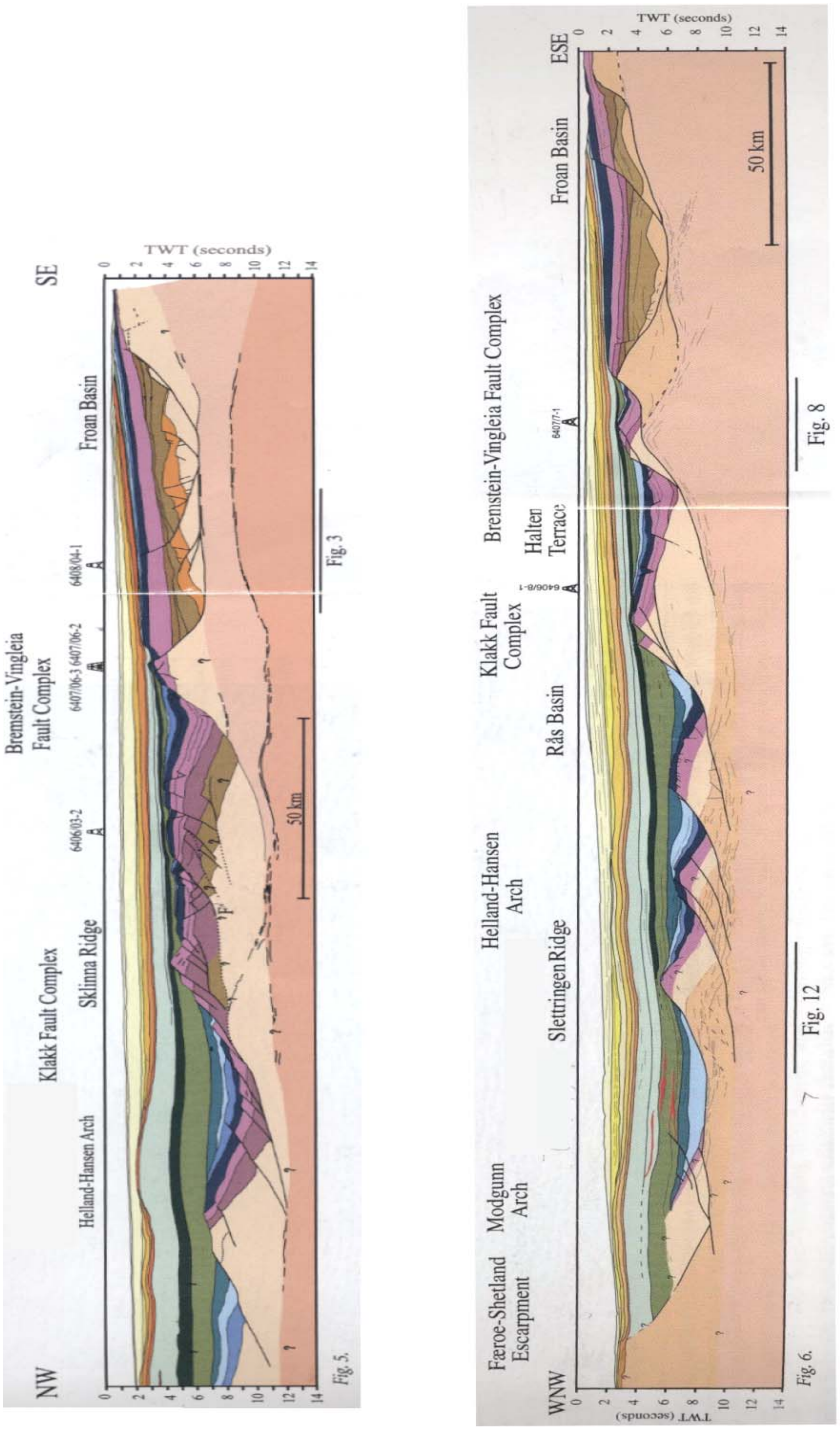

Figure 7.4: Interpreted seismic profiles from Osmundsen et al. (2002). The upper and lower models correspond respectively to the profiles GMNR-94-310 and GMNR-94-104.

7.2. Extensional models for the crustal thinning

In this section we discuss the correlation between the Moho uplifts and the deep Cretaceous sedimentary basins observed in our deep crustal profiles. Two different configurations are observed in the crustal transects (Figs 7.1 to 7.3); the first one corresponds to a superposition of the Moho uplifts and the deep basin areas as seen very clearly in the profile 2 east and west of the Slettringen Ridge (Fig. 7.1). The other configuration is showing a shift between the elevation of the Moho and the location of the deep basin as seen west of the Grip High in Profile 4 (Fig. 7.2). These differences of deep crustal configuration can be explained by a rifting model that combines a pure-shear and a simple shear extensional model Fig. 7.5)

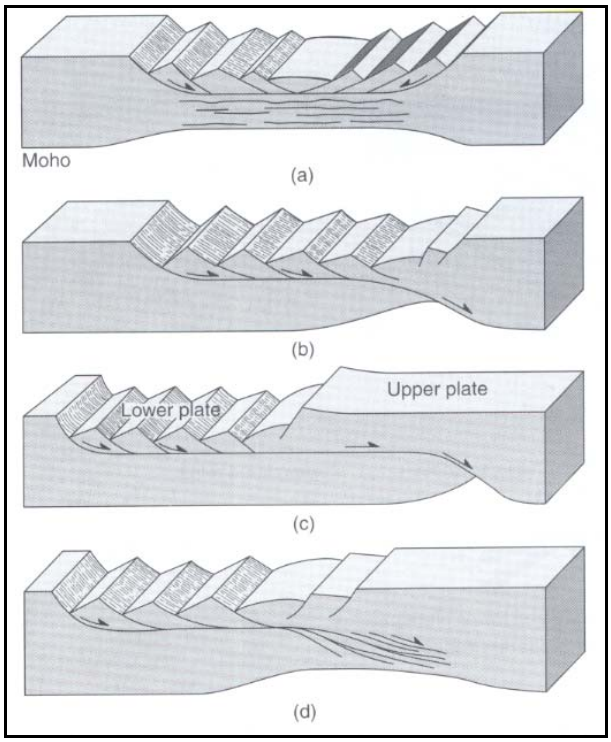

Figure 7.5. Models of rifting at crustal scale (van der Pluijm and Marshak, 2004). (a) Pure-shear model; (b and c) simple-shear models; (d) hybrid model (simple shear plus broad zone of distributed shear at depth).

Pure shear model

In this symmetric rifting model (Fig. 7.5a), normal faults dip toward each other outlining a graben. The detachment of the base of this upper crustal normal faulting lies in the vicinity of the brittle-plastic transition in the crust. The crust is stretched in a horizontal direction in the

form of ductile deformation or by the movement on an array of connected shear zones. In this rifting model, the maximum crustal thinning is located under the deepest basin area. It also implies steep faults that extend in the lower crystalline crust as observed for example east and west of the Slettringen Ridge in profile 2 (Fig. 7.2).

Simple shear model

This rifting model (Fig. 7.5b and c) is defined as asymmetric where the upper-crustal extension is accommodated by displacement on arrays of subparallel normal faults dipping mostly in the same direction. Profile 5 (Fig 7.3) is characterized by the structural configuration; an array of parallel faults. In a simple shear model, the normal faults merge at depth with a detachment zone. This detachment can extend horizontally over large distance before it cuts through the lower crystalline crust. In this extensional model, the faults are defined by a low angle flattening at depth. This configuration is observed in profile 3 (Fig. 7.2) in the Klakk Fault Complex area. In the east of profile 1 and 3, under the southern part of the Trøndelag platform, the faults merge into a subhorizontal detachment level. Osmundsen et al. (2002) have also interpreted a common detachment level (Fig. 7.4).

In the transition between the Møre and Vøring margins, as structural configuration from both rifting models were observed, the most appropriate rifting model would be a hybrid model (Fig. 7.5d).

7.3. Distribution of lower crustal intrusions

A lower crustal body (LCB) characterized by high velocities (7 + km/s) and densities (2.95–3.0 g/cm^3) are found widespread on the Vøring margin. Mjelde et al. (2003) mapped the thickness and distribution of the LCB.

An important observation from our deep crustal transects is the absence of a lower crustal high velocity body. At the gravity modelling stage, we did not need to include such a layer to achieve a good match between the observed and calculated gravity data. The article published by Mjelde et al. (2003) presents the landwards extension of this lower crustal body north of our study area and this interpretation was possible based on the present OBS-database (Fig.

7.6). The longest southeastward extent of the body is found between the Gleipne Lineament and the L Lineament; the latter is defined as a new transfer zone by Mjelde et al. (2003). We display two OBS profiles, 10-96 and 12-96 (Fig. 7.7), to show the pinching out of the lower crustal body towards SE and SW respectively. In addition, we display the OBS transect, 8-96, located south of the Jan Mayen Lineament, where a lower crustal high-velocity body reappears (Raum, 2000). According to Berndt et al. (2001), the limited landward extent of lower crustal intrusion between the Jan Mayen Fracture Zone/Lineament and the new lineament L (Fig. 7.6) can be explained by lateral heat transport from the oceanic lithosphere to the adjacent continental lithosphere, which decreased the ambient mantle temperature and melt production along the transform. This might indicate that these lineaments have been constraining the emplacement of magma at the transition zone between Møre and Vøring margins.

New OBS data need to be acquired east of the Jan Mayen Lineament to couple the observations from the south and the north of our study area in order to delimit the extent of the lower crustal high-velocity body across the transition zone between the Møre and Vøring margins.

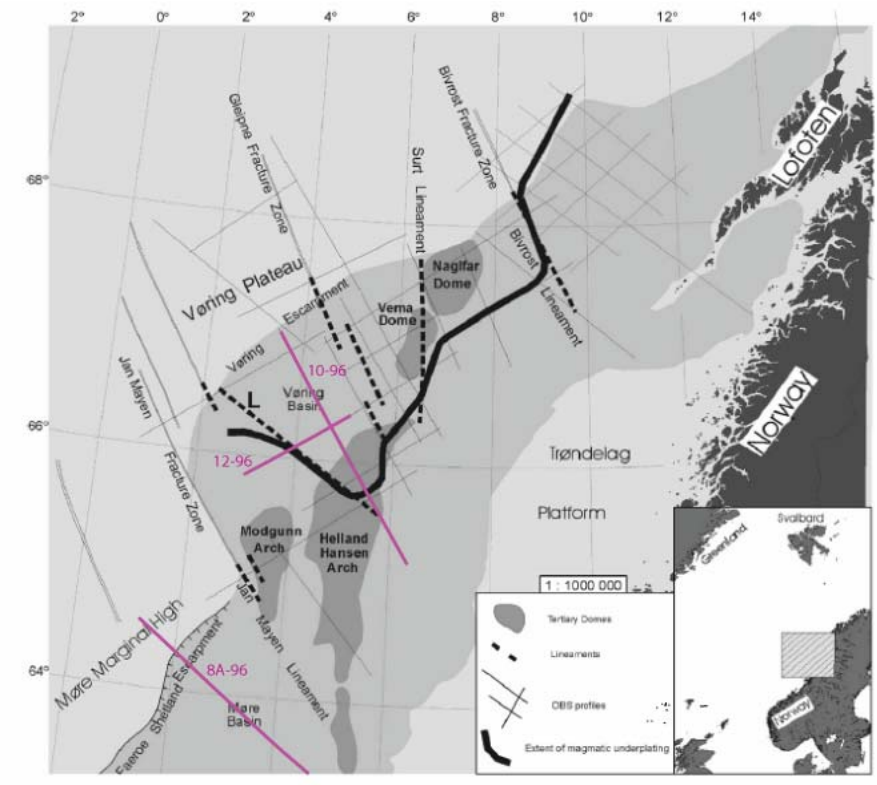

Figure 7.6: Simplified structural map (modified from Mjelde et al., 2003) showing in solid black line the landward extent of lower crustal body (LCB) and in pink and red the OBS transects shown in Figure 7.7.

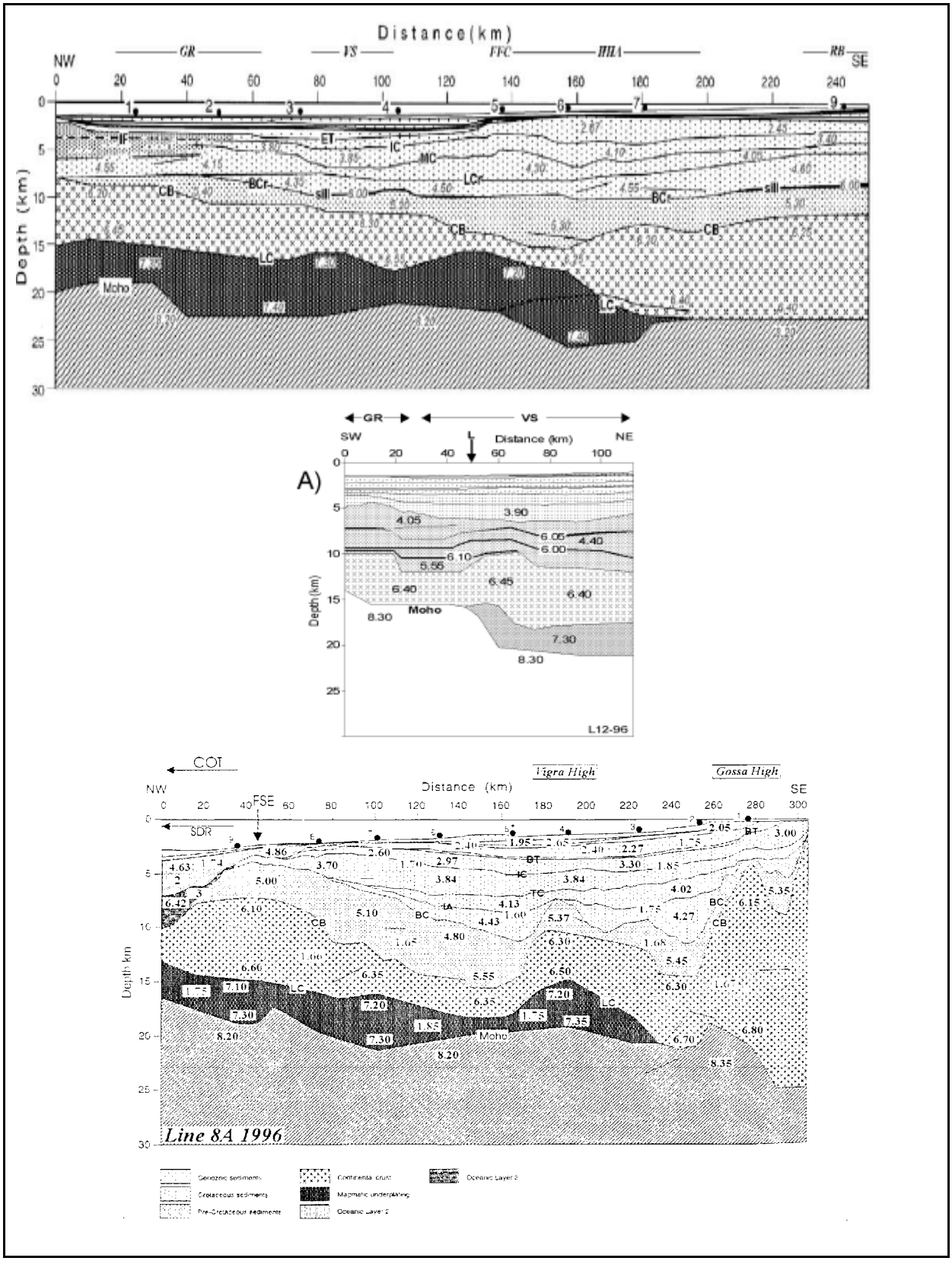

Figure 7.7. OBS transects 10-96 (Raum et al. 2002), 12-96 (Mjelde et al. 2003) and 8A-96 (Raum, 2000) showing the extent of the lowet crustal body north and south of the transition between the Vøring and Møre margins.

8. Summary and conclusions

This study addresses the deep basin and crustal configuration of the transition between the Møre and Vøring margins. The results of the integrated analysis of expanded spread profiles (ESP), multichannel seismic and gravity data has allowed us to construct deep regional crustal transects across the study area. The regional transects provided valuable information on the topography of and depth to Moho, the amount of crustal thinning, the distribution of the sedimentary units across the transition area with focus on the thickness of the Cretaceous sequence, structural trends and structural elements.

The topography of Moho shows a clear correlation between the upper mantle uplifts and the deep Cretaceous basins. Observations from the crustal transects indicate that there is a relative superposition between the two features. Another remark can be made about the depth to Moho; the general trend along the profiles show a seaward shallowing of the discontinuity, from depths of 32 km under the Trøndelag Platform to 11 km in the oceanic domain in the western part of the northernmost profile.

Another interesting feature observed in the transects is the crustal thinning. The variations in the thickness of the crystalline crust are very important; from 30 km under the Trøndelag Platform to a thickness of 3 to 5 km under the deep sedimentary basin at the western flank of the Slettringen Ridge. This really shows that the area has undergone a very long period of extensional tectonic activity.

The Klakk Fault Complex constitutes a clear boundary between the platform area and the deep sub-basins to the west along all the profiles. These deep Cretaceous depocentres are defined by extreme sedimentary thicknesses**.** The maximum observed depth to the base Cretaceous is c. 14.5 km in the north of the study area west of Slettringen Ridge.

All profiles show a similar structural trend with W-dipping normal faults cutting the lower crystalline crust. It is though very difficult to trace the continuation of the faults at depth in the areas of important crustal thinning. The geometry of the faults in eastern parts of the profiles 1 and 3 indicates normal faults merging at depth with a detachment zone, which infer an asymmetric rifting model.

One of the main objectives of this study was the analysis of a new set of ESP's. The information obtained from these wide-angle seismic profiles has contributed to better velocity control in our study area. However, they do not provide full control on the entire crust. It was therefore crucial to combine the ESP data with OBS data that reach the upper mantle in order to constrain the deep structures. OBS data has played an important part in the construction of the deep crustal transects presented in this study, though there is a general lack of OBS data to the east of the Jan Mayen Lineament. It would be relevant to acquire more OBS data in the transition zone between the Møre and Vøring margins to obtain improved velocity control for the deep basin and crustal configuration. New data could also contribute to the mapping of the landward extension of the high-velocity lower crustal body across this transition area.

References

Andresen, O. B., Knudsen, P., 1998. Global marine gravity field from the ERS-1 and Geosat geodetic mission altimetry. *Journal of Geophysical Research*, ***103*** (C4), p. 8129.

Berndt, C., Mjelde, R., Planke, S., Shimamura, H., Faleide, J., I., 2001. Controls on the tectono-magmatic evolution of a volcanic transform margin: the Vøring Transform Margin, NE Atlantic. Marine Geophysical Researches, **22**, 133-152.

Bjørnseth, H. M., Grant, S. M., Hansen, E. K., Hossack, J. R., Roberts, D. G., & Thompson, M.,1997. Structural evolution of the Vøring Basin, Norway, during the Late Cretaceous and Palaeogene. *Journal of the Geological Society, London*, ***154***, 559-563.

Blystad, P., Brekke, H., Færseth, R. B., Larsen, B.T., Skogseid, J., & Tørudbakken, B.,1995. Structural elements of the Norwegian continental shelf. *NPD Bulletin*, ***8***, 45pp.

Brekke, H.,2000. The tectonic evolution of the Norwegian Sea Continental Margin with emphasis on the Vøring and Møre Basins. In A. Nøttvedt, *Dynamics of the Norwegian Margin. Geological Society London Special Publication*, ***167***, 327-378.

Brekke, H., Sjulstad, H. I., Magnus, C., & Williams, R. W.,2001. Sedimentary environments offshore Norway-an overview. In O. J. Martinsen & T. Dreyer, *Palaeozoic to Recent*. *NPF Special Publication*, ***10***, 7-37.

Brekke, H., Dahlgren, S., Nyland, B., & Magnus, C.,1999. The prospectivity of the Vøring and Møre basins on the Norwegian Sea continental margin. In A. J. Fleet & S. A. R. Boldy, *Petroleum Geology of Northwest Europe*: *Proceedings of the 5th Conference*. The Geological Society, London (pp. 261-274).

Diebold, J. B., & Stoffa, P. L., 1981. The traveltime equation, tau-p mapping, and inversion of common midpoint data. *Geophysics*, **46**, 238-254.

Doré, A. G., Lundin, E. R., Fichler, C., & Olesen, O.,1997. Patterns of basement structure and reactivation along the NE Atlantic margin. *Journal of the Geological Society, London*, ***154***, 85-92.

Doré, A. G., Lundin, E. R., Jensen, L. N., Birkeland, Ø., Eliassen, P. E., & Fichler, C.,1999. Principal tectonic events in the evolution of the northwest European Atlantic margin. In A. J. Fleet & S. A. R. Boldy, *Petroleum Geology of Northwest Europe*: *Proceedings of the 5th Conference*. The Geological Society, London (pp. 41-61).

Eldholm, O., 2002. G38x: Marine Seismic Wide-Angle Data. *Course Manual*, Dept. of Geology, University of Oslo.

Flakstad, B., 1998. Forlengelsen av Jan Mayen bruddsonen på den midt-norske marginen. *Hovedfag thesis*. Dept of Geology. University of Oslo.

Keary, P. & Brooks M., 1984, An introduction to geophysical exploration. 4, Oxford, United Kingdom, Blackwell Sci. Publ., pp. 296.

Ludwig, W. J., Nafe, J. E., and Drake, C. L, 1970. Seismic refraction, in *The Sea*, A. E. Maxwell (Editor), Vol. 4, Wiley-Interscience, New York, 53–84.

Lundin, E. R., & Doré, A. G.,1997. A tectonic model for the Norwegian passive margin with implications for the NE Atlantic Early Cretaceous to break-up. *Journal of the Geological Society, London, **154***, 545-550.

Mjelde, R., Shimamura, H., Kanazawa, T., Kodaira, S., Raum, T., Shiobara, H., 2003c. Crustal lineament, distribution of lower crustal intrusives and structural evolution of the Vøring Margin, NE Atlantic; new insight from wide-angle seismic models. *Tectonophysics*, **369**, 199-218.

Olafsson, I., Sundvor, E., Eldholm, O., & Grue, K., 1992. Møre Margin: Crustal Structure from analysis of expanded spread profiles. *Marine Geophysical Researches*, **14**, 137-162.

Osmundsen, P., T., Sommaruga, A., Skilbrei, J., R., Olesen O., 2002. Deep structure of the Mid Norway rifted margin. *Norwegian Journal of Geology*, **82**, 205-224.

Planke, S., 1993. **VELO**: *Seismic refraction/wide-angle reflection velocity database program*. Version 3.2. Computer program/database documentation series no.1., Geophysics Research Group, Dept. of Geology, University of Oslo.

Planke, S., 1993. **SECTION***: Section plotting, digitizing, and utility program*. Version 1.0, Computer program/database documentation series no. 4., Geophysics Research Group, Dept. of Geology, University of Oslo.

Planke, S., 1995. **XSP**. *Processing and Modelling of Expanded Spread Profiles and Other Seismic Refraction Data*. Computer program/database documentation series no. 1x. Version 1.0. Geophysics Research Group, Dept. of Geology, University of Oslo.

Raum, T., 2000. Crustal structure and evolution of the Færoe, Møre and Vøring margins from wide-angle seismic and gravity data. *Phd. Thesis*. Institute of solid earth physics, University of Bergen.

Raum, T., Mjelde, R., Digranes, P., Shimamura, H., Shiobara, H., Kodaira, S., Haatvedt, G., Sørenes, N., Thorbjørnsen, T., 2002. Crustal structure of the southern part of the Vøring

Basin, mid-Norway margin, from wide-angle seismic and gravity data. *Tectonophysics*, **355**, 99-126.

Raum, T., Mjelde, R., Shimamura, H., Murai, Y., Bråstein, E., Karpuz, R. M., Kravik, K., Kolstø, H. J., 2006. Crustal structure and evolution of the southern Vøring Basin and Vøring Transform Margin, NE Atlantic. *Tectonophysics*, **415**, 167-202.

Skilbrei, J. R., Kihle, O., Olesen, O., Gellein, J., Sindre, A., Solheim, D., Nyland, B.,2000. Gravity anomaly map, Norway and adjacent areas, scale 1:3 million. Map and digital data, Geol. Surv. Norway (http://www.ngu.no/), DRAGON project, 7491 Trondheim, Norway.

Skogseid, J., Pedersen, T., & Larsen, V. B.,1992. Vøring Basin : subsidence and tectonic evolution. *In*: Larsen, R. M., Brekke, H., Larsen, B. T. & Talleraas, E. (eds) *Structural and Tectonic Modelling and its Application to Petroleum Geology*, Norwegian Petroleum Society Special Publications, ***1***, Elsevier, Amsterdam, 55-82.

Skogseid, J., Planke, S, Faleide, J. I., Pedersen, T., Eldholm, O., & Neverdal, F.,2000. NE Atlantic continental rifting and volcanic margin formation. In A. Nøttvedt, *Dynamics of the Norwegian Margin. Geological Society London Special Publication*, ***167***, 295-326.

Smith, W., H., F., & Sandwell, D., T., 1997. Global sea floor topography from satellite altimetry & ship depth soundings. *Science*, **277**, 1956-1962.

Stoffa, P. L., Buhl, P., Diebold, J. B. & Wenzel, F., 1981. Direct mapping of seismic data to the domain of intercept time and ray parameter: a plane wave decomposition. *Geophysics*, **46**, 255-267.

Stoffa, P. L., Buhl P., Diebold J. B., 1983. The seismic reflection/refraction method: wide aperture data obtained from multiship experiments. In: Structure and development of the Iceland-Scotland Ridge. Plenum Press, p. 219-256.

Van der Pluijm, B., A., Marshak, S., 2004. Earth structure: an introduction to structural geology and tectonics – 2nd ed, WCB/McGraw-Hill, 656 pp.

Wessel P., & Smith, W., H., F., 1998. New, improved version of the Generic Mapping Tools released, EOS Trans. AGU, **79**, 579.

Wilson, J., 2003, Regionale skorpeprofiler over nordøstlig del av Vøringmarginen. *Hovedfag thesis*. Dept. of Geology. University of Oslo.